LONG-TERM BEHAVIOUR OF MODEL PIERS IN WEAK ROCK

LONG-TERM BEHAVIOUR OF MODEL PIERS IN WEAK ROCK

BY

KYU-JONG CHAE, B.Sc.

A Thesis

Submitted to the School of Graduate Studies

in Partial Fulfilment of the Requirements

for the Degree

Master of Engineering

McMaster University

May 1984

MASTER OF ENGINEERING (1984) McMASTER UNIVERSITY
(Civil Engineering) Hamilton, Ontario

TITLE: Long-Term Behaviour of Model Piers in Weak Rock

AUTHOR: Kyu-Jong Chae, B.Sc. (Agri. Eng.)
(Kun-Kook University, Seoul, Korea)

SUPERVISOR: Dr. R.G. Horvath

NUMBER OF PAGES: xxiii, 180

ABSTRACT

The research contained in this thesis is concerned with long-term behaviour of drilled piers socketed in weak rock. The experimental work involved testing of two steel and seven concrete model piers. The 25.4 mm (1.0 in) diameter steel piers had relatively smooth socket walls (RF = 0.033) and were socketed into pseudo-rock material. The concrete piers were 76.2 mm (3.0 in) in diameter and were socketed into weak rock (Queenston Shale). The concrete piers were of two types: conventional socketed piers with relatively smooth socket walls (RF = 0.025) and grooved piers with relatively rough socket walls (RF = 0.081 and 0.303).

The piers were tested under two condition of load support, shaft resistance only and combined shaft resistance and end-bearing support conditions.

In case of steel piers, electrical resistance strain gauges were mounted on the pier shaft to measure the load distribution along the shaft of the piers. For concrete piers under combined shaft resistance and end-bearing support conditions, flat jack load cells with Marsh and Budenberg pressure gauges and/or electrical pressure transducers were used to measure the load transfer at the base.

All model piers were axially loaded in the laboratory using load frames designed and fabricated for this purpose. The axial loads were

applied by the air cylinders and held constant throughout the period of testing using a regulated air pressure supply.

The test results confirmed that performance of socketed piers can be significantly improved by increasing the roughness of the pier-rock interface. Both the primary creep rate and the load transfer with time were larger for piers with small shaft roughness.

A second stage of creep having a much lower creep rate was observed for all model tests. The time to the end of primary creep was found to depend on the roughness of the socket wall. The primary and secondary creep rate appeared to be dependent on the stress level, shaft roughness, compressive strength of weak rock and support conditions.

The results of the model tests are compared with available test data and with values predicted using methods based on viscoelastic analysis. This method of analysis for piles in clay soils has been modified for application to socket piers in weak rock. It is suggested that the modifications can be used to estimate the long-term settlement of socket piers in weak rock

ACKNOWLEDGEMENTS

The author wishes to express his sincere sense of gratitude and appreciation to Dr. R.G. Horvath for his guidance, assistance and interest at every stage of this study. It has truly been a rewarding experience to work under his supervision.

The author also would like to thank:

His colleagues, Mr. S. Chakrabarti, Mr. D. Chong, and Mr. G. D'Souza for their friendship and discussions during the period of the syudy.

The technical staff of the Civil Engineering and Engineering Mechanics laboratory, Mr. P. Koudys, Mr. M. Forget, Mr. D. Perret and Mr. L. McAndrew for their help during the testing program.

To the McMaster University for offering the financial assistance and Natural Sciences and Engineering Research Council of Canada for the research grant without which the present study would not have been possible.

Last but not least, the author is deeply moved by the kindness, patience and encouragement shown to him by his dear wife Sook-Ja and his sons, Benjamin Jr and Harold and his families.

TABLE OF CONTENTS

LIST OF TABLES

LIST OF FIGURES

LIST OF PLATES

LIST OF SYMBOLS

A	creep function parameter
A_s	surface area of socket pier
B	creep function parameter
C_r	primary creep rate
C_{rn}	normalized creep rate
C_{rs}	secondary creep rate
c	cohesion
D	diameter of socket pier
d	diameter of pile
d_b	diameter of base of pile
E	Young's modulus
E'	drained Young's modulus
E_c	Young's modulus of concrete
E_r	Young's modulus of rock
E_s	secant Young's modulus
E_0	instantaneous Young's modulus
E_1, E_3	spring stiffness for viscoelastic model
h	asperity height
I	settlement influence factor for rigid pile in elastic soil
I_{d1}	first cycle slake-durability index
I_{d2}	second cycle slake-durability index
I_p	plasticity index
I_s	settlement influence factor for socket pier in rock

$J(t)$	creep function
$J(t)^*$	modified creep function
K	modulus ratio
L	length
L_s	length of socket
L_t	total travel distance along the socket wall profile
LVDT	linear variable displacement transducer
l_s	groove length
n	factor
Q	load
Q_a	applied load
Q_b	load support by base resistance
Q_E	load at linear elastic limit
Q_s	load support by shaft resistance
Q_{sf}	load support by shaft resistance at failure
Q_t	total applied load
Q_u	ultimate load
q_s	shaft resistance
q_{sf}	shaft resistance at failure
q_{sm}	maximum shaft resistance
RF	roughness factor
r	radius
r_s	radius of socket
$\bar{\Delta r}$	average asperity height

S	settlement (displacement)
S_L	observed long-term settlement (displacement)
S_{Ln}	normalized long-term settlement (displacement)
S_N	normalized settlement (displacement)
S_s	observed short-term settlement (displacement)
S_{sn}	normalized short-term settlement (displacement)
$S(t)$	total settlement at any time,t
s_f	settlement (displacement) at failure
t	time
t_p	time to end of primary creep
W	moisture content
W_L	liquid limit
w	groove step width
α	creep function parameter
ε	uniaxial strain
η_2	dashpot viscosity
ν	poisson's ratio
ν_r	poisson's ratio of rock
σ	uniaxial stress
σ_c	uniaxial compressive strength
σ_{cw}	compressive strength of weaker material
σ_t	tensile strength
σ_y	yield strength
ϕ	angle of frictional resistance

ASTM	American Society for Testing and Materials
BS	British Standard
ISRM	International Society for Rock Mechanics

CHAPTER 1

INTRODUCTION

1.1 GENERAL

During the past decades, the use of socketed pier foundations has rapidly increased because they provide an economical method to transfer heavy concentrated load, for example, bridges, high-rise buildings, waterfront structures etc., to underlying competent rock. Socketed piers in weak rock are also being used more often.

The long-term settlement and load transfer behaviour of socketed piers in rock is being questioned because most structures are subjected to a long-term sustained load. This study examines the behaviour of drilled piers socketed into weak rock (Queenston Shale) under sustained working loads. For obvious economic reasons, small-scale laboratory model tests were performed for the present research and the data are compared with available full-scale data for an understanding of socketed pier behaviour under sustained load.

1.2 DEFINITION OF SOCKETED PIERS

In this study the term socketed piers refers to piers which are constructed by drilling a socket of required length into the rock and then filling the socket with concrete to form the piers. There are two type of piers, conventional piers (Fig. 1.1) with smooth socket walls

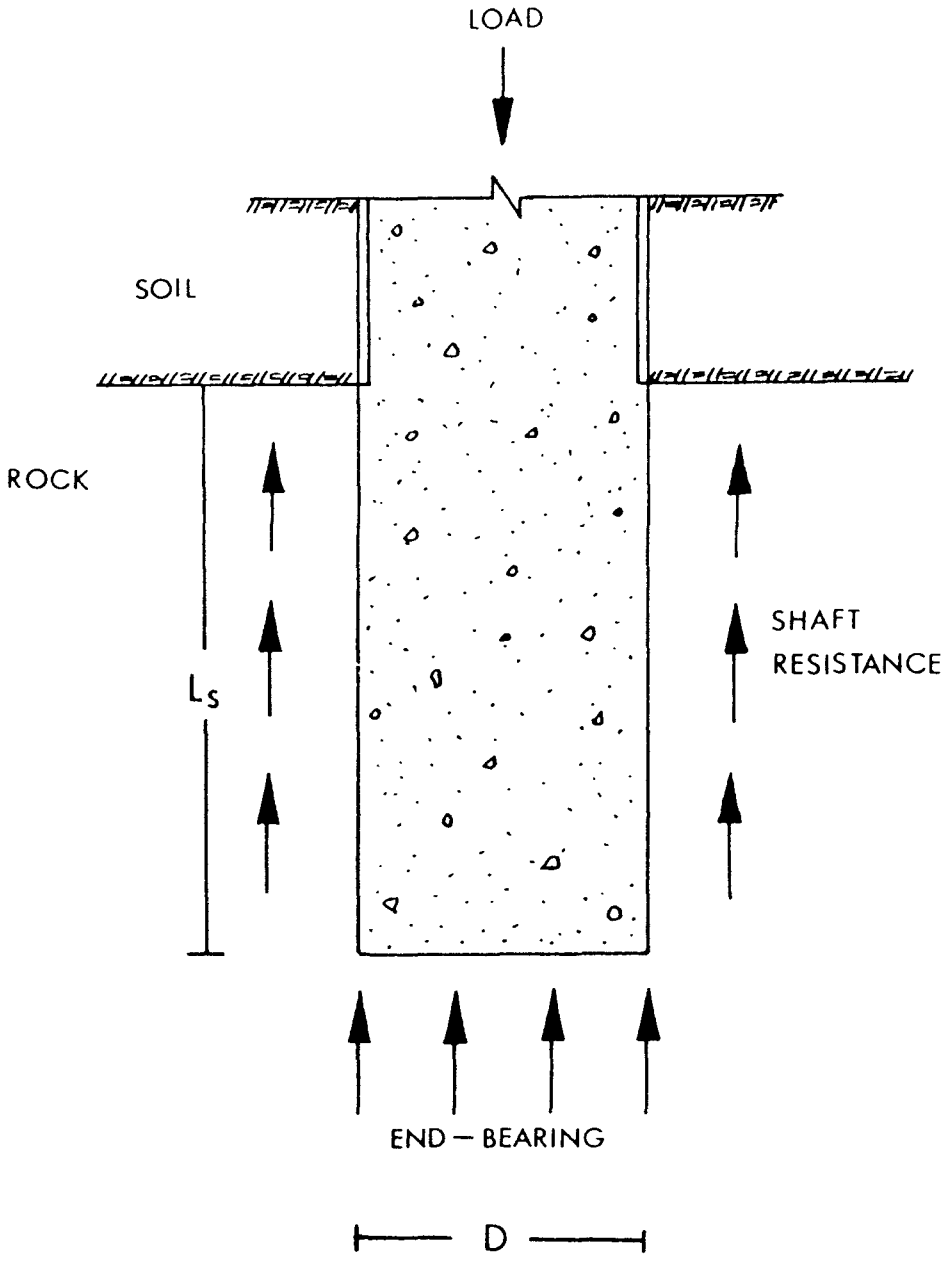

Fig. 1.1 Typical conventional socketed pier to resist axial compression load.

and grooved piers (Fig. 1.2) with socket walls roughened by making grooves.

1.3 RESEARCH AIMS

The main purposes of this study were:

1) To measure the influence of time on displacement of drilled socketed piers under long-term load.

2) To observe the influence of time on load transfer and load distribution in socketed pier foundations.

3) To examine the influence of the relative roughness of the pier-rock interface on long-term behaviour.

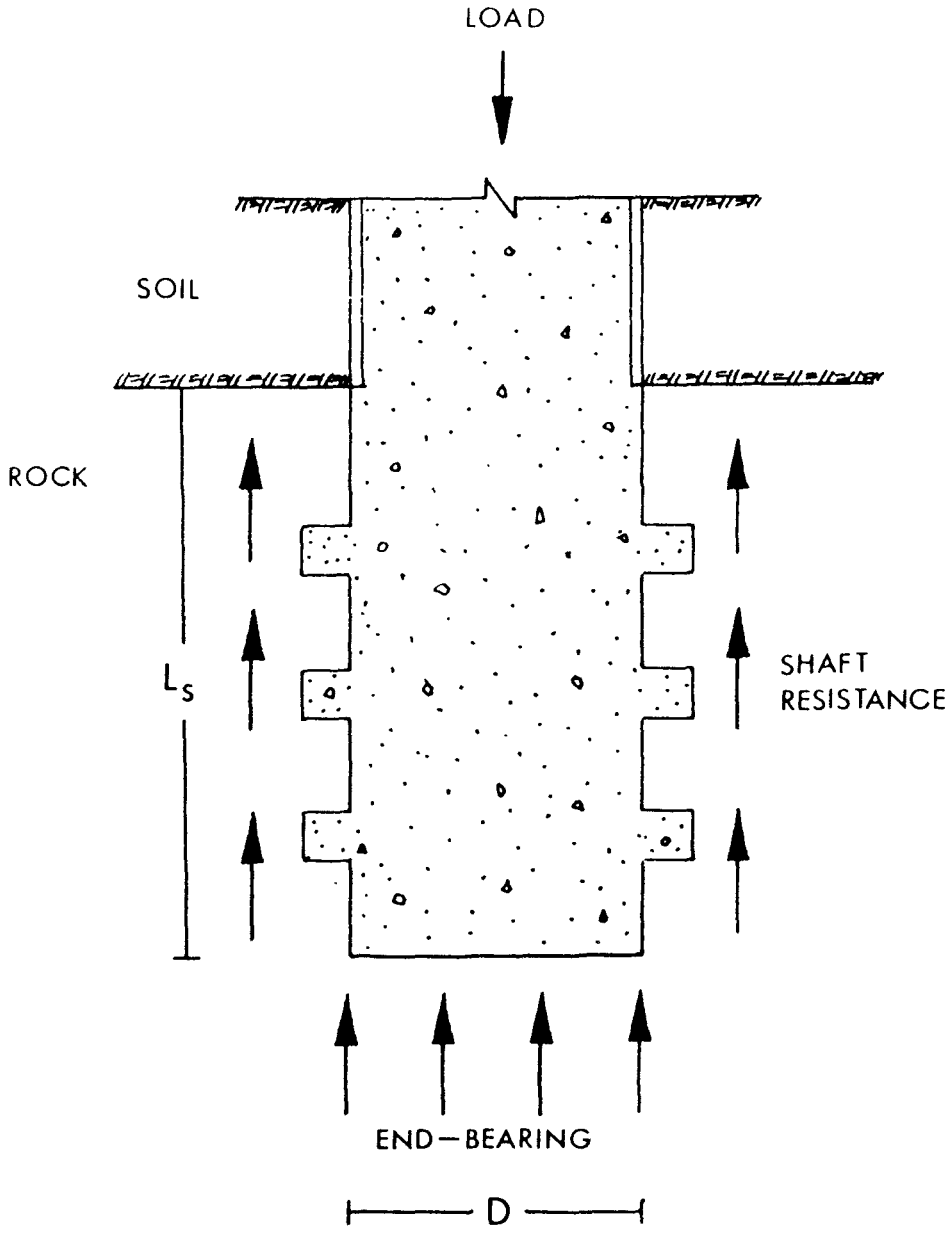

Fig. 1.2 Typical grooved socketed pier to resist axial compression load.

CHAPTER 2

REVIEW OF LITERATURE

2.1 GENERAL

A number of studies have been made in the past few decades to examine the effects of various factors on the design, construction and performance of socketed piers, for example, rock strength, construction technique, socket geometry etc. Most of these studies have been based on short-term response of the materials and comparatively little attention has been paid to long-term behaviour of socketed piers. However, since most engineering structures are subjected to sustained loading, the long-term behaviour of these foundations is important.

2.2 LOAD TRANSFER MECHANISM

Several theoretical studies (Coates and Yu 1970; Ellison et al. 1971; Osterberg and Gill 1973) and instrumented full-scale tests (Aurora and Reese 1976; Bauer 1980; Gibson 1973; Glos and Briggs 1983; Horvath 1982; Jackson et al. 1973; Koutsoftas 1981; Vijavergiya et al. 1969; Williams 1980) have been made in the past to investigate the load transfer mechanisms for drilled socketed piers. These studies, in general, indicate that the magnitude of load transfer is significantly affected by various factors, for example, the ratio of the Elastic Modululi of the pier material and rock, E_c/E_r, depth of pier embedment, Poisson's ratio, ν, and presence of weaker seams in underlying rock etc.

Most of the above studies do not consider the effects of time on the load transfer behaviour. It has been recognized by several researchers (O'Neill and Reese 1970; Peck 1965; Wooley and Reese 1974) that sustained loading results in a "load-shedding" behaviour (Fig. 2.1) wherein the load is gradually transferred from the upper portion to the lower portion of the pier shaft with time. This "load-shedding" behaviour may be influenced by creep of the concrete in the piers, creep of the rock material and creep along the pier-rock interface.

2.3 CREEP IN CONCRETE

Although the overall effect of creep has been reasonably well understood, the magnitude of creep strain in concrete may be rather difficult to predict. The creep in concrete is dependent on several factors (England 1965; Freudenthal and Roll 1958; Neville 1972; Ngab et al. 1981; Troxell et al. 1958; York et al. 1970): 1) humidity, 2) concrete properties, 3) aggregate size and shape, 4) aggregate properties, 5) temperature, 6) water-cement ratio, and 7) curing history.

Neville (1972) and Ngab et al. (1981) reported that sustained load strength is dependent on the strength of concrete. The ratio between the sustained-load strength and short-term strength was found to be higher with high strength than with normal strength concrete (Ngab et al. 1981).

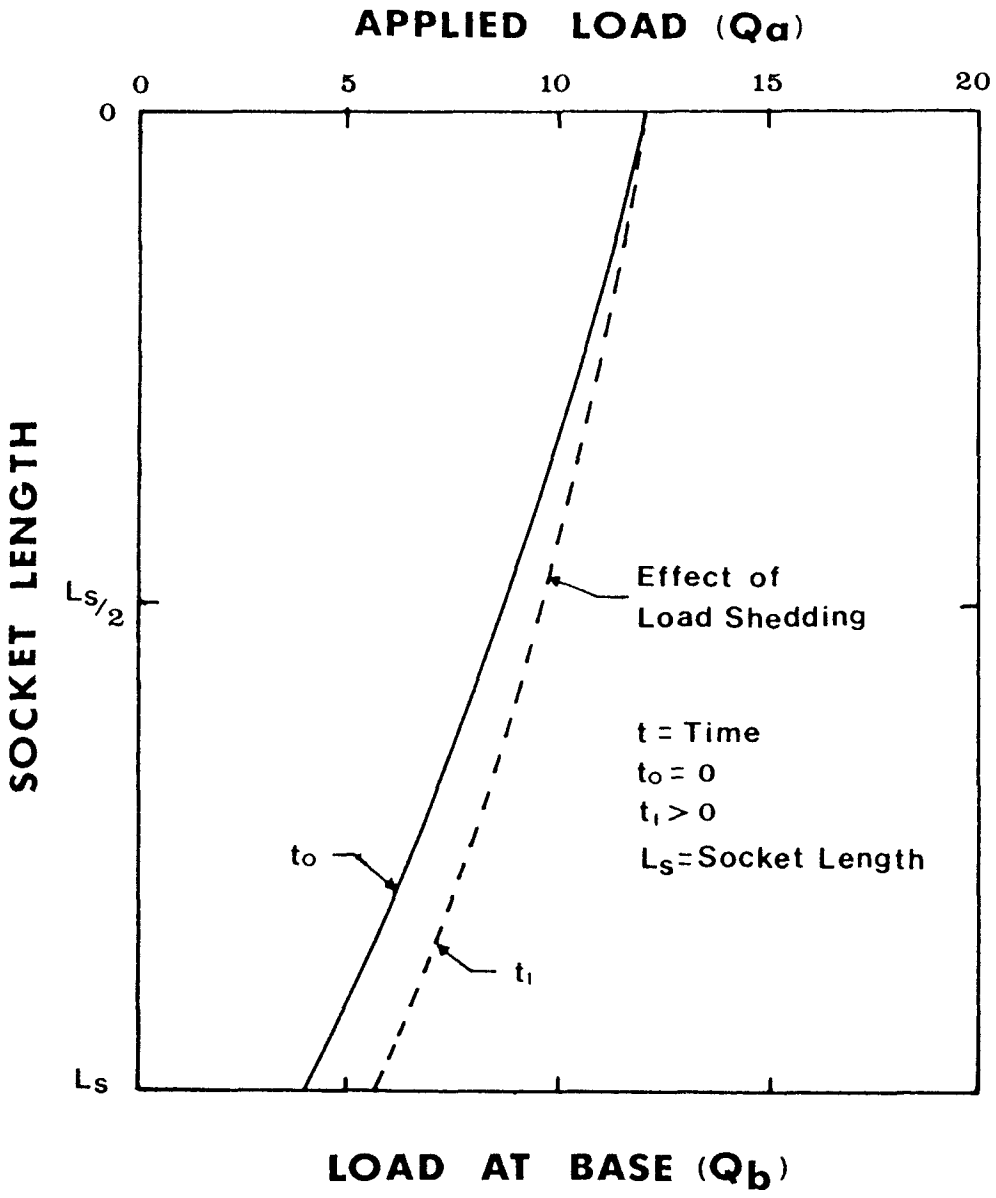

Fig. 2.1 Effect of load-shedding due to sustained loading.

2.4 CREEP IN WEAK ROCK

It has been generally recognized that weak rocks invariably suffer a loss of strength when subjected to sustained load. Casagrande and Wilson (1951) reported that the shear strength of clay-shale lost about 40 % of the compressive strength in 30 days.

There are two distinct types of creep mechanisms for rocks. In the first type, the creep deformation occurs at relatively low deviatoric stresses. This type is associated with comparatively weaker rocks like shales. The second type occurs with hard rocks like granite and take place at comparatively higher stress level, sufficient enough to initiate cracks in the rock (Goodman 1980).

Shales are classified as overconsolidated plastic clays with well or strongly developed diagenetic bonds (Bjerrum 1967; Scott and Brooker 1968). Creep in shale may, therefore, involve significant migration of moisture and/or reorientation of the clay platelets (Goodman 1980). While dealing with shale, it is therefore, of considerable importance to briefly summarize the understanding of the creep mechanism for clay soils.

Bjerrum (1973) proposed a creep mechanism to explain the effect of time on the shear strength of clays. According to this hypothesis, under action of the sustained loading, the cohesive component will attain a peak value at a certain amount of strain and then will decrease, whereas the frictional component increases steadily with the strain (Fig. 2.2) (Schmertmann and Osterberg 1961). Creep movement between

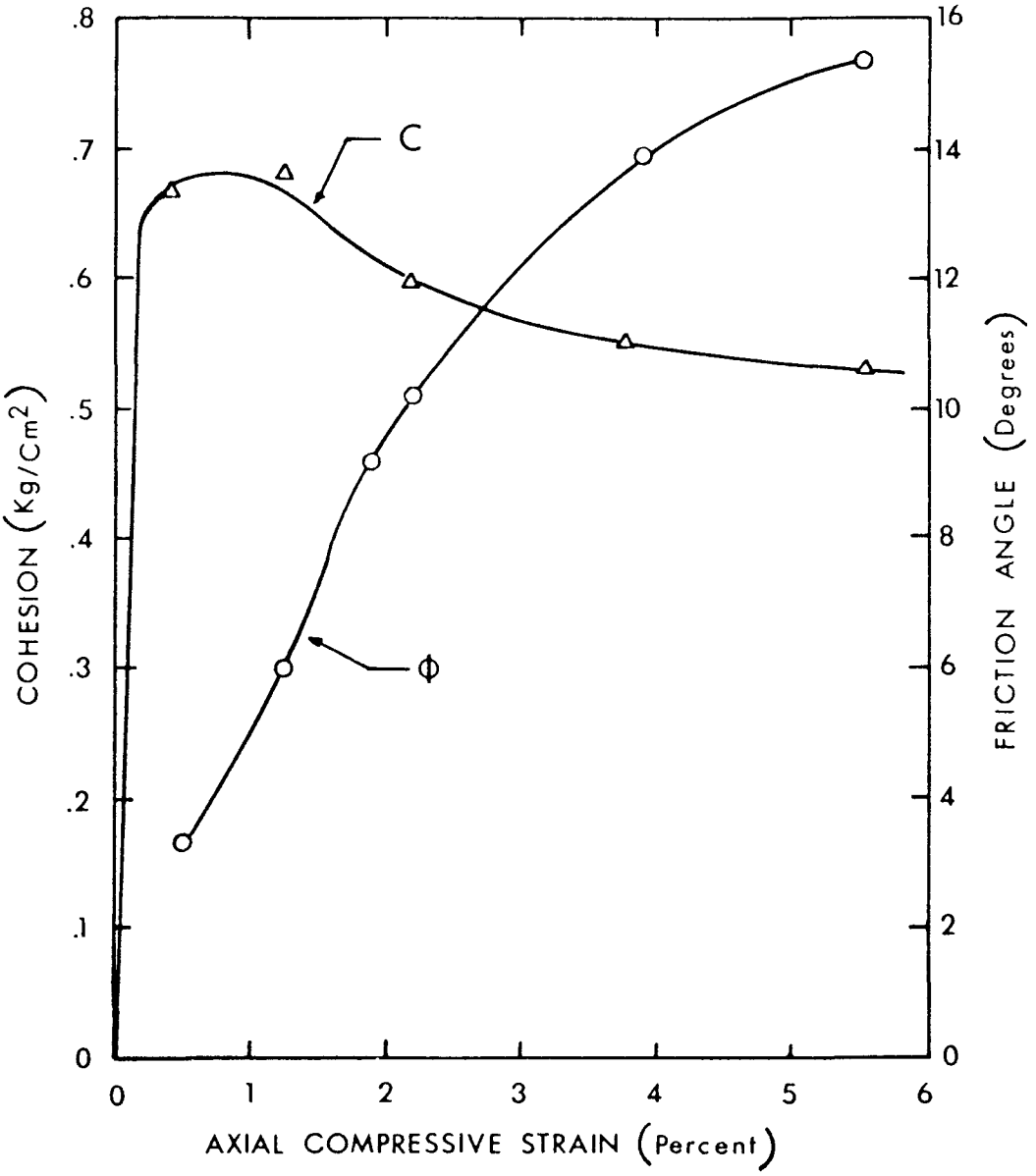

Fig. 2.2 Mobilization of effective cohesion and friction with increasing strain for an undisturbed sample of Boston Blue Clay (after Schmertmann and Osterberg 1961).

particles will continue until a change in the geometry takes place. It has been pointed out by several researchers (Bjerrum 1973; Nelson and Tompson 1977; Terzaghi 1936) that the contact point or interparticle bond may fail at this time. It can, however, be understood that the clay will fail quickly, if the sustained loading is rather high. Smaller stress levels, on the other hand, will require longer time to fail.

It can be seen from the above brief description of creep mechanisms in clays, that the load carrying contact point can fail under sustained loading conditions even if the applied stress is smaller than the shear strength of the soil. However, weak rock like shales are well consolidated and thus, have a well developed mineral-to-mineral contact. The shale will, therefore, creep at a much slower rate than ordinary clay soils which do not have a well developed mineral-to-mineral contact system.

2.5 CREEP IN SOCKETED PIER

As mentioned earlier, time-dependent settlement for socketed piers in weak rock will be affected by creep in the pier material, creep in rock as well as creep along the pier-rock interface.

As explained in section 2.4, the shear strength of weak rocks consists of two components: 1) Cohesion, 2) Friction. Under sustained loading, the decrease in the cohesive component will cause an increase in the frictional component. This process will lead to a reduction in the shear strength of the weak rock which in turn would cause creep

settlements. The magnitude of such creep settlements would depend on several factors (Al-Shaikh-Ali 1977; Gibson 1973; Horvath 1982; Wooley and Reese 1974): 1) stress level, 2) shaft roughness, 3) rock strength, 4) rate of loading, 5) stress history, 6) temperature variation etc.

Williams (1980) reported that piers with relatively smooth socket walls fail initially due to loss of bond between the pier material and rock and then because of low normal stress due to small interface dilation and Poisson's ratio effects.

The failure mechanism of roughened or grooved socket piers, on the other hand, may be controlled by the progressive shearing failure of the asperities or grooves. This mechanism produces significant dilation across the pier-rock interface (Horvath 1982).

From the above, it appears that for conventional piers with smooth socket walls, creep may primarily take place along the pier-rock interface. The creep in grooved socket piers may, however, involve the combined effect of creep in rock and slippage or creep at the pier-rock interface.

2.6 ROUGHNESS FACTOR (RF)

The roughness of the socket wall has been reported to be an important factor determining the shaft resistance and load-displacement behaviour of socketed piers (Horvath 1982; Kenney 1977; Pells et al. 1980; Williams 1980). In the past few years, many researcher's have reported

roughness classifications for socket piers based on semi-qualitative methods (Pells 1978; Pells et al. 1980) and equations (Williams 1980) for the measure of the surface roughness based on the standard deviation of the asperity height and the tangent of the asperity angle.

For present research, the Roughness Factor (RF) proposed by Horvath (1982) and Horvath et al. (1983) has been used. Roughness Factor (RF) is given by:

$$(2.1) \quad RF = \frac{\overline{\Delta r}}{r_s} \times \frac{L_t}{L_s}$$

where $\overline{\Delta r}$ is average height of asperities,

r_s is nominal socket radius,

L_t is total travel distance along the socket wall profile, and

L_s is nominal socket length.

2.7 IMPROVING THE LONG-TERM BEHAVIOUR: GROOVED SOCKETS

It has been generally recognized that under short-term loading conditions, the shaft load capacity of full-scale socket piers is primarily dependent on the roughness of the pier-rock interface. Grooved socket piers were reported to have an average of twice the shaft load capacity of the conventional piers with relatively smooth socket walls (Horvath 1982). Horvath (1982) also reported the settlement behaviour for two socketed piers under sustained loading for a period of 40 hours maximum. Both the settlement and creep rate were found to be significantly less for the grooved socketed piers as compared to conventional

socketed piers. Also, the base load did not increase much with time for the grooved piers as compared to the conventional pier. This suggests that "load-shedding" or creep effects may be less significant for grooved socket piers.

2.8 DESIGN METHODS FOR SOCKET PIERS

The design methods for socket piers can be broadly classified under two categories:

1) Empirical Methods

2) Theoretical Analysis

The empirical methods (Aurora and Reese 1976; Chellis 1951; Davies et al. 1979; Freeman et al. 1972; Horvath 1982; Leach and Thompson 1979; Matich and Kozicki 1967; Rosenberg and Journeaux 1976; Williams 1980; and others) are based on the results of the model studies and loading tests on small and large piers, local experience and other related aspects.

The theoretical approach (Donald et al. 1980; Ellison et al. 1971; Ladanyi1977; Osterberg and Gill 1973; Pells and Turner 1979; Poulos and Davis 1968; and others) is based on idealized behaviour of the pier and the supporting foundation medium. The idealization of the pier foundation interaction is usually based on an elastic or elasto-plastic approach to the problem. Although the theoretical analysis can lead to a better understanding of the behaviour of socket piers, there is a growing concern as to the applicability of the results for

the prediction of actual behaviour in the field.

For socket piers in weak rock, creep may play an important role (Cole and Stroud 1977). There are no widely accepted methods for the estimation of creep for socket piers in weak rock. There are, however, several methods for the estimation of creep for piles in clay soils. One such important and attractive method is that proposed by Booker and Poulos (1976). The method is simple and requires only a few parameters which can be easily determined and/or estimated. The Booker and Poulos (1976) method is described in Chapter 10 while discussing the long-term settlement of socket piers.

2.9 SUMMARY OF SOCKET PIERS UNDER SUSTAINED LOADS

From the foregoing discussions, it appears that several factors may affect the long-term behaviour of socket piers in weak rock. The major factors are rock properties, load applications, applied loading, shaft roughness, and creep parameters of the rock etc.

The rational method for the estimation of the settlement due to the creep of the weak rock should be based on the consideration of load-displacement curve, the magnitude of the load transferred to the base and rate of creep. It has been generally accepted that "load-shedding" could result in a steeper load distribution curve (Fig. 2.1) (O'Neill and Reese 1970; Peck 1965; Wooley and Reese 1974). This decrease in slope of the load distribution curve is due to the gradual transfer of load to the base of the pier shaft. This increase in the base pressure could result

in additional settlement of the pier.

CHAPTER 3

PROBLEM AND INVESTIGATION

3.1 GENERAL

The present research was directed towards the study of load-displacement and load transfer behaviour of model socketed piers under long-term loading.

3.2 STATEMENT OF THE PROBLEM

This investigation attempted to answer the following questions regarding the behaviour of drilled piers socketed into weak rock.

1) Is the long-term behaviour of a socketed pier significantly different than behaviour predicted using short-term load test?

2) If so, can the time-displacement behaviour for socketed piers be predicted?

3) Can the load-displacement and load transfer behaviour of socketed piers under long-term loading conditions be improved significantly by increasing the roughness of the pier-rock interface?

4) If so, is there any relationship between creep behaviour and relative roughness of the interface?

During the course of the research, the following additional aspects attracted attention for a better understanding of "load-shedding"

behaviour of socketed piers.

5) Are "load-shedding" effects observable in model socketed piers for long-term sustained loading?

6) If so, then how is load transferred to the base during long-term loading?

3.3 PROGRAM OF INVESTIGATION

A laboratory investigation on model socketed piers was done in the following major stages:

1 st: Preliminary tests were performed on two model steel piers in pseudo-rock. These tests were done in order to evaluate the feasibility of the study and to standardize the testing procedure.

2 nd: Suitable load frames were designed and constructed.

3 rd: Two model concrete piers in weak rock were loaded to failure. The main objectives of these tests were:

1) The design loads for the long-term tests were estimated from these tests.

2) The test data from the model piers were compared with full-scale socketed piers test results.

4 th: Five model concrete piers were tested for long-term behaviour under sustained load.

5 th: A method for estimating the long-term settlement of

socketed piers in weak rock based on a viscoelastic model was suggested.

The details of the material properties of model piers and testing programs are given in Chapter 4 and 5 respectively. The discussion of the test results are presented in Chapter 6 through 9. A method for the estimating the long-term creep settlements of the socketed piers is suggested in Chapter 10.

CHAPTER 4

MATERIAL PROPERTIES

4.1 GENERAL

The present research is concerned with the long-term load-displacement and load transfer behaviour of two different model piers socketed in weak rock. The small model steel piers socketed in pseudo-rock and concrete piers socketed in weak rock (Queenston Shale) were tested.

A brief description of the materials used in the models and their engineering properties are given in the following sections.

4.2 STEEL MODEL PIERS

4.2.1 Pseudo-Rock Material

For the model tests using small steel piers, a special concrete mix was used to model the weak rock. Cement, fine sand, bentonite and water were mixed to obtain a concrete which had strength and deformation behaviour similar to that of weak rock (Kenney et al. 1975). The proportions of cement, fine sand, bentonite and water for the concrete mix are given in Table 4.1.

The compressive strength, Young's modulus and Poisson's ratio of the pseudo-rock were determined from the results of uniaxial compressive tests on twelve standard control cylinders. The compressometer

TABLE 4.1 THE PROPORTIONS OF CONCRETE MIX.

Material Name	Proportion (%)
High Early Strength Cement	21.27
Fine Sand	53.20
Bentonite	4.26
Water	21.27

TABLE 4.2 ENGINEERING PROPERTIES OF PSEUDO-ROCK MATERIAL.

Uniaxial Compression Tests	Test Results	
	Range	Ave.
Compressive Strength, σc (Mpa)	12.40-20.73	16.57
Secant Elastic Modulus, E_s (Gpa)	5.45 - 5.90	5.68
Poisson's Ratio, ν	0.21 - 0.23	0.22

TABLE 4.3 MILD STEEL PROPERTIES IN SMALL MODEL STEEL PIERS.

	Range	Ave.
Tensile Strength, σ_t (Mpa)	400 - 455	428
Yield Strength, σ_y (Mpa)	221 - 352	286
Young's Modulus, E (Gpa)	-	206

and four electrical resistance strain gauges were used to measure both axial and circumferential displacements of the concrete cylinders during the uniaxial compression tests. All tests were done strictly in accordance with the methods recommened by American Society for Testing and Materials (ASTM).

The results of these tests are summarized in Table 4.2 and are plotted on Deere's (1968) engineering classification chart (Fig. 4.1) as modified by Peck (1976).

More details of the determination of the compressive strength and the rate of strength gains are provided in Appendix A.

4.2.2 Steel Pier Properties

Two model steel piers were made using low-carbon cold rolled mild steel bars. The properties of the mild steel used are given in Table 4.3.

4.3 CONCRETE MODEL PIERS

4.3.1 Weak Rock Properties

The engineering properties of the weak rock (Queenston Shale) used for the present research were determined by the appropriate laboratory tests. All tests were done strictly in accordance with relevant standards for testing such materials (ASTM; BS 1377; ISRM).

A summary of the engineering properties of the weak rock is given

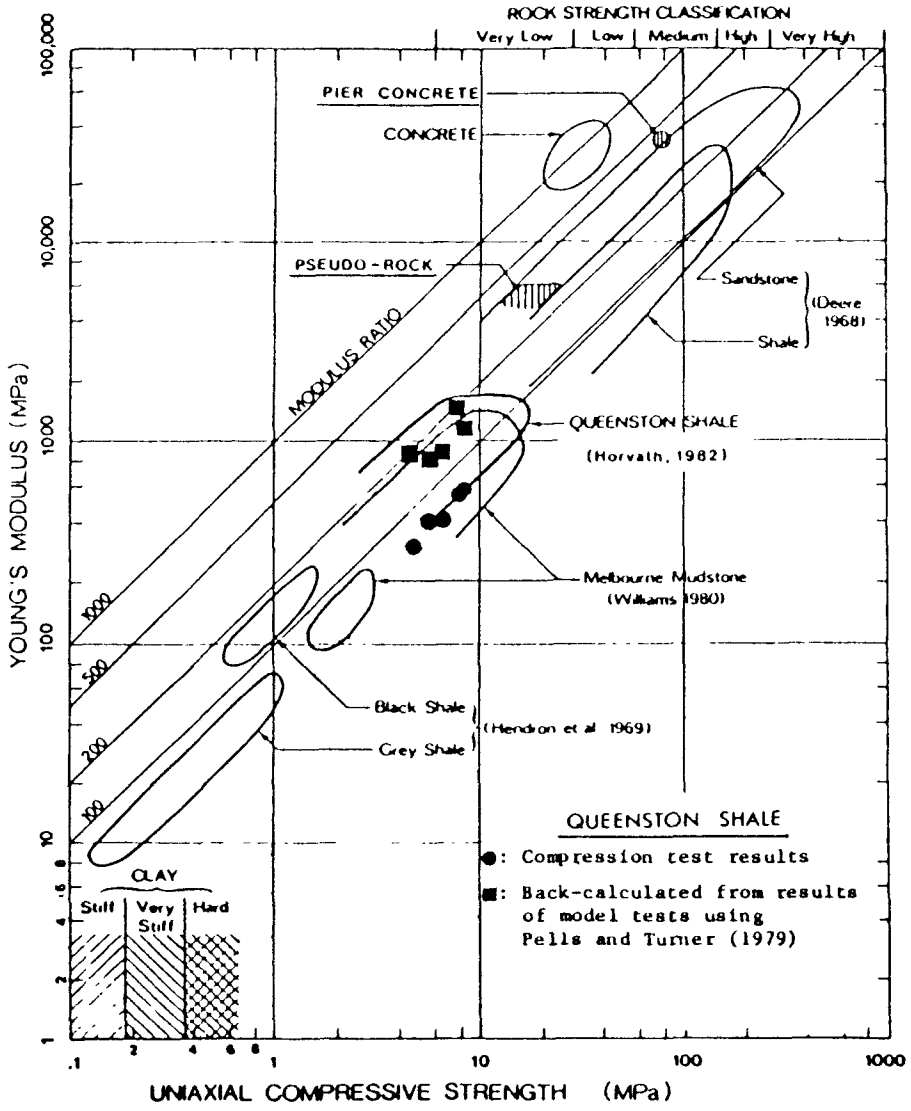

Fig. 4.1 Engineering classification for intact rocks (after Deere 1968).

in Table 4.4. The details of the weak rock are provided in Appendix B.

4.3.1.1 Classification Testing

The following tests were performed to determine the characteristics of the weak rock (Queenston Shale) used for the study:

Atterberg Limits and Cone Penetrometer

Slake Durability

The results of the Atterberg Limits and Cone Penetrometer tests indicated that the shale consists of weakly plastic inorganic clays as per Casagrande's (1948) plasticity chart.

The results of the Slake Durability tests indicated that the shale has low durability as per Gamble's (1971) classification. The shale was also observed to rapidly deteriorate when left exposed in the open.

4.3.1.2 Compressive Strength Testing

The strength and the elastic properties of the shale were determined from the results of undrained uniaxial compression test of core samples, 66.0 mm (2.6 in) in diameter and 165.0 mm (6.5 in) in length. Four electrical resistance strain gauges were used to measure both axial and circumferential displacement of each core sample during the compression testing. The tests were performed to determine the compressive strength, Young's modulus and Poisson's ratio of the test samples.

The results of these tests are summarized in Table 4.4 and are

TABLE 4.4 ENGINEERING PROPERTIES OF WEAK ROCK (QUEENSTON SHALE).

Test Description	Test Results	
	Range	Ave.
Moisture Content, W (%)	5.1 - 5.7	5.6
Liquid Limit, W_L (%)	20.8 - 22.4	21.6
Plastic Index, I_P (%)	8.6 - 9.0	8.8
Slaking Test, I_{d1}	66.3 - 86.2	76.5
Slaking Test, I_{d2}	38.5 - 68.4	54.1
Uniaxial Compression Test		
Compression Strength, σ_c (Mpa)	3.20 - 8.58	6.5
Secant Elastic Modulus, E_s (Mpa)	427 - 545	500
Poisson's Ratio, ν	0.28 - 0.34	0.31

TABLE 4.5 ENGINEERING PROPERTIES OF CONCRETE IN TEST PIERS.

Uniaxial Compression Test	Test Results	
	Range	Ave.
Compression Strength, σ_c (Mpa)	60.0 - 68.5	63.4
Secant Elastic Modulus, E_s (Gpa)	31.5 - 32.1	31.9
Poisson's Ratio, ν	0.21 - 0.23	0.22

also plotted in Fig. 4.1.

4.3.2 Concrete Pier Properties

Medows pre-mix V-3 non-shrink grout was used for the concrete piers.

Twelve standard control cylinders were cast and tested for uni-axial compressive strength tests. The results of these tests are given in Table 4.5 and are plotted in Fig. 4.1.

The typical properties of the non-shrink grout as supplied by the manufacturer and the rate of strength gain with time are provided in Appendix C.

CHAPTER 5

TESTING EQUIPMENT AND PROCEDURES

5.1 GENERAL

Two types of model piers were tested for the present investigation. The first set of model tests were performed on steel piers socketed in pseudo-rock designed to simulate the behaviour of weak rocks. The other set of model tests were carried out on concrete piers socketed into weak rock.

The designation scheme for the tests is shown in Fig. 5.1.

The laboratory work comprised of the following major steps:

1) For tests on steel piers, suitable pseudo-rock was designed to model weak rock. For concrete piers, representative large block samples of the weak rock (Queenston Shale) were collected.

2) Suitable load frames were designed and constructed.

3) Model piers were constructed and suitable instrumentation schemes were designed and installed.

4) The model piers were load tested.

A summary of the testing program is given in Table 5.1.

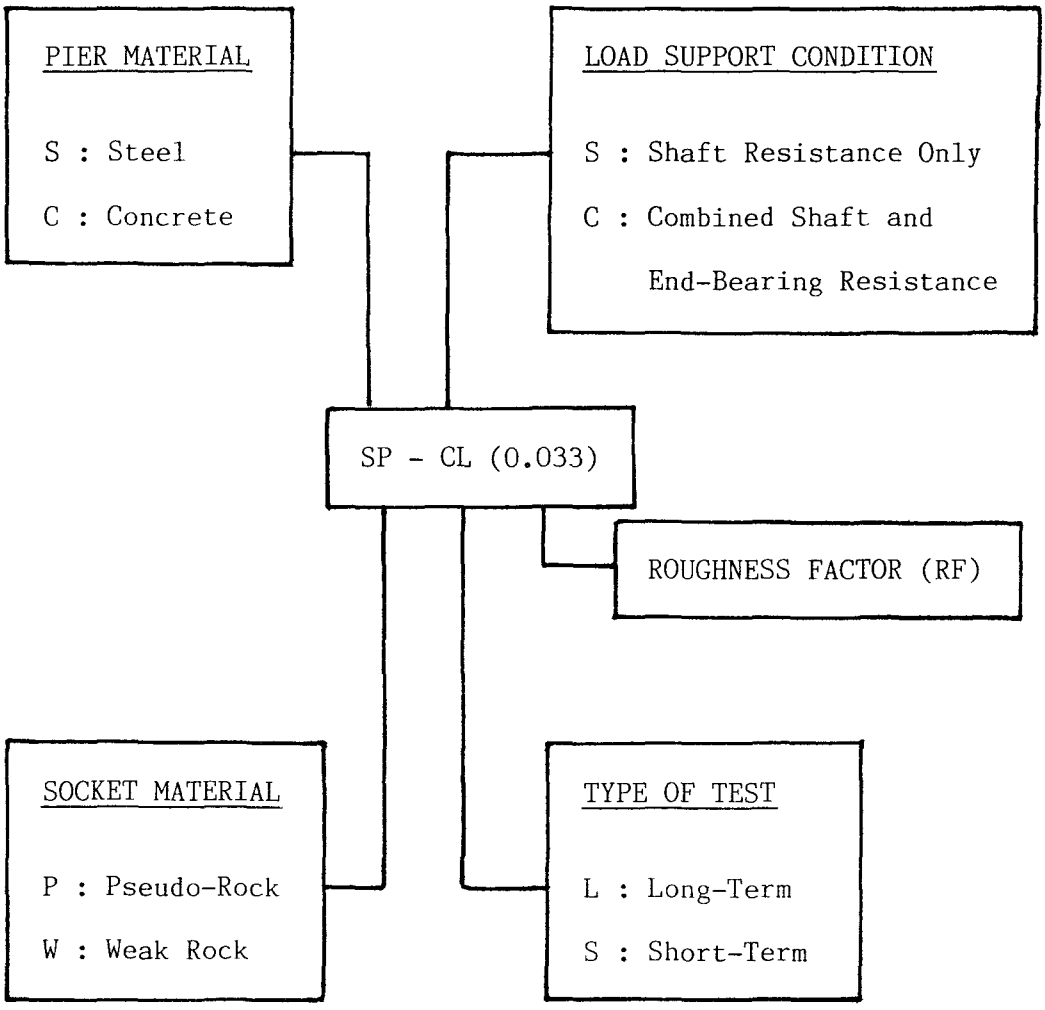

Fig. 5.1 Test designation scheme.

TABLE 5.1 SUMMARY OF TESTING PROGRAM.

Pier Material	Test Pier	D (mm)	L_s/D	No. of Tests		Remarks
				Short Term	Long Term	
Steel	SP-SL(0.033)	25.4	4		1	Test continued
	SP-CL(0.033)	25.4	4		1	for 240days
Concrete	CW-SS(0.025)	76.2	2	1		Loaded to
	CW-CS(0.303)	76.2	2	1		failure
	CW-SL(0.025)	76.2	2		1	Long-term test continuing; data for 200 days are presented
	CW-CL(0.025)	76.2	2		1	
	CW-SL(0.081)	76.2	2		1	
	CW-SL(0.303)	76.2	2		1	
	CW-CL(0.303)	76.2	2		1	

D = Socket Diameter L_s = Socket Length

5.2 EQUIPMENT

5.2.1 Load Testing Frame (Short-Term Test)

The larger model concrete socketed piers were tested in RIEHLE Testing Machine with a capacity of 25,000 kN (5,620,000 lb). A spherical load platen and steel ball was used at the top of the test pier to ensure axial loading (Plate 5.1).

5.2.2 Load Frame (Long-Term Test)

Two types of load frames were used for the model pier tests. Two small load frames with a capacity of 5.34 kN (1,200 lb) and 15.6 kN (3,500 lb) for small and large Bellofram Air Cylinder respectively, were available in the laboratory. This load frame (Fig. 5.2) was used for the tests on small model steel piers socketed into pseudo-rock materials.

Load frames of higher capacities 80.0 kN (18,000 lb) were designed and fabricated for the larger model concrete piers socketed into weak rock. Five such higher capacity load frames were made of structural steel sections. The essential details of these frames are shown in Fig. 5.3.

5.2.3 Load Measurement

A Bellofram Air Cylinder was used to apply the axial load. The desired pressure was applied and maintained constant by connecting the air cylinder to a regulated air pressure supply. The load on the air cylinder-ram was measured with a calibrated Marsh and Budenberg gauges

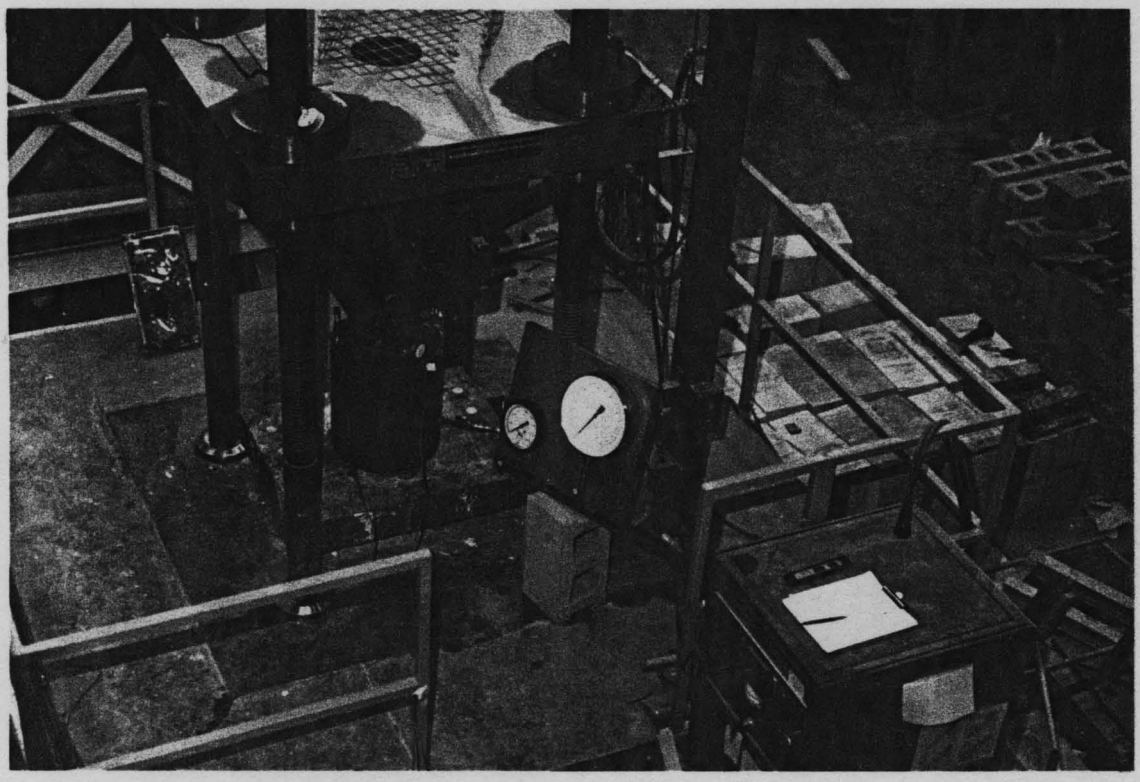

Plate 5.1 View of short-term load frame and typical instrumentation arrangement for measuring device.

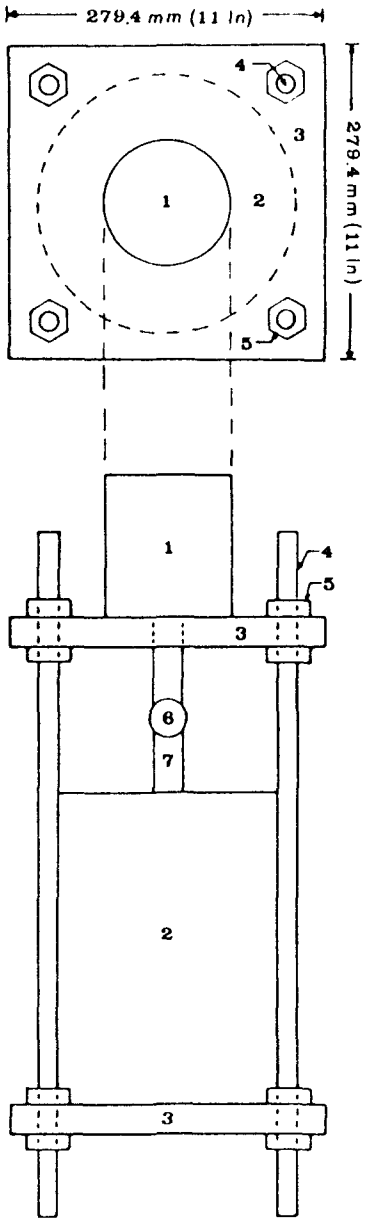

1) Bellofram Air Cylinder 2) Pseudo-Rock
3) 25.4 mm (1.0 in) Thick Steel Plate
4) 19.1 mm (3/4 in) Threaded Rod
5) 19.1 mm (3/4 in) Nut 6) 25.4 mm (1.0 in) Dia. Steel Ball 7) Steel Pier

Fig. 5.2 Load frame for model steel pier.

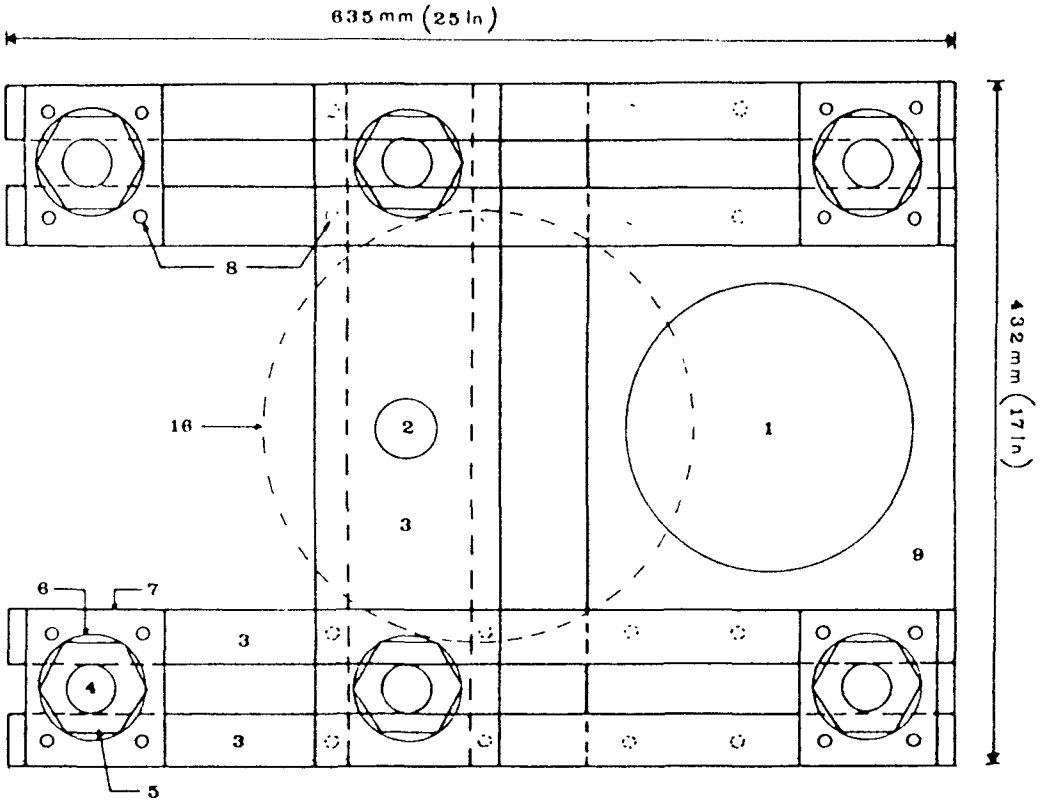

1) Bellofram Air Cylinder 2) 38.1 mm (1.5 in) Dia. Threaded Rod
3) C4 x 7.25 Channel 4) 25.4 mm (1.0 in) Dia. Threaded Rod
5) 25.4 mm (1.0 in) Nut 6) Washer 7) 12.7 mm (0.5 in) Thick Steel Plate 8) 25.4 mm (1.0 in) Dia. Steel Ball
9) C10 x 25 Channel 10) 50.8 mm (2.0 in) x 50.8 mm (2.0 in) Cold Rolled Bar 11) Thrust Bearing (Model NICE 1005J BF08)
12) 38.1 mm (1.5 in) Dia. Steel Ball 13) Air Bubble Level
14) 1 : 6 Ratio Lever 15) Model Concrete Pier 16) Steel Pipe

Top View

Fig. 5.3 Load frame for model concrete piers.

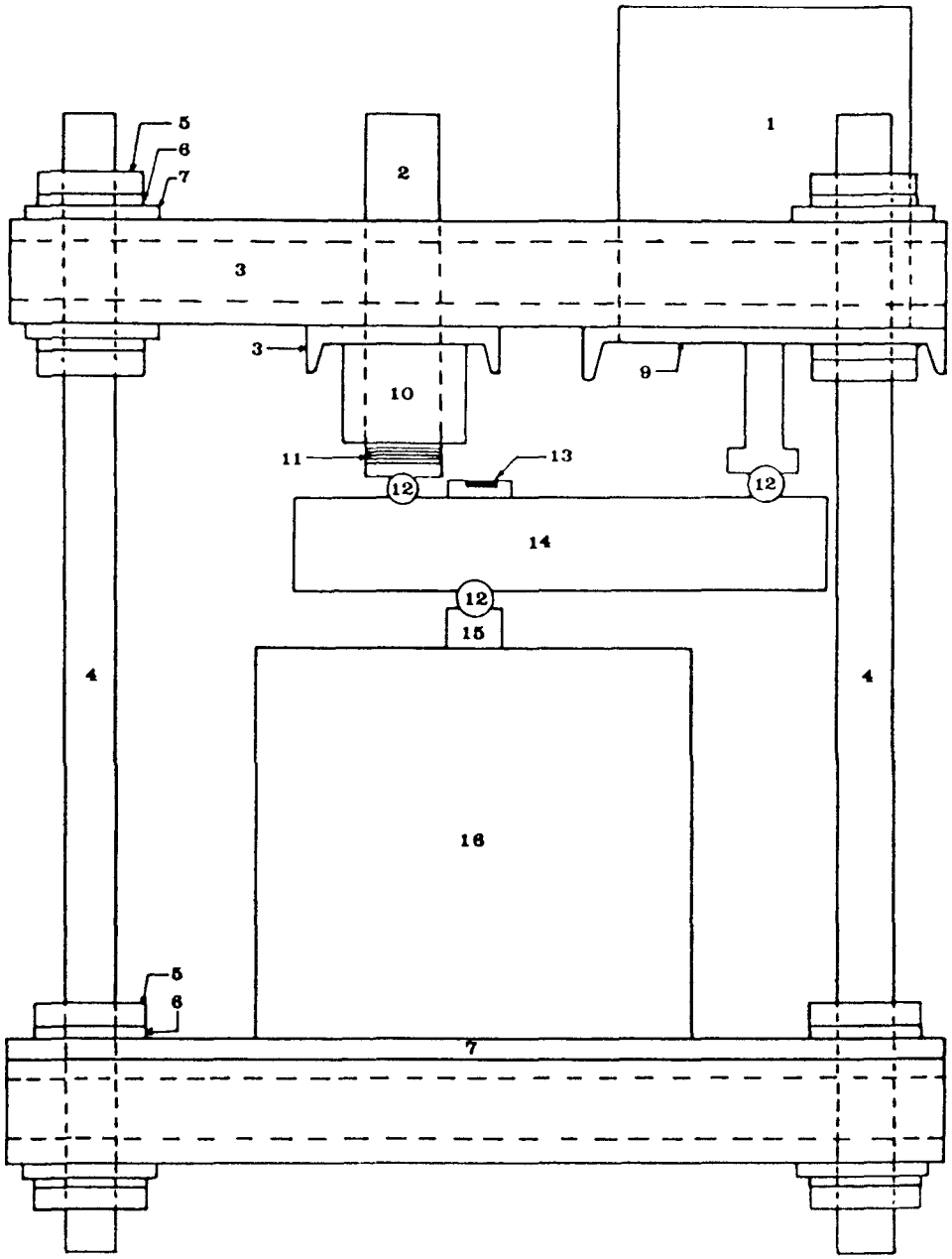

Side View

Fig. 5.3 Load frame for model concrete piers.

for small model steel piers and large model concrete piers respectively.

For small model steel piers, the ram-load was directly applied to the top of the test pier. However, for large model concrete piers the ram-load was applied through a lever with a lever-arm rati of 1 : 6. The load on the pier was, therefore, six times the load on the ram.

5.3 STEEL PIERS IN PSEUDO-ROCK

5.3.1 General

Two steel piers were tested. These steel piers were made out of 31.7 mm (1.25 in) diameter mild steel cold rolled bars. The bars were prestressed before machining to the desired size and shape. The final size of the completed piers was 25.4 mm (1.0 in) diameter by 177.8 mm (7.0 in) long. Typical details of the steel piers are shown in Fig. 5.4.

5.3.2 Fabrication

The major steps in the fabrication of the model steel piers were:

1) The surface of the two halves were roughened by twenty small grooves, 2.54 mm (0.1 in) deep and 0.33 mm (0.013 in) wide, equally spaced in bottom 101.6 mm (4.0 in) of length of each piers.

2) A channel, 9.53 mm (0.375 in) wide and 3.81 mm (0.15 in) deep, was milled inside each half-pier. This channel provided room for the installation of the electrical resistance strain

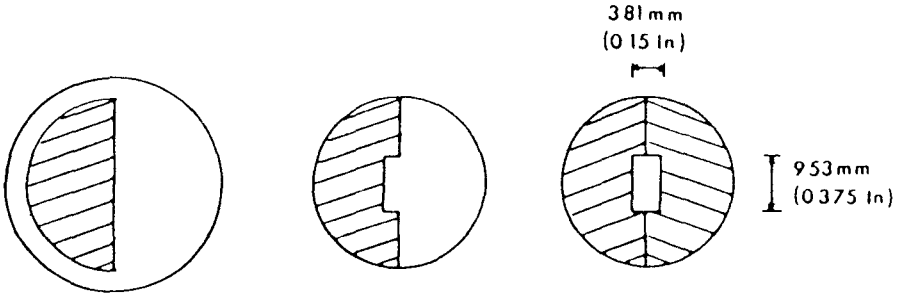

a) Stages of Machining

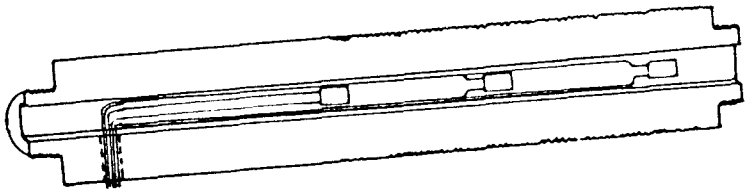

b) Electrical Resistance Strain Gauges in Channel

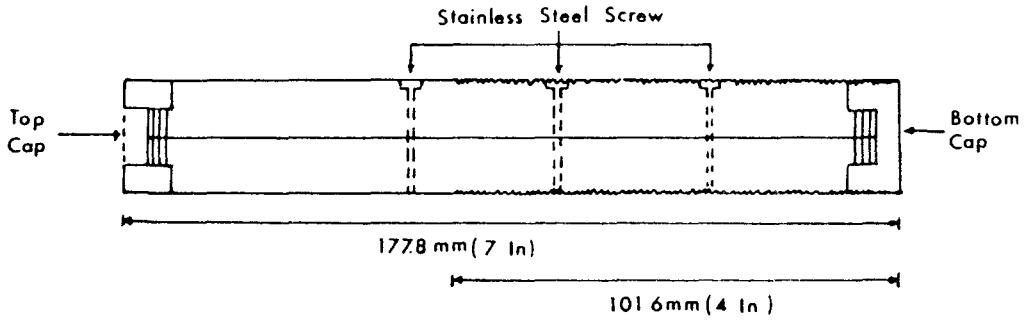

c) Assembled Steel Pier

Fig. 5.4 Typical details of steel model pier.

gauges and connection wires.

3) Each pier was Cadmium Plated so as to protect the piers from rusting.

4) Three 10 mm (0.393 in) long electrical resistance strain gauges were bonded inside the channel of each pier. The electrical resistance strain gauges were installed on each side of the pier at the same height and were protected from moisture by using a rubber coating. Further protection was provided by filling up the channel with silicone vacuum grease.

5) The two halves of the pier were secured using three stainless steel screws placed equal distances apart. The top and bottom sides of the steel piers were provided with cadmium plated steel caps.

6) The assembled piers were placed on a loading frame. The electrical resistance strain gauges were checked and the piers were calibrated for load.

5.3.3 Instrumentation

5.3.3.1 Load Transfer Measurements

Electrical resistance strain gauges were used to determine load transfer along the pier length. A strain box was used to record the strain gauge readings (Plate 5.2).

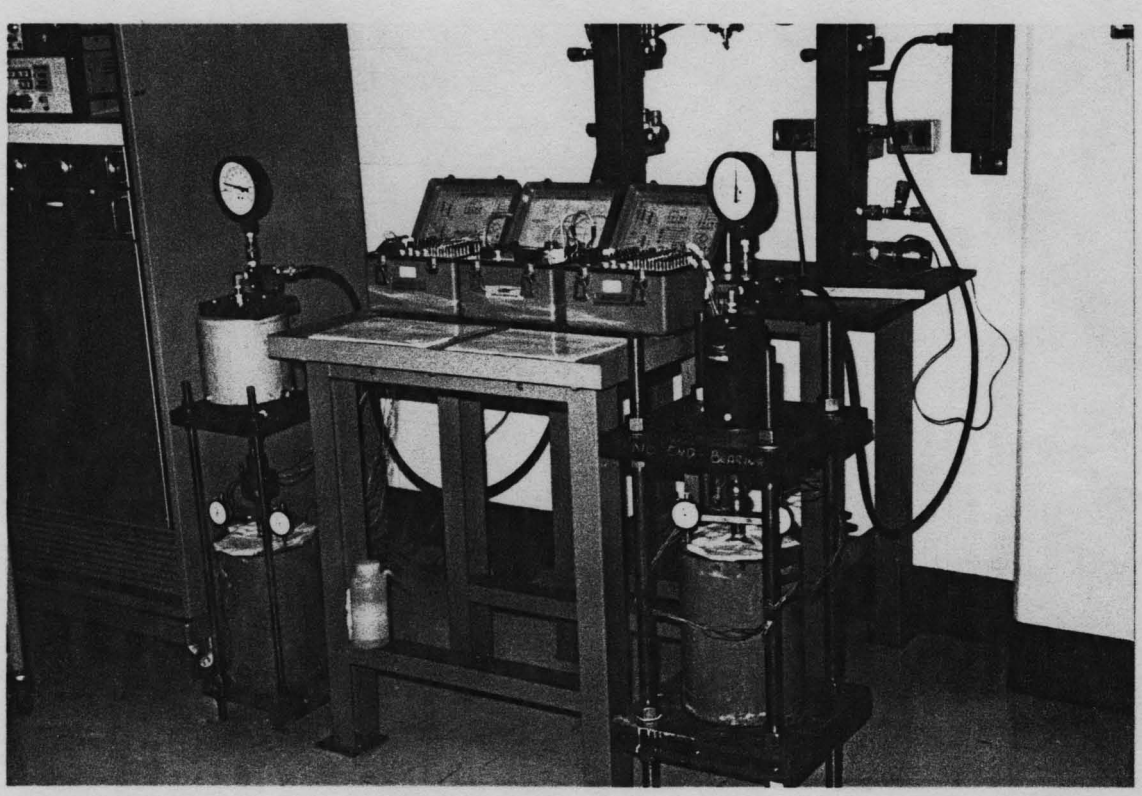

Plate 5.2 View of typical instrumentation arrangement for measuring device and load frame.

5.3.3.2 Displacement Measurements

Two dial indicator gauges, 0.00254 mm (0.0001 in) to 50.8 mm (2.0 in), placed diametrically opposite were used to measure the vertical displacement at the top of the test piers (plate 5.2). The dial indicator gauge shafts were glued to the top of the confining steel pipe by epoxy so as to avoid any disturbance due to slipping ets., during the testing time.

5.3.4 Installation

The major steps followed for the installation of small model steel piers were:

1) The steel pier was centered and held in proper position with the help of a specially designed removable template inside a steel pipe, 225.0 mm (8.86 in) diameter by 305.0 mm (12.0 in) height. The steel pipe was 3.2 mm (0.125 in) thickness.

2) The pseudo-rock concrete materials were poured into the pipe. The model steel pier tested had an embedment length of 101.6 mm (4.0 in). This embedment length gave a L_s/D ratio of 4.0. The model steel pier with shaft resistance only, SP-SL(0.033), a 25.4 mm (1.0 in) thick waxed styrofoam plug was fastened to the base of pier to essentially eliminate end-bearing (simulating a void at the pier base).

3) The pseudo-rock material in the steel pipe with the pier held in position was kept for 9 days in a curing room. The curing

room was kept at 100 % humidity and at 23^{o}C during the curing period.

4) After the curing period was over, the model was taken out from the curing room and was placed on the loading frame. The model was kept in the laboratory room for 3 days so that it could reach the laboratory room temperature of 22 ^{o}C± 0.5. Moist burlap was used to protect the concrete from moisture changes.

5) At the end of second day the template used to hold the steel pier was removed.

5.3.5 Testing Procedure

5.3.5.1 General

After the measuring instruments were installed and checked, the small model steel piers were ready for testing. The axial load on the test pier was applied by using the Bellofram Air Cylinders.

5.3.5.2 Steel Pier with Shaft Resistance Only (Void at the Base)

The test pier was loaded incrementally, similar to the method used by Horvath (1982). Each load increment was applied until the total load on the pier reached 2.22 kN (500.0 lb). This load of 2.22 kN (500.0 lb) was held constant for a period of 26 days.

After the end of 26 days, the test pier was subjected to further incremental load until the total load on the test reached 4.45 kN

(1,000.0 lb). This load 4.45 kN (1,000.0 lb) was kept constant for a period of 14 days.

At the end of above stage of loading, the test pier was further loaded in steps until the total load on the pier reached 5.34 kN (1,200.0 lb). This load was held constant for 180 days.

At the end of this period, the load was released and the model was removed from the load frame and was placed on a higher capacity load frame. The small model steel pier was reloaded in steps of 0.445 kN (100.0 lb) which were kept constant for 2 days after which a further load increment was added. The test pier exhibited large deformations when the total load was 10.23 kN (2,300.0 lb) and the test was terminated.

5.3.5.3 Steel Pier with Combined Shaft and End-Bearing Resistance

The model steel pier with combined shaft and end-bearing resistance, SP-CL(0.033), was tested up to 5.34 kN (1,200.0 lb) which was held constant for a period of 180 days.

After this period of loading, the test pier was loaded in steps of 0.455 kN (100.0 lb) which were applied every 48 hours. The total applied load was 10.23 kN (2,300.0 lb) and the test pier did not exhibit any tendency towards failure. This was reasonable because the test pier had both shaft and end-bearing resistance.

The test was terminated at the load frame capacity of 15.6 kn (3,500.0 lb).

The strain gauges and dial indicator gauges readings were recorded at all stages of loading for both the test piers.

5.4 CONCRETE PIERS IN WEAK ROCK

5.4.1 General

A total of seven large model concrete piers were tested. These piers were tested under two different support conditions:

1) Shaft resistance only (void at the base).
2) Combined shaft and end-bearing resistance (load cell at the base).

Three of these piers were designed as conventional model socketed piers and had relatively smooth socket wall (RF = 0.025). The remaining four piers were roughened by grooving (RF = 0.081 and 0.303).

The nominal pier dimensions were: diameter, D, 76.2 mm (3.0 in) and socket length, L_s, 152.4 mm (6.0 in). The socket length-diameter ratio (L_s/D) was equal to 2.0.

The details of the piers are shown in Figs. 5.5 and 5.6 and Table 5.2.

5.4.2 Construction

Each pier was constructed individualy so that the concrete was placed on same day that the socket shaft was drilled into the weak rock. The major steps for the construction of the large model concrete

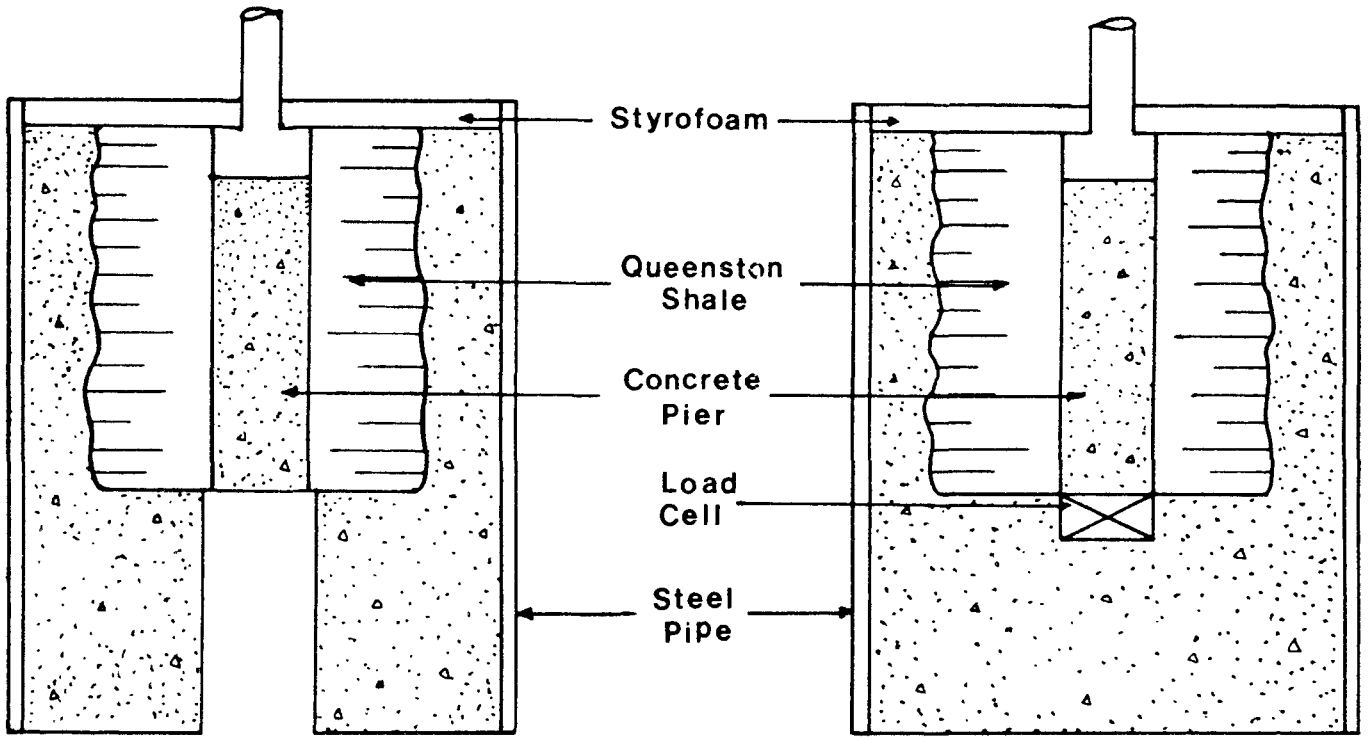

a) Shaft Resistance Only (Void at the Base).

b) Combined Shaft and End-Bearing Resistance (Load Cell at the Base).

Fig. 5.5 Conventional concrete model socketed piers.

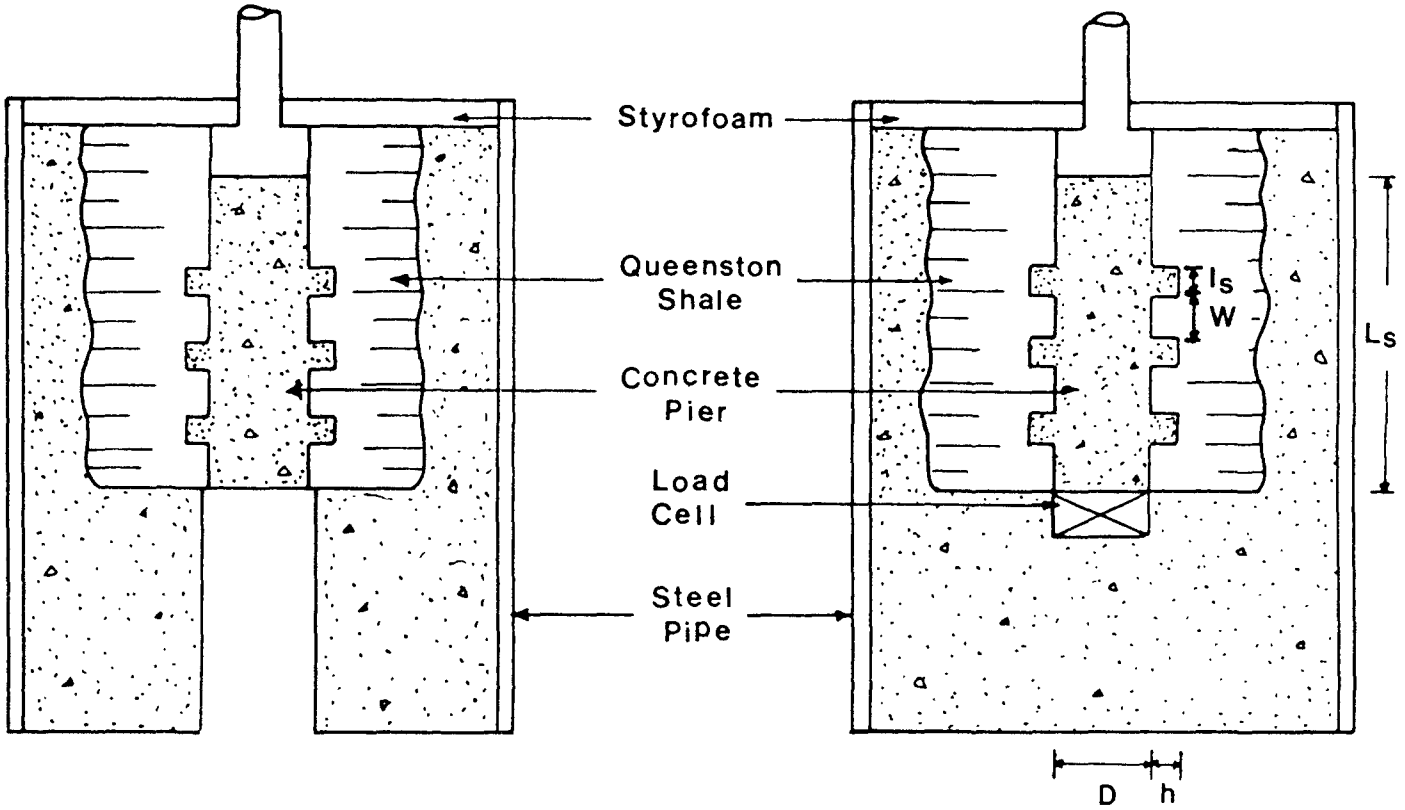

a) Shaft Resistance Only (Void at the Base).

b) Combined Shaft and End-Bearing Resistance (Load Cell at the Base).

Fig. 5.6 Grooved concrete model socketed piers.

TABLE 5.2 DETAILS OF GROOVED SOCKET PIERS.

Test Pier	CW-SL(0.081)	CW-SL(0.303)	CW-CL(0.303)
Roughness Factor (RF)	0.081	0.303	0.303
Socket Diameter, D (mm)	76.2 (3.0)	76.2 (3.0)	76.2 (3.0)
Socket Length, L_s (mm)	152.4 (6.0)	152.4 (6.0)	152.4 (6.0)
$L_{s/D}$	2.0	2.0	2.0
Step Width, w (mm)	29.46 (1.16)	29.46 (1.16)	29.46 (1.16)
Groove Depth, h (mm)	2.79 (0.11)	8.64 (0.34)	8.64 (0.34)
Groove Length, l_s (mm)	17.78 (0.70)	17.78 (0.70)	17.78 (0.70)

* Dimensions in inches in brackets

piers were:

1) Large block samples of the weak rock (Queenston Shale) were collected in National Sewer Pipe quarry in Burlington, Ontario. These samples were trimmed using a diamond saw to blocks of 254.0 mm (10.0 in) long x 254.0 mm (10.0 in) wide x 229.0 mm (9.0 in) deep.

2) These block samples of weak rock were placed into a steel pipe, 356.0 mm (14.0 in) diameter x 406.0 mm (16.0 in) deep x 6.4 mm (0.25 in) thick. Concrete was then poured so as to fill the space in the between the steel pipe and the weak rock. The concrete was poured and vibrated up to the top of the weak rock sample.

3) The steel pipe with the concrete and weak rock was kept inside the curing room for seven days.

4) At the end of seven days curing period, the model was brought outside and the pier socket was drilled using a 76.2 mm (3.0 in) diameter thin-walled diamond coring bit. For grooved piers, grooving of the socket wall was made with special "Ankerbonder" tool by Allen-Fyfe Equipment Limited of Toronto.

5) For piers with void at the base, a paper-board tube, 101.6 mm (4.0 in) in outside diameter by 203.0 mm (8.0 in) length was placed under the socket and concrete was poured around it and let cure for three days. For piers with a end-bearing

support, a FREYSSI Flat Jack Load Cell unit was placed in position at the base of the socket. The concrete was then poured around it and let cure for three days.

6) The concrete was then poured into the rock socket and vi-rated and let cure for eleven days. The curing room maintained at constant temperature 23 ^{o}C and 100 % humidity for all curing period.

7) After curing, the model was removed from curing room and was placed on the loading frame. The model was kept in the laboratory room for three days so that it could come to the laboratory room temperature of 22 ^{o}C ± 0.5. For piers with void at the base, the paper-board tubes installed below the piers were removed before placing the models on the load frame.

8) A mild steel bar, 38.0 mm (1.5 in) diameter x 50.8 mm (2.0 in) thickness, was placed on the top of the pier. The vertical side of the steel plate was smeared with vacuum grease to reduce friction. This mild steel bar was used to act as a column to transmit the applied load on the test pier and also to hold the dial indicator gauges and Linear Variable Displacement Transducers (LVDT) for recording the displacement.

5.4.3 Instrumentation

5.4.3.1 General

Suitable equipments were selected to determine the load response

behaviour of the model concrete piers. Measurements of vertical displacements and the load transfer to the test pier base were consider to be a major importance for the present study.

5.4.3.2 Displacement Measurements

Vertical displacements at the top of test piers were measured using a set of two dial indicator gauges and a set of two Linear Variable Displacement Transducers. The dial indicator gauges and LVDT's were attached to the loading column and positioned at equal spacing the circumference of the shaft. The arrangement of the measuring devices is shown in Fig. 5.7.

The dial indicator gauges had a travel of 50.8 mm (2.0 in) and a accuracy of 0.00254 mm (0.0001 in).

The LVDT's ranges and accuracey are shown in Table 5.3.

For test pier with shaft resistance only, CW-SL(0.081), the vertical displacement at the tip was emasured using a LVDT positioned as shown in Fig. 5.7.

All dial indicator gauges and LVDT's core rods were glued to the top of the confining steel pipe or glued to the bottom of test pier by epoxy so as to avoid any disturbance due to slipping etc. during the long period of testing time.

A digital voltmeter, HP 3480A, and HP DC range unit (100 mV - 1000 V), HP 3482A, connected to the LVDT through a switch box was used

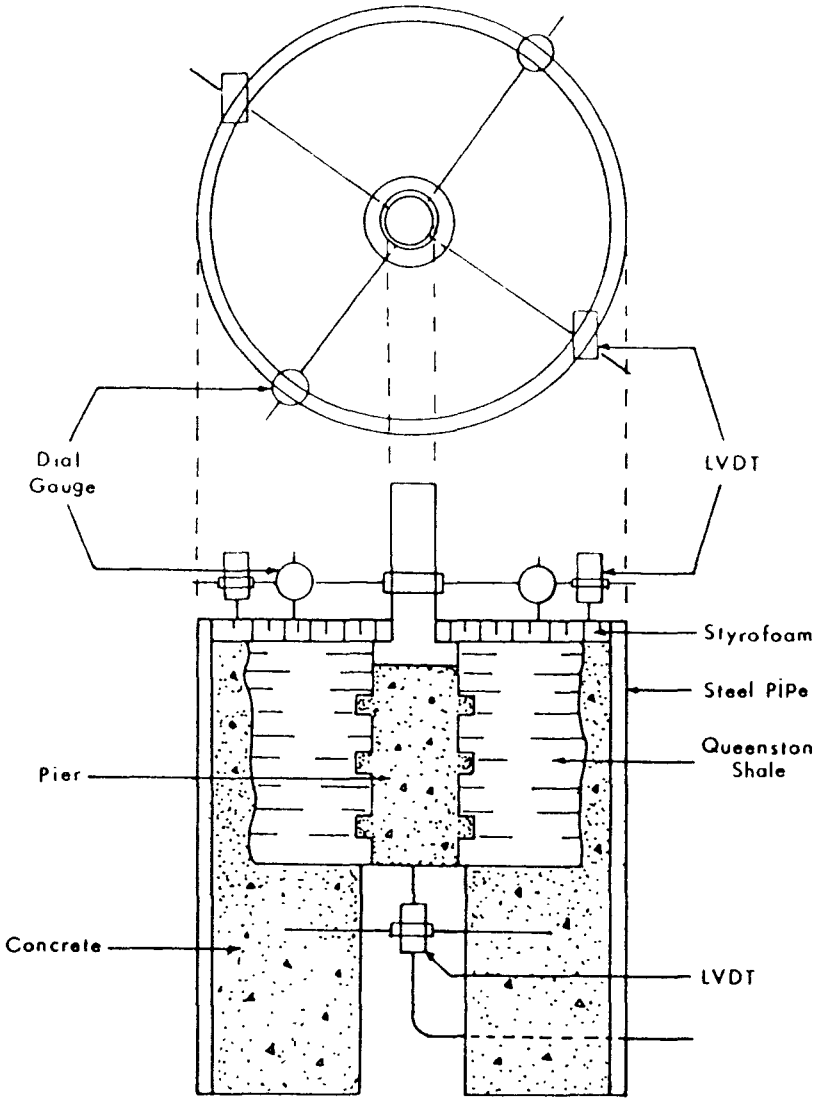

Fig. 5.7 Typical arrangement of the measuring devices.

TABLE 5.3 DISPLACEMENT RANGES AND ACCURACY OF L.V.D.T.

Model	Displacement Range Full Scale (in)	Maximum Non-Linearity (% of full scale)
7DCDT-050	0.05	±0.5
7DCDT-100	0.10	±0.5
7DCDT-250	0.25	±0.5
7DCDT-1000	1.00	±0.5
24DCDT-050	0.05	±0.5

to record the vertical displacement at the top of the test piers.

5.4.3.3 Base Load Measurements

For piers with end-bearing support, the loads transferred to the base of the piers were measured by means of a load cell unit. Each of these load cell unit consisted of a FREYSSI Flat Jack and four steel bearing plates. The flat jacks had a capacity of 20.0 kN (4,496.0 lb) and were capable of expanding to a maximum opening of 16.0 mm (0.63 in). The essential details of the flat jacks and load cell unit are shown in Fig. 5.8 and 5.9.

A set of one Budenberg pressure gauge (0 - 1.17 kPa (170.0 psi)) and one Marsh pressure gauge (0 - 13,790.0 kPa (2,000.0 psi)) was used to measure the applied load transferred to the test pier base. The schematic arrangement of measuring system is shown in Fig. 5.10.

These pressure gauges were found to be not very effective and were replaced with two pressure transducers (0 - 6,895.0 kPa (1,000.0 psi)).

5.4.4 Testing Procedure

As in small model steel piers, a constant rate of loading was used for the test. Load increments of 112.4 N (500.0 lb) were applied at 15 minute intervals. Each load increment was maintained for 15 minutes and then next load increment was added.

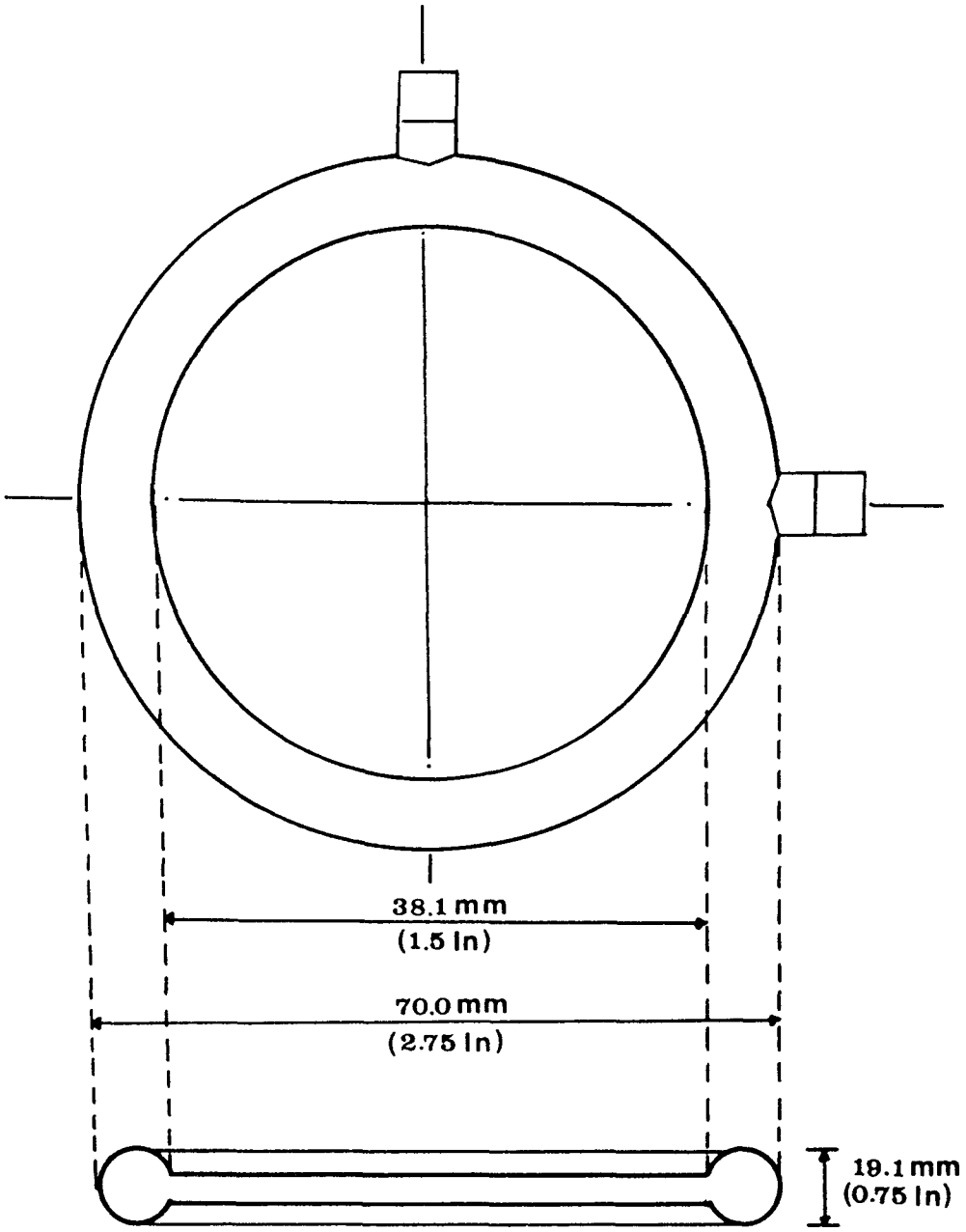

Fig. 5.8 Details of FRESSI flat jack.

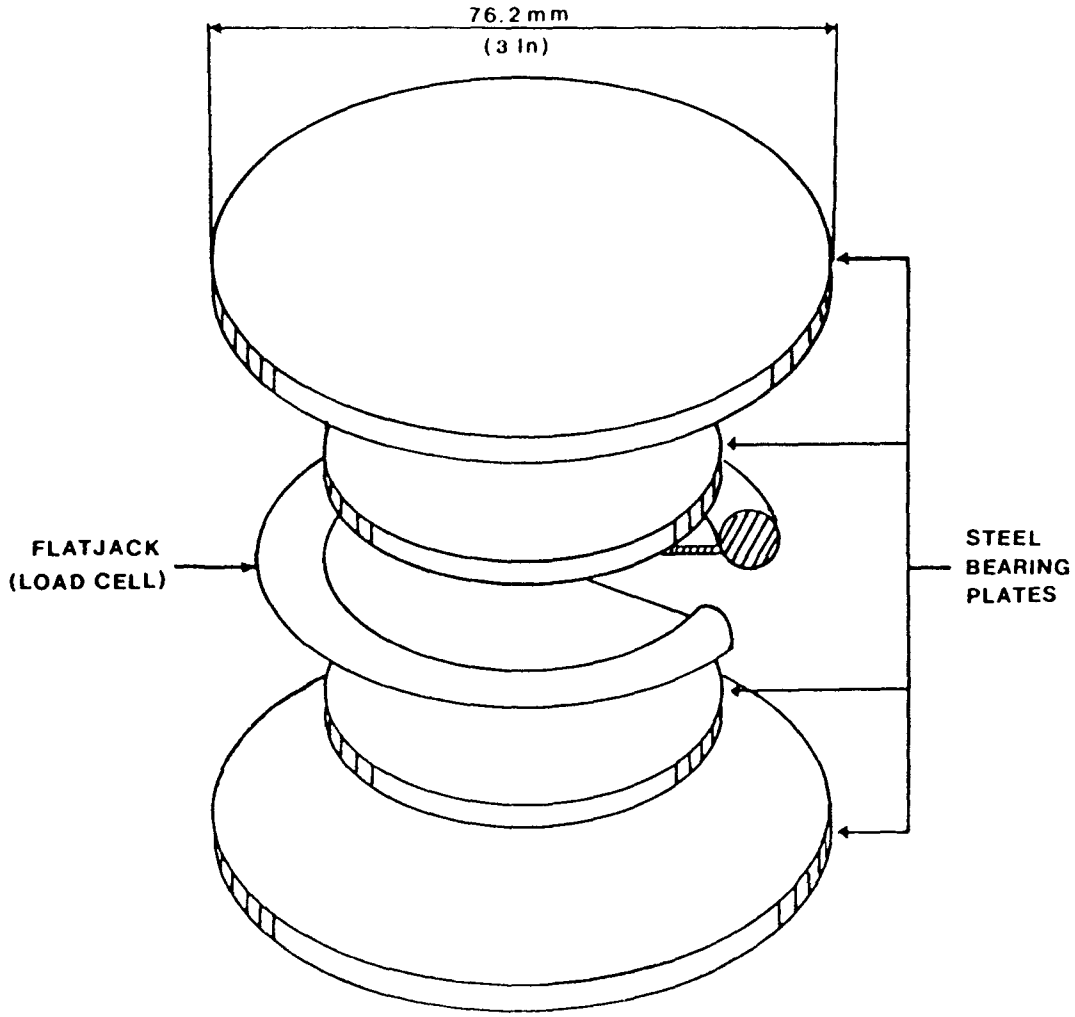

Fig. 5.9 Base load cell unit.

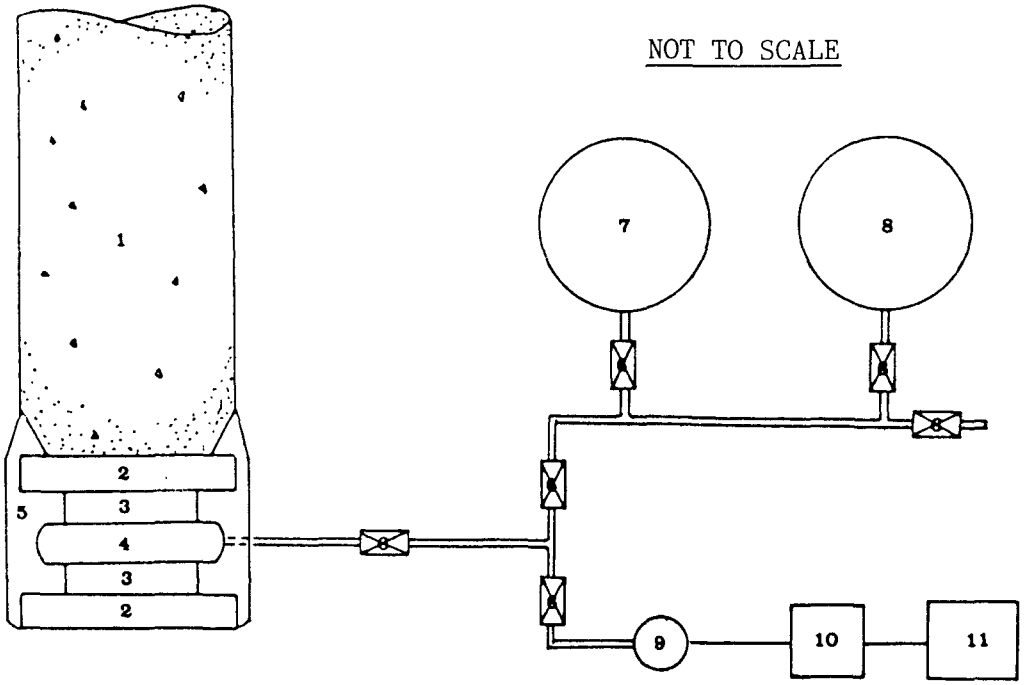

1) Concrete Pier 2&3) Steel Bearing Plate 4) Flat Jack (Load Cell)
5) Plasticine 6) Plug Valve 7) Low Pressure Reading Gauge
8) High Pressure Reading Gauge 9) Electrical Pressure Transducer
10) Regulate Power Supply 11) Digital Voltimeter

Fig. 5.10 Base load measuring system arrangement.

For short-term tests, the load increments were applied till the test piers failed by excessive vertical displacements.

For long-term tests, the test piers were subjected to a sustained loading after the desired level of loading was reached.

CHAPTER 6

SHORT-TERM TESTS ON MODEL PIERS: SHAFT RESISTANCE

6.1 GENERAL

Short-term testing is widely used in practice to estimate the ultimate load capacity of socketed piers. A total of four model piers were tested for the present study using short-term loading, in order to determine the appropriate load for the long-term testing. The second objective was to investigate where the model tests can be correlated with full-scale test results.

The relevent data from these test are presented in the following section of this Chapter.

6.2 METHOD OF CALCULATION

The average shaft resistance, q_s, of socket piers is usually calculated by:

$$(6.1) \quad q_s = \frac{Q_s}{A_s}$$

where Q_s is load supported by shaft resistance, and

A_s is surface area of socket pier (πDL_s).

For the present study, the load support by shaft resistance, Q_s, was measured directly for piers with shaft resistance only (void at the base), SP-SL(0.033) and CW-SS(0.025). For piers with combined shaft and end-bearing resistance, electrical resistance strain gauges and a load cell unit (Fig. 5.9) were used to determine the magnitude of load transferred to the base. The values of Q_s for these piers with support at the base were, therefore, calculated as per:

(6.2) $Q_s = Q_t - Q_b$

where Q_t is total applied load, and

Q_b is support by end-bearing resistance.

6.3 CONVENTIONAL PIERS

6.3.1 Steel Piers

Two model steel piers were designed as conventional piers, SP-SL (0.033) and SP-CL(0.033). In order to achieve a surface roughness equivalent to that of conventional piers, twenty small grooves, 0.33 mm (0.013 in) wide and 2.54 mm (0.1 in) deep, were made along the socket length.

A summary of the results for the steel piers are given in Table 6.1. The load-displacement behaviour of the two piers are shown in Figs. 6.1 and 6.2.

It can be seen from Figs. 6.1 and 6.2, that the test did not show a definite peak value of the load. The shaft resistance at failure,

TABLE 6.1 MEASURED VALUES OF SHAFT RESISTANCE FOR CONVENTIONAL MODEL STEEL PIERS.

Test Pier	D (mm)	L_s (mm)	L_s/D	RF	Displacement in $s_f/D \times 100$	Ave. Shaft Resistance At Failure q_{sf} (MPa)	Ave. Shaft Resistance At Maximum q_{sm} (MPa)	References
SP-SL(0.033)	25.4	101.6	4	0.033	0.53	1.21	1.31	This Study
SP-CL(0.033)	25.4	101.6	4	0.033	0.47	1.23	1.37	This Study

D = Socket Diameter L_s = Socket Length

RF = Roughness Factor s_f = Displacement at Failure

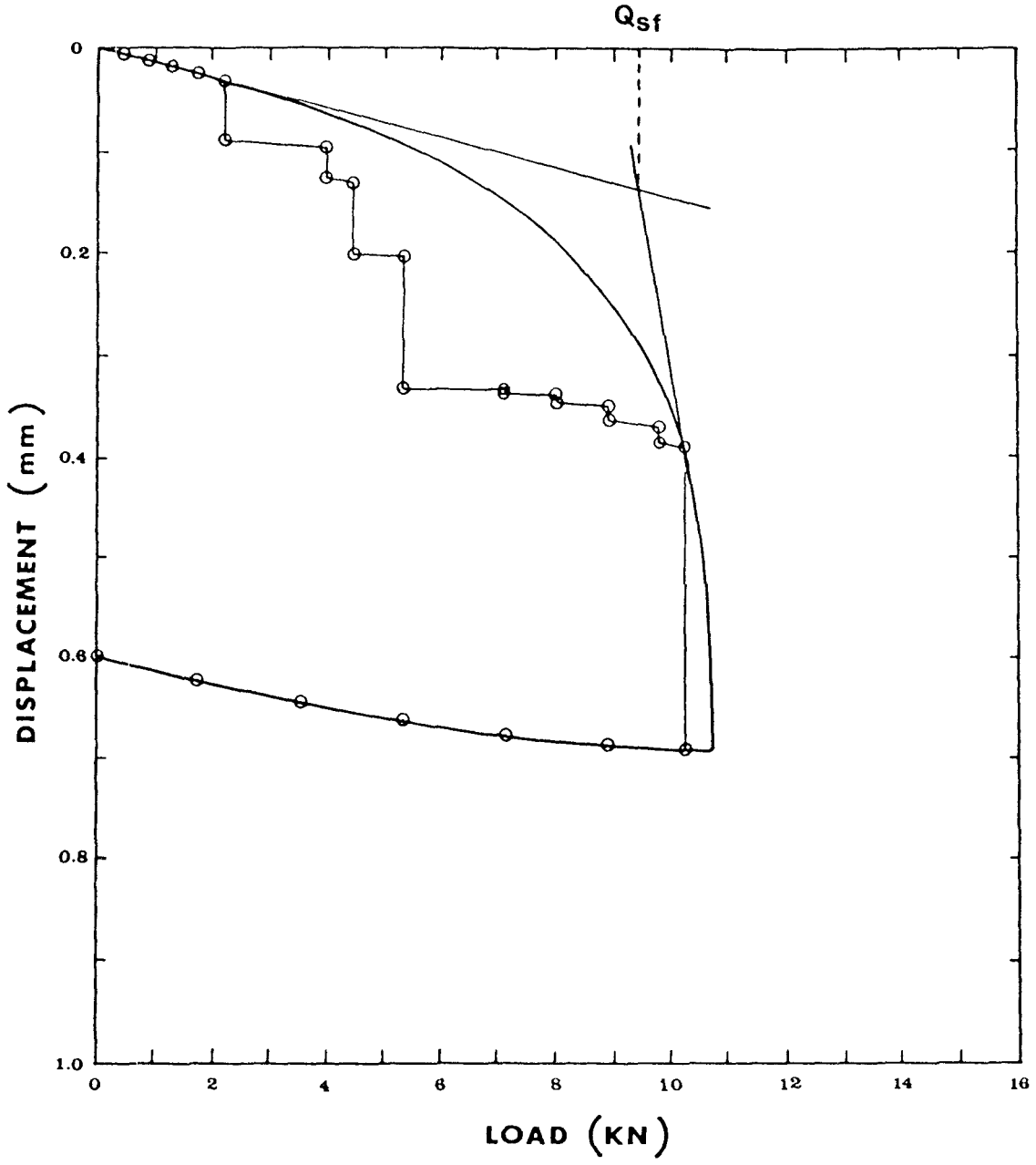

Fig. 6.1 Load-displacement behaviour for steel pier with shaft resistance only, SP-SL(0.033).

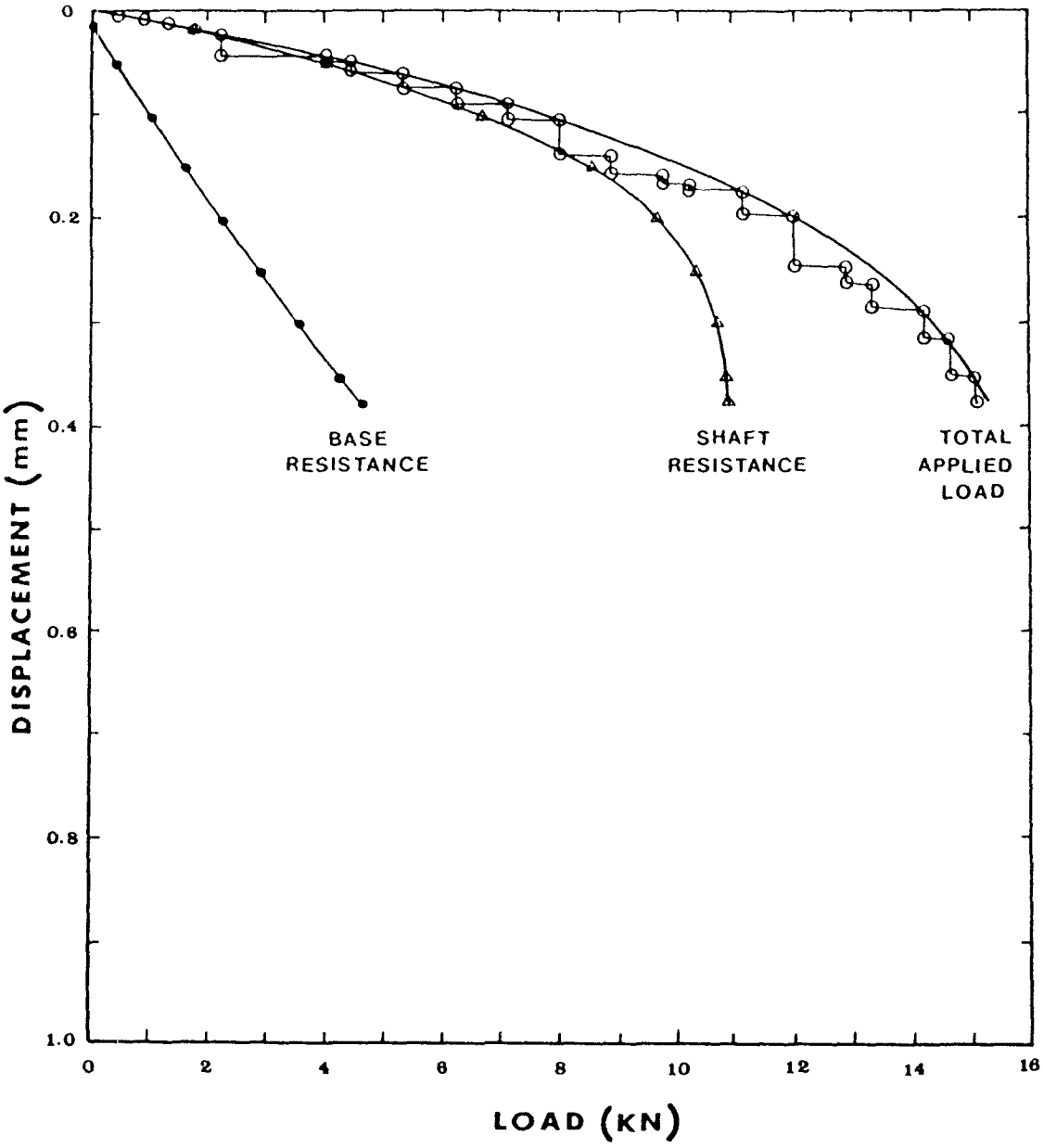

Fig. 6.2 Load-displacement behaviour for steel pier with combined shaft and end-bearing resistance, SP-CL(0.033).

q_{sf}, for this pier was, therefore, calculated on the basis of the load corresponding to the point of intersection of the two tangent line (Fig. 6.1). This method was based on recommendation by Butler and Hoy (1977), O'Neill and Reese (1970) and Sowers (1962).

It can be seen from Table 6.1 and Figs. 6.1 and 6.2, that the shaft resistance behaviour of the two piers was similar irrespective of the end conditions used in the tests. The pier with shaft resistance only, SP-SL(0.033), developed about the same shaft resistance as that by the pier with combined shaft and end-bearing resistance, SP-CL(0.033).

6.3.2 Concrete Pier

Only one concrete pier with shaft resistance only, CW-SS(0.025), was tested for short-term load. The pier socket wall was relatively smooth and had a roughness factor of 0.025. This test pier was used to estimate the appropriate design load for the long-term tests and also for the comparison with available data from full-scale tests.

The relevant data for this test are compared with available data from full-scale tests (Horvath 1982) in Table 6.2.

The load-displacement curve for the test pier is shown in Fig. 6.3.

It can be seen for Table 6.2, that the shaft resistance values for the small-scale model pier test results compared very well with the full-scale socketed piers.

TABLE 6.2 COMPARISON OF SHAFT RESISTANCE VALUE FOR CONVENTIONAL SOCKETED PIERS IN QUEENSTON SHALE.

Test Pier	D (mm)	L_s (mm)	L_s/D	RF	Displacement in $s_f/D \times 100$	Ave. Shaft Resistance At Failure q_{sf} (MPa)	Ave. Shaft Resistance At Maximum q_{sm} (MPa)	References
CW-SS(0.025)	76.2	160	2.10	0.025	0.29	1.10	1.40	This Study
P1	710	1370	1.93	0.036	0.73	1.11	1.54	Horvath (1982)
P2	710	1370	1.93	0.025	0.90	1.11	1.45	Horvath (1982)
P5	710	1370	1.93	0.039	0.89	1.09	1.37	Horvath (1982)

D = Socket Diameter L_s = Socket Length

RF = Roughness Factor s_f = Displacement at Failure

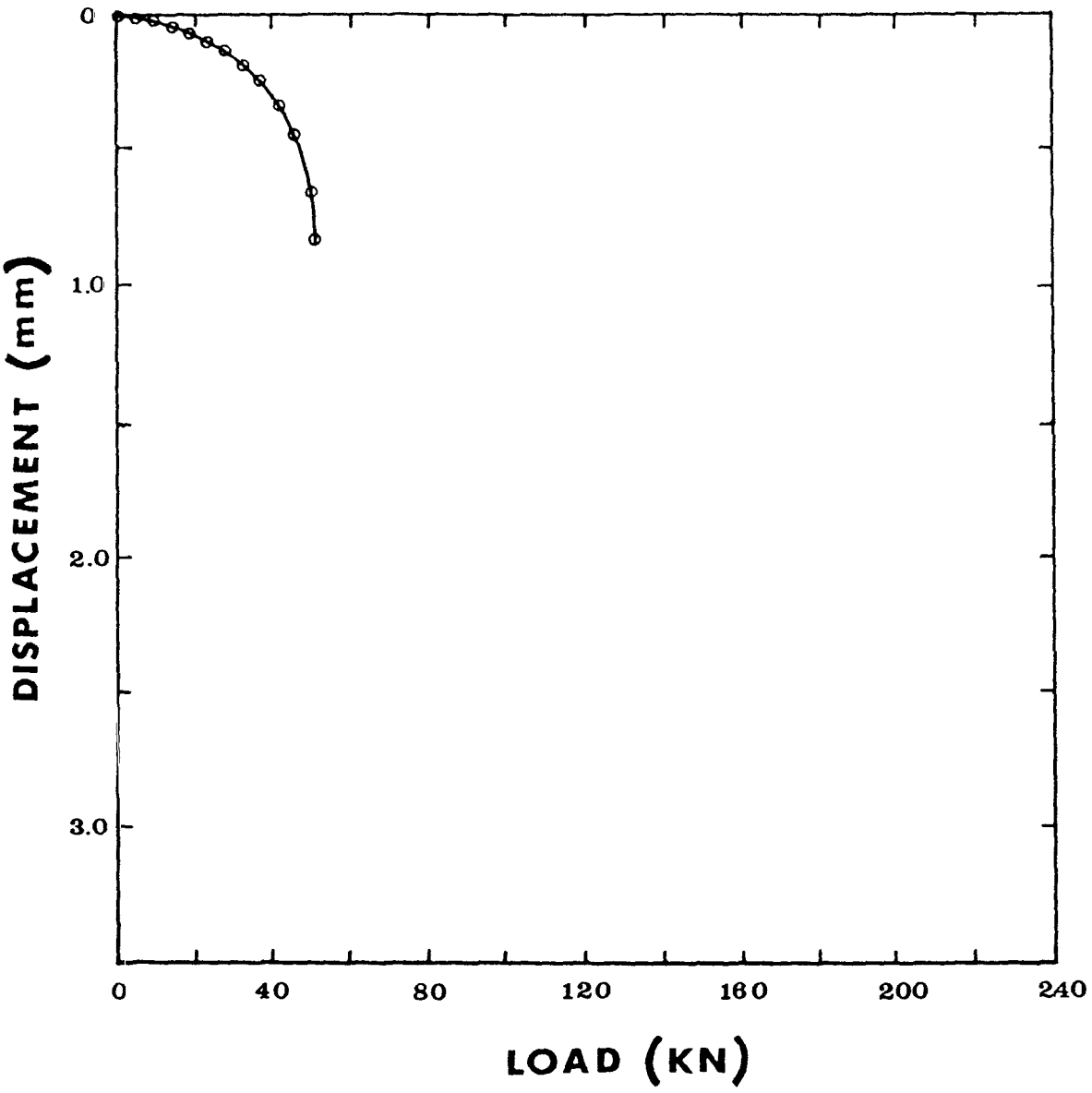

Fig. 6.3 Load-displacement behaviour for conventional concrete pier with shaft resistance only, CW-SS(0.025).

Regarding the magnitude of displacements, the field and model piers behaved differently. While the displacement at failure (reported as $S_f/_D$ x 100) occured at 0.73 % - 0.9 % for full-scale tests in field (Horvath 1982), the model pier for the present study showed failure at 0.29 % of the shaft diameter. Large variation (0.06 % - 1.21 %) of the displacement at failure loads for eleven full-scal piers have been reported by Williams (1980). Although the result of the present tests fall within the range reported by Williams (1980), the definite reasons for the differences between model test and the data from Horvath (1982) are not known. It is, however, believed that possible scale effects may have contributed to some extent. It must also be point out that the present tests were performed at controlled conditions in the laboratory and on carefully selected homogeneous block samples of shale. Furthermore, the samples were uniformly supported radially by the steel pipes during the course of testing program, whereas, the study by Horvath (1982) was on full-scale field tests on large diameter piers socketed into shale. The shale in-situ may have had clay seams, bedding planes, small pockets and other irregularities which were not present in the models.

6.4 GROOVED CONCRETE PIER

One grooved concrete pier with combined shaft and end-bearing resistance, CW-CS(0.303), was tested using short-term loading. The socket wall of this pier had three grooves, 8.64 mm (0.34 in) deep and 17.78 mm (0.7 in) wide.

The shaft resistance for the test pier was determined from the load test data by using equation 6.2. The values of shaft resistance obtained from the this study are compared with the available data from the full-scale test (Horvath 1982) in Table 6.3.

The load-displacement curves for the model test pier are shown in Fig. 6.4.

A comparison of Table 6.2 and 6.3, shows the grooved test pier required about 3 times more displacement than the conventional test pier for the full mobilization of the shaft resistance. The trend is reasonable as the grooved pier will have a larger shaft resistance capacity as compared to the conventional pier and will thus show less displacement at a particular load. When loaded to failure, conventional piers will attain full mobilization of the shaft resistance at a relatively smaller displacements as compared to the grooved piers.

Pells et al. (1980) reported peak failure (brittle behaviour) for the smooth socketed piers in sandstone. No such peak failures were observed for the model piers in this study (Fig. 6.3) and for the full-scale conventional piers in Queenston Shale (Horvath 1982). The brittle behaviour observed in case of sandstone (Pells et al. 1980) is believed to be due to very low Roughness Factor (RF $\leqq$ 0.015 compared against RF = 0.025 - 0.036 used in the present study and in Horvath's (1982) study) of the piers and the nature of the sandstone itself.

TABLE 6.3 COMPARISON OF SHAFT RESISTANCE VALUE FOR GROOVED SOCKETED PIERS IN QUEENSTON SHALE.

Test Pier	D (mm)	L_s (mm)	L_s/D	RF	Displacement in $s_f/D \times 100$	Ave. Shaft Resistance At Failure q_{sf} (MPa)	Ave. Shaft Resistance At Maximum q_{sm} (MPa)	Source
CW-CS(0.303)	76.2	152.4	2.0	0.303	0.85	3.53	3.90	This Study
P3	710	1370	1.93	0.076	2.0	2.0	2.11	Horvath (1982)
P6B	710	1370	1.93	0.1	1.55*	-	2.45*	Horvath (1982)

* Failure in shaft resistance not achived due to limiting capacity of the load frame.

D = Socket Diameter L_s = Socket Length

RF = Roughness Factor s_f = Displacement at Failure

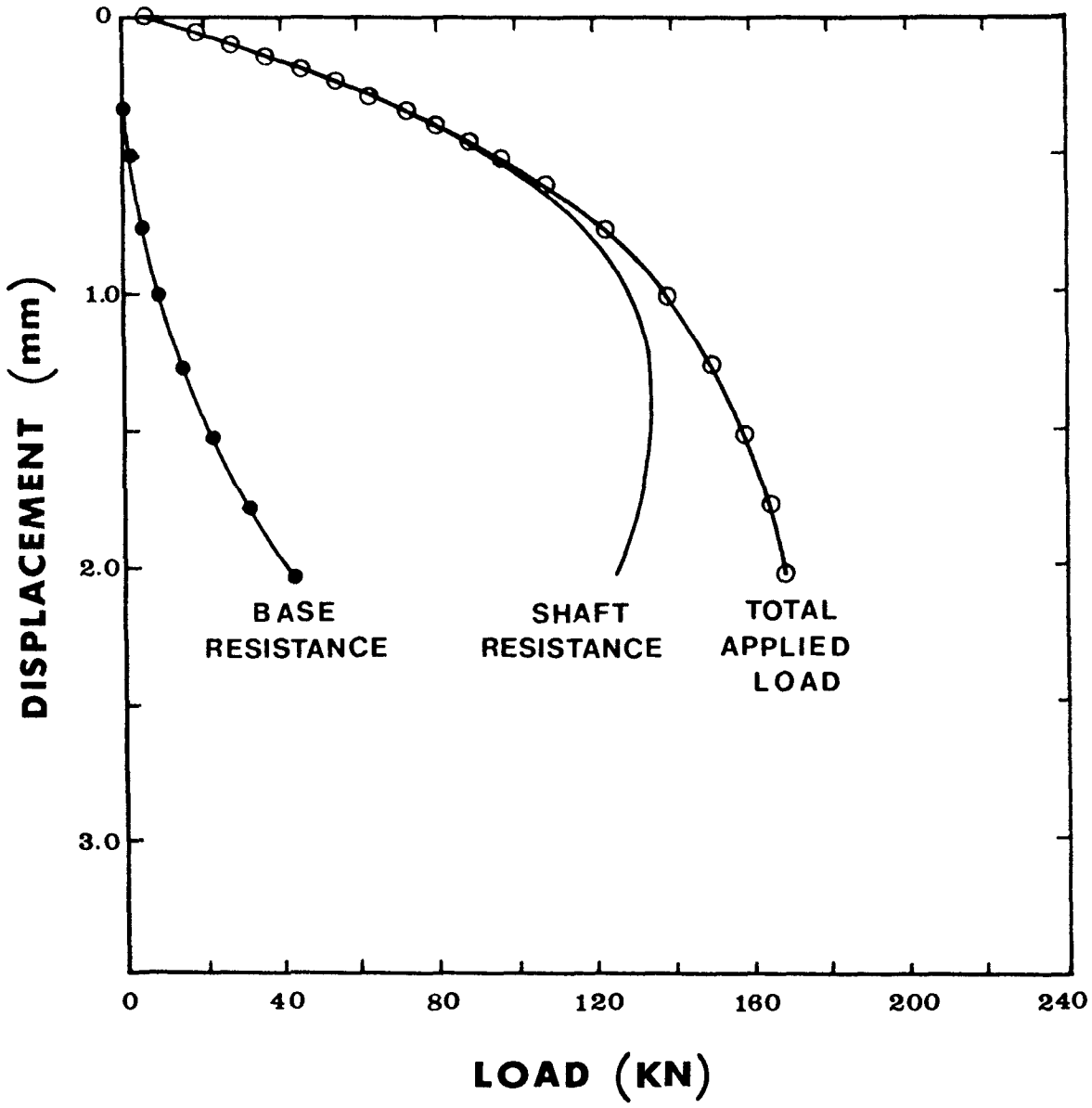

Fig. 6.4 Load-displacement behaviour for grooved concrete pier with combined shaft and end-bearing resistance, CW-CS(0.303).

6.5 COMPARISON OF CONVENTIONAL AND GROOVED PIERS

The shaft resistance behaviour of conventional concrete pier, CW-SS(0.025) and grooved concrete piers, CW-SL(0.081) and CW-SL(0.303), with shaft resistance only are compared in Fig. 6.5. Similarly the load-displacement behaviour of conventional concrete pier, CW-CL(0.025), and grooved concrete pier, CW-CL(0.303), with combined shaft and end-bearing resistance are compared in Fig. 6.6.

It can be seen from Figs. 6.5 and 6.6, that the piers with higher values of pier-rock interface roughness exhibited superior load-displacement behaviour.

The shaft resistance developed in case of the test pier with combined shaft and end-bearing resistance was determined indirectly by subtracting the load transferred to the base from the total applied load as per equation 6.2. It is interesting to note that the shaft resistance of the grooved concrete pier, CW-CS(0.303), was found to be 3.2 times the shaft resistance of the conventional concrete pier, CW-SS(0.025) and 2.9 times for the conventional steel piers, SP-SL(0.033) and SP-CL(0.033). Similar trends have been reported for full-scale socketed piers by Horvath (1982).

The value of shaft resistance for conventional and grooved piers of this study are summarized in Table 6.4.

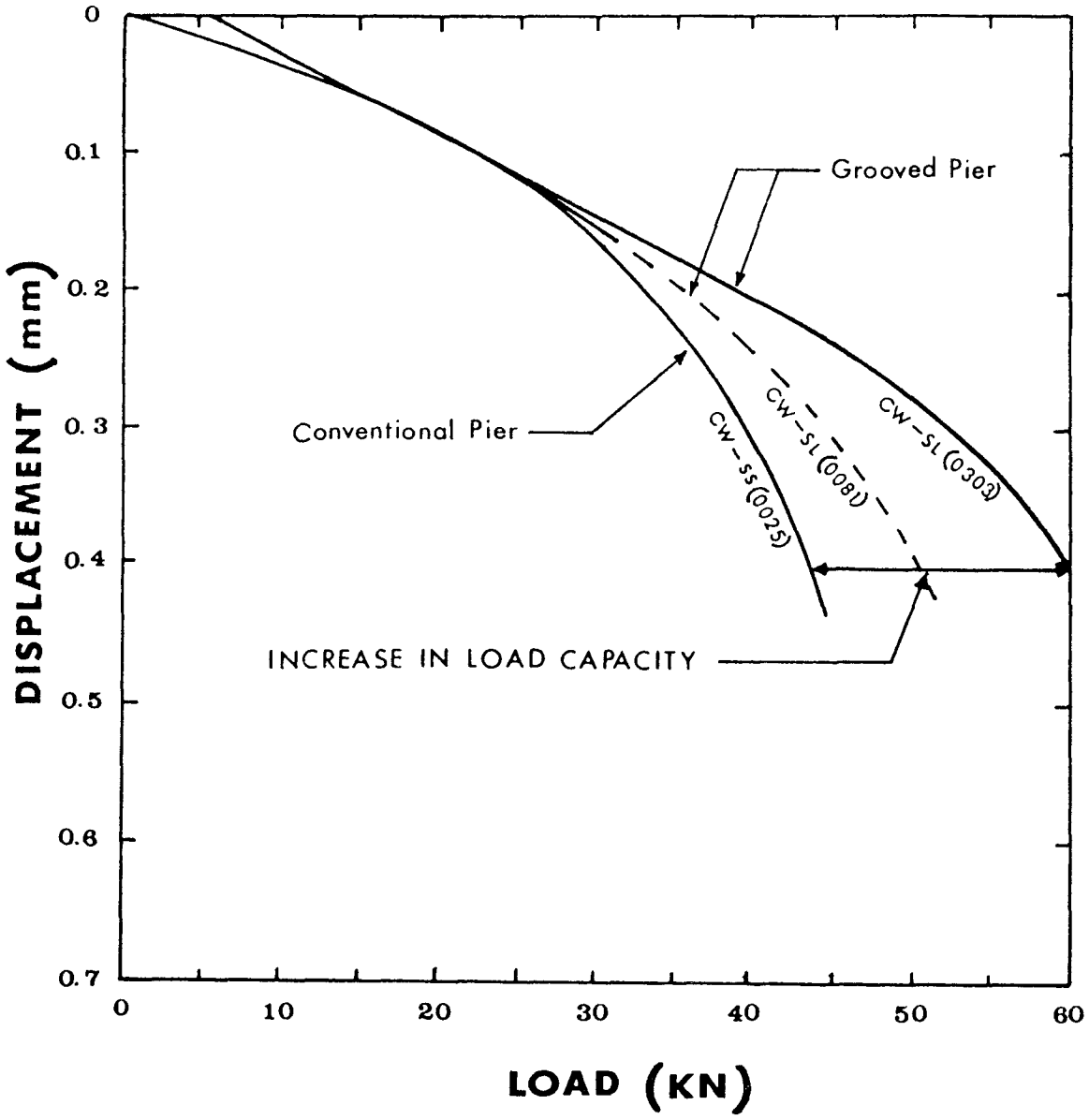

Fig. 6.5 Comparison of load-displacement behaviour of conventional and grooved piers with shaft resistance only.

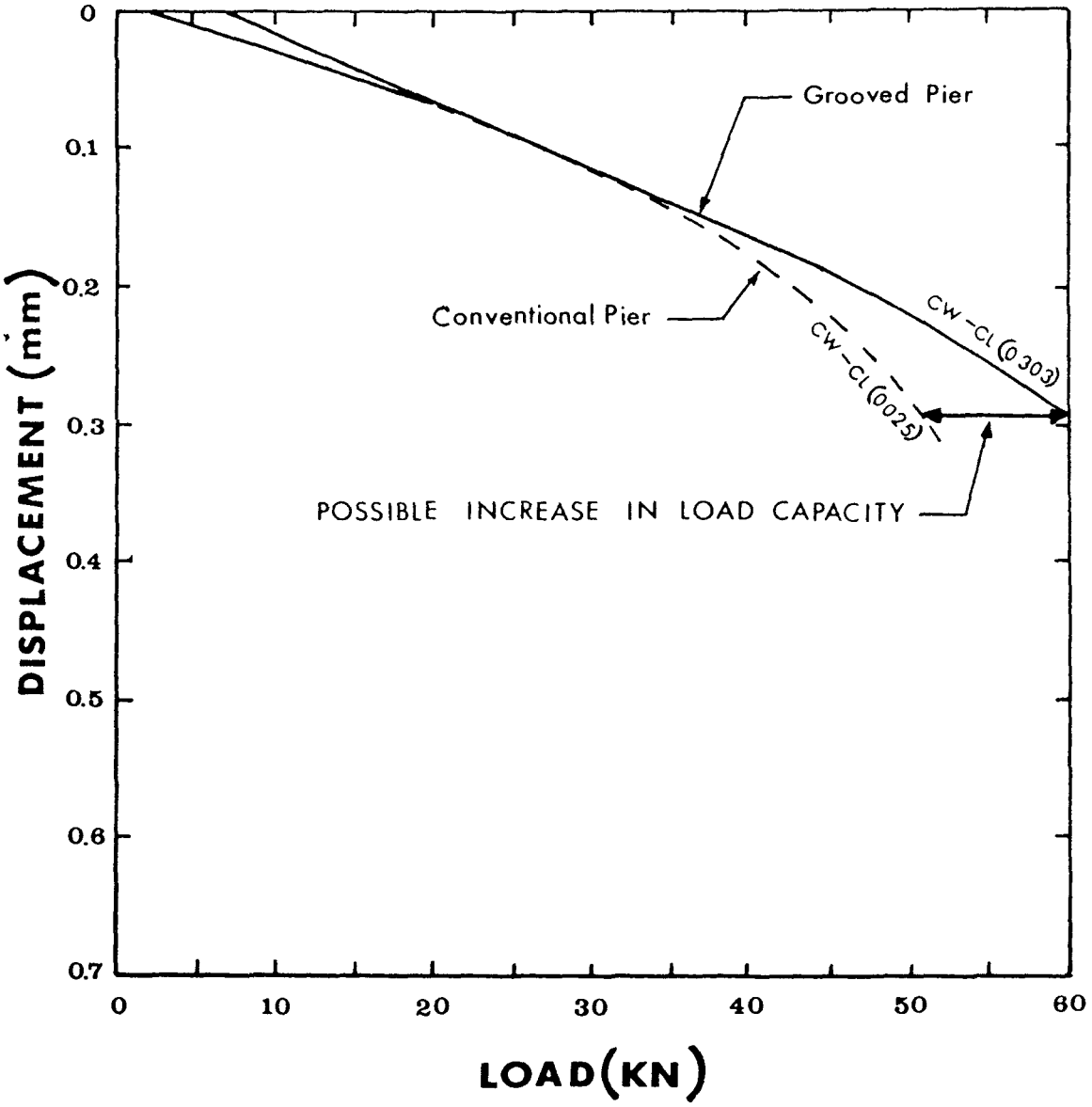

Fig. 6.6 Comparison of load-displacement behaviour of conventional and grooved piers with combined shaft and end-bearing resistance.

TABLE 6.4 COMPARISON OF SHAFT RESISTANCE VALUE FOR CONVENTIONAL AND GROOVED MODEL PIERS.

Socket Type	Pier Material	Test Pier	D (mm)	L_s (mm)	L_s/D	RF	Displacement in $s_f/D \times 100$	Ave. Shaft Resistance At Failure q_{sf} (MPa)	Ave. Shaft Resistance At Maximum q_{sm} (MPa)
Conventional	Steel	SP-SL(0.033)	25.4	101.6	4	0.033	0.53	1.21	1.31
		SP-CL(0.033)	25.4	101.6	4	0.033	0.47	1.23	1.37
	Concrete	CW-SS(0.025)	76.2	160.0	2.1	0.025	0.29	1.10	1.40
Grooved	Concrete	CW-CS(0.303)	76.2	160.0	2.0	0.303	0.85	3.53	3.90

D = Socket Diameter

L_s = Socket Length

RF = Roughness Factor

s_f = Displacement at Failure

6.6 COMPARISON WITH AVAILABLE RESULTS

6.6.1 Conventional Piers

For conventional piers, Horvath et al. (1983) presented a correlation between shaft resistance and the compressive strength of the weaker material (Fig. 6.7). It can be seen from Fig. 6.7, that the results of the present study are in excellent agreement with Horvath et al. (1983) findings. Since the data point of the present study lie around the 0.1 σ_{cw} line, it appears that bond failure is of major concern for these piers.

As mentioned before, the steel piers with Roughness Factor of 0.033 and concrete piers with Roughness Factor of 0.025 were used as conventional piers for the present study. The test results of these piers were compared against the correlation between the Roughness Factor (RF) and the normalized shaft resistance for grooved piers (Horvath et al. 1980; Horvath 1982) (Fig. 6.8). It can be seen from Fig. 6.8, that the present results agree very well with the findings of Horvath et al. (1980) and Horvath (1982).

6.6.2 Grooved Piers

It can be seen from Fig. 6.8, that the results of the model test on grooved piers also agree with the correlation proposed for grooved piers by Horvath et al. (1980) and Horvath (1982).

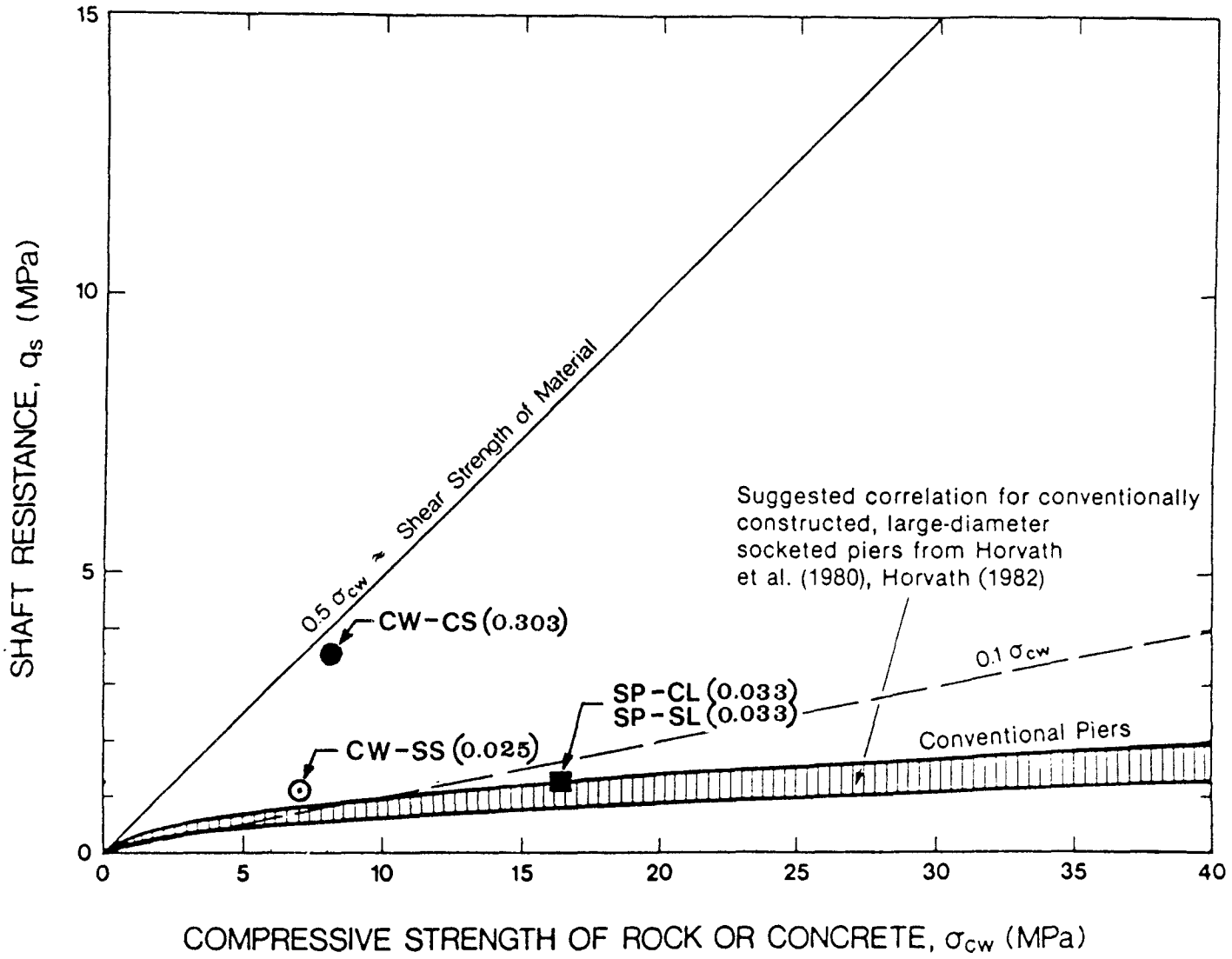

Fig. 6.7 Comparison of shaft resistance data for test piers with correlation for large diameter conventional piers (after Horvath et al. 1983).

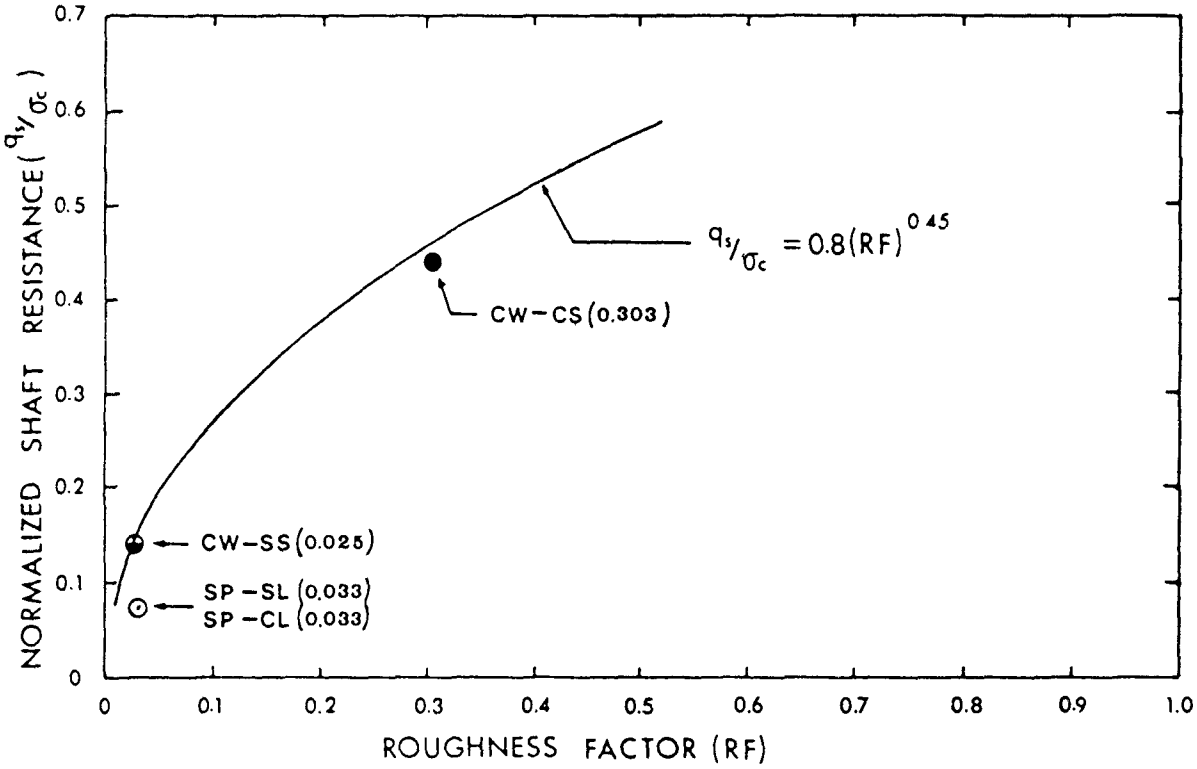

Fig. 6.8 Normalized shaft resistance versus roughness factor (after Horvath et al. 1980; Horvath 1982).

Only one grooved concrete pier with a Roughness Factor of 0.303 was tested for the present study. The shaft resistance value for this pier was calculated as per equation 6.2 and was plotted in Fig. 6.7. The fact that the data point lies just below the 0.5 σ_{cw} line indicates that the shear strength of the weaker material is the important factor controlling the behaviour of this pier.

After completion of the tests, the concrete piers were split into two halves (Plates 6.1 to 6.4). It can be seen from Plates 6.1 and 6.2, that the conventional pier, CW-SS(0.025), failed along pier-rock interface only. For the grooved pier, CW-CS(0.303), a shear plane in the zone adjacent to the grooves can be visibly seen (Plates 6.3 and 6.4).

Plate 6.1 Conventional concrete test pier, CW-SS(0.025), after load testing (cut-section).

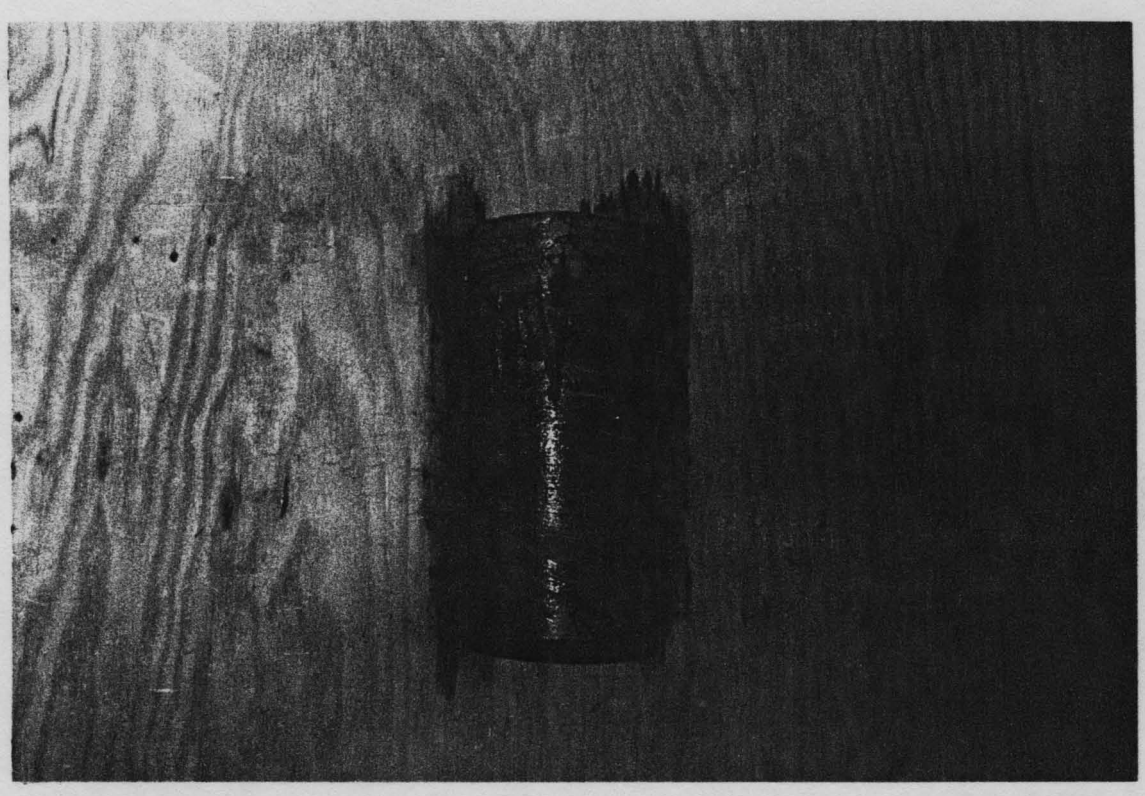

Plate 6.2 Conventional concrete test pier shaft, CW-SS(0.025), after load testing (cut-section).

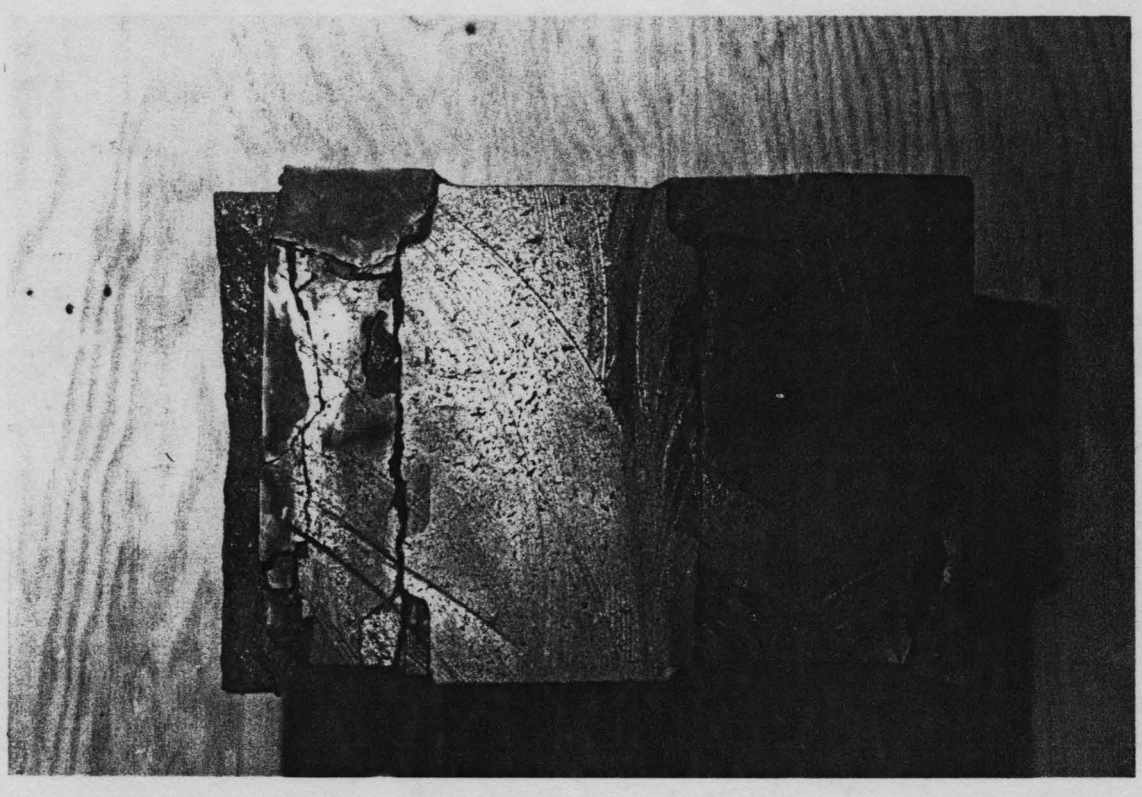

Plate 6.3 Grooved concrete test pier, CW-CS(0.303), after load testing (cut-section).

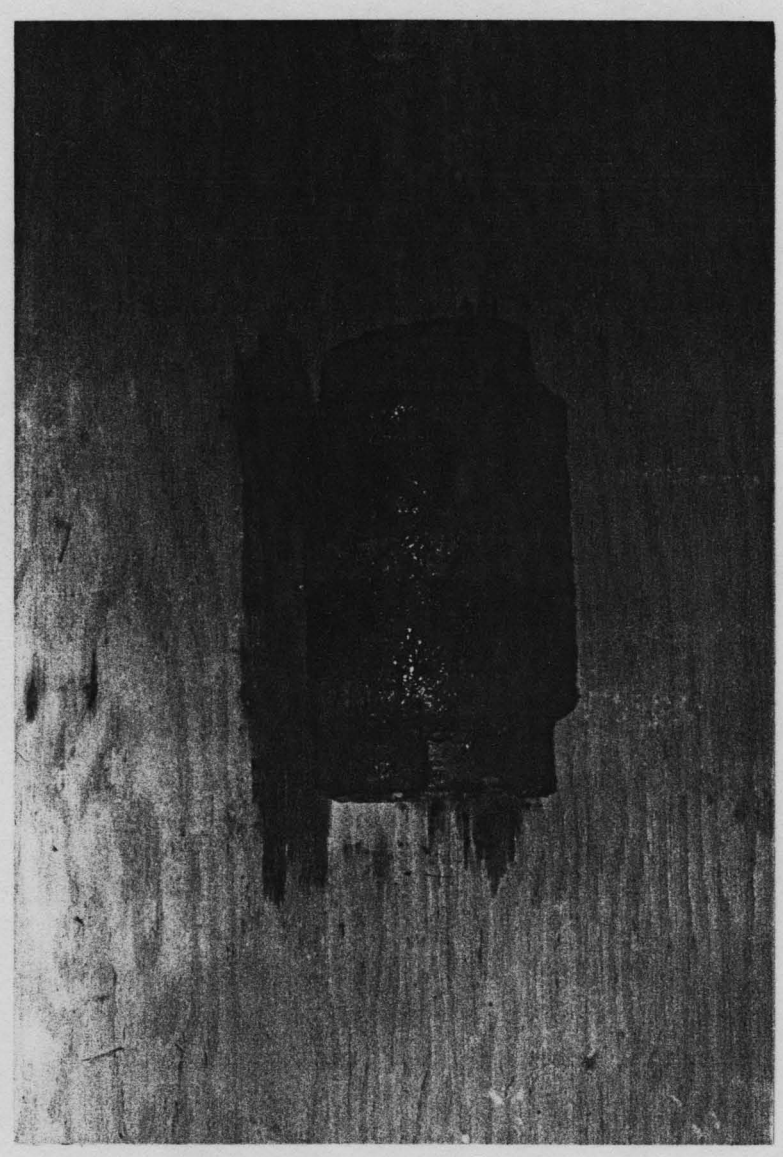

Plate 6.4 Grooved concrete test pier shaft, CW-CS(0.303), after load testing (cut-section).

CHAPTER 7

SHORT-TERM TESTS ON MODEL PIERS: LOAD TRANSFER

7.1 GENERAL

One steel pier, SP-CL(0.033), and one concrete pier, CW-CS(0.303), with combined shaft and end-bearing resistance and one steel pier with shaft resistance only, SP-SL(0.033), were tested using the short-term loading tests. Load transfer behaviour for these piers was monitored.

As shown in Fig. 5.4, the model steel piers were provided with electrical resistance strain gauges at three locations along the shaft length of the piers. The load distribution along the shaft length of the steel pier could, therefore, be determined during loading. For the pier with shaft resistance only, the end-bearing resistance was assumed to be zero and the load distribution curves (Fig. 7.1) below the lowest strain gauge point were extended to pass through zero load at the bottom of the test pier. For the pier with combined shaft and end-bearing resistance, the load distribution curves (Fig. 7.2) were extended to cut the load-axis at the bottom of the test pier. The load transfer to the end-bearing for this pier was determined by straight line distribution curve for each incremental loading.

The load transfer results are discussed in the following sections.

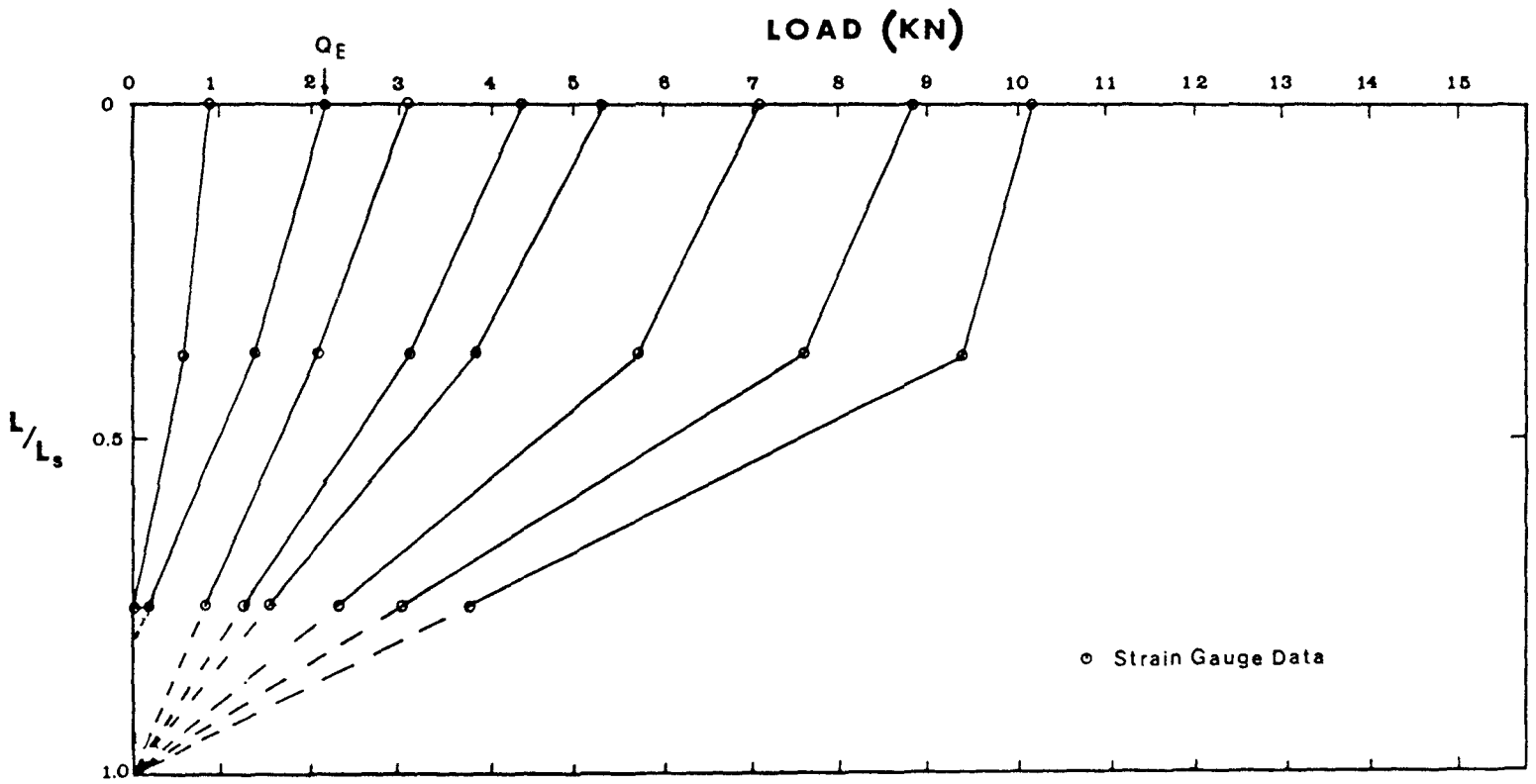

Fig. 7.1 Load distribution curves for steel pier with shaft resistance only, SP-SL(0.033).

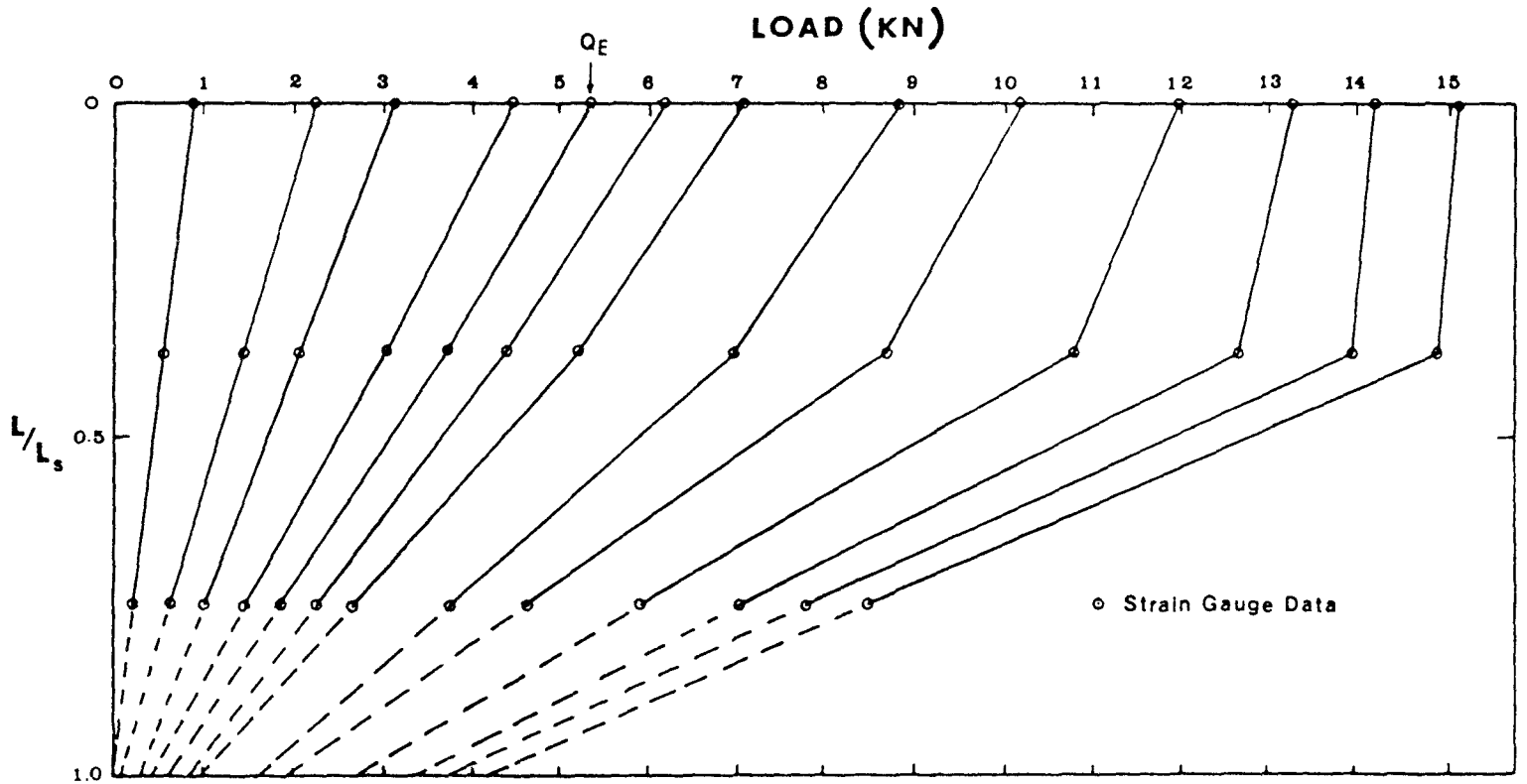

Fig. 7.2 Load distribution curves for steel pier with combined shaft and end-bearing resistance, SP-CL(0.033).

7.2 CONVENTIONAL SOCKETED PIER: STEEL PIER

7.2.1 Distribution of Shaft Resistance

The load distribution along the shaft of the model piers, SP-SL (0.033) and SP-CL(0.033), at various increments of load are shown in Figs. 7.1 and 7.2.

It can be seen from Fig. 7.1, that the load distribution along the embeded shaft length of test pier with shaft resistance only, SP-SL (0.033), was uniform up to an applied load, Q_a = 2.22 kN (500.0 lb). This value of load was the limit of the elastic range (Fig. 6.1). The results of this test are, therefore, in agreement with theoretical studies by Osterberg and Gill (1973), who suggest that all load distributions for loads within the elastic range of loading should be linear.

For the applied loads beyond the elastic range, $Q_E > 2.22$ kN (500.0 lb), the behaviour changed. As higher loads were applied, the load carried by the upper portion of the pier was found to be smaller compared to the load carried by the bottom portion of the pier (Fig. 7.1). This non-uniform distribution behaviour is thought to be due to the progressive failure of the bond between the steel pier and pseudo-rock as higher loads were applied. This behaviour is consistent with the theoretical prediction for bored piles reported by Ellison et al. (1971) and for socketed piers by Osterberg and Gill (1973). This bond-failure of the upper portion of the test pier was observed, when the model was split into two halves after the completion of the test.

Similar trends were also observed for the test pier with combined shaft and end-bearing resistance, SP-CL(0.033), (Fig. 7.2). The test pier exhibited uniform distribution of shaft resistance as long as the applied loads were within the elastic loading range, $Q_E \leq 5.34$ kN (1,200.0 lb), (Fig. 7.2). The results of this test are also consistant with the theoretical studies by Osterberg and Gill (1973).

At applied loads beyoned the elastic loading range, $Q_E > 5.34$ kN (1,200.0 lb), the load was no longer uniformly distributed along the shaft length, and the upper portion of the pier was observed to carry less load.

7.2.2 Load Transfer to the Base

The portion of the applied load transferred to the base of the test pier at selected load increments is summarized in Table 7.1.

It can be seen that load transferred to the base increased as higher loads were applied to the test pier. The load transmitted to the base increased from 0.0 % at Q_a = 0.89 kN (200.0 lb) to 28.1 % at Q_a = 15.12 kN (3,400.0 lb) (See Table 7.1). For applied load, Q_a = 5.34 kN (1,200.0 lb), which was equal to the limit of the elastic range, the base load was 11.3 % of the applied load.

The percentage of the applied load carried by the base at the elastic loading limit $Q_a = Q_E$ = 5.34 kn (1,200.0), is compared with the values estimated by the lineae elastic solution proposed by Donald

TABLE 7.1 SUMMARY OF LOAD TRANSFER DATA FOR CONVENTIONAL MODEL STEEL PIER, SP-CL(0.033).

Applied Load Q_a (kN)	Base Load Q_b (kN)	Q_b/Q_a (%)
0.89	0.00	0.0
2.22	0.11	5.0
3.11	0.29	9.3
4.45	0.45	10.1
5.34*	0.60	11.3
6.23	0.84	13.5
7.12	1.01	15.2
8.90	1.58	17.8
10.23	1.92	18.8
12.00	2.81	23.4
13.34	3.38	25.3
14.23	3.75	26.4
15.12	4.25	28.1

* Elastic Loading Limit

et al. (1980) and Pells and Turner (1979) (Table 7.2). It is interesting to note that the results of the present study are in excellent agreement with these theoretical solutions.

Based on the test results for full-scale piers, Williams et al. (1980) proposed a correlation between the load transfer at the base and the embedment ratio. It is also interesting to note that the present data are in good agreement with the Williams et al. (1980) findings (Fig. 7.3).

7.3 GROOVED SOCKETED PIER: CONCRETE PIER

The values of load transferred to the base at various load increments for the grooved pier with combined shaft and end-bearing resistance, CW-CS(0.303), are summarized in Table 7.3.

The grooved concrete pier behaved a little differently from the conventional steel pier. Up to the elastic loading limit, Q_E = 62.3 kN (1,400.0 lb), virtually no load was transferred to the base (Fig. 6.4 and Table 7.3). However, the load transferred to the base was found to increase when loads exceed the elastic limit. About 5.0 % of total load was found to be transferred to the base at initial failure of shaft resistance, Q_S = 124.5 kN (28,000.0 lb).

Donald et al. (1980) and Pells and Turner (1979) proposed methods for estimating the load transfer to the base. These methods are based on elastic analysis and predict higher values of load transferred to the base as the Young's modulus ratio (E_c/E_r) increases. The test re-

TABLE 7.2 COMPARISON OF LOAD TRANSFER BEHAVIOUR IN ELASTIC RANGE FOR CONVENTIONAL MODEL STEEL PIER.

	% Load Transfer to the Base (Q_b/Q_a)
This Study	
Steel Pier, SP-CL(0.033)	11.3
Elastic Solutions	
Pells and Turner (1979)	11.0
Donald et al. (1980)	12.1

$L_{s/D}$ = 4.0, $K = {}^{E}/_{E_c}$ = 36.3

Q_a = Applied Load

Q_b = Base Load

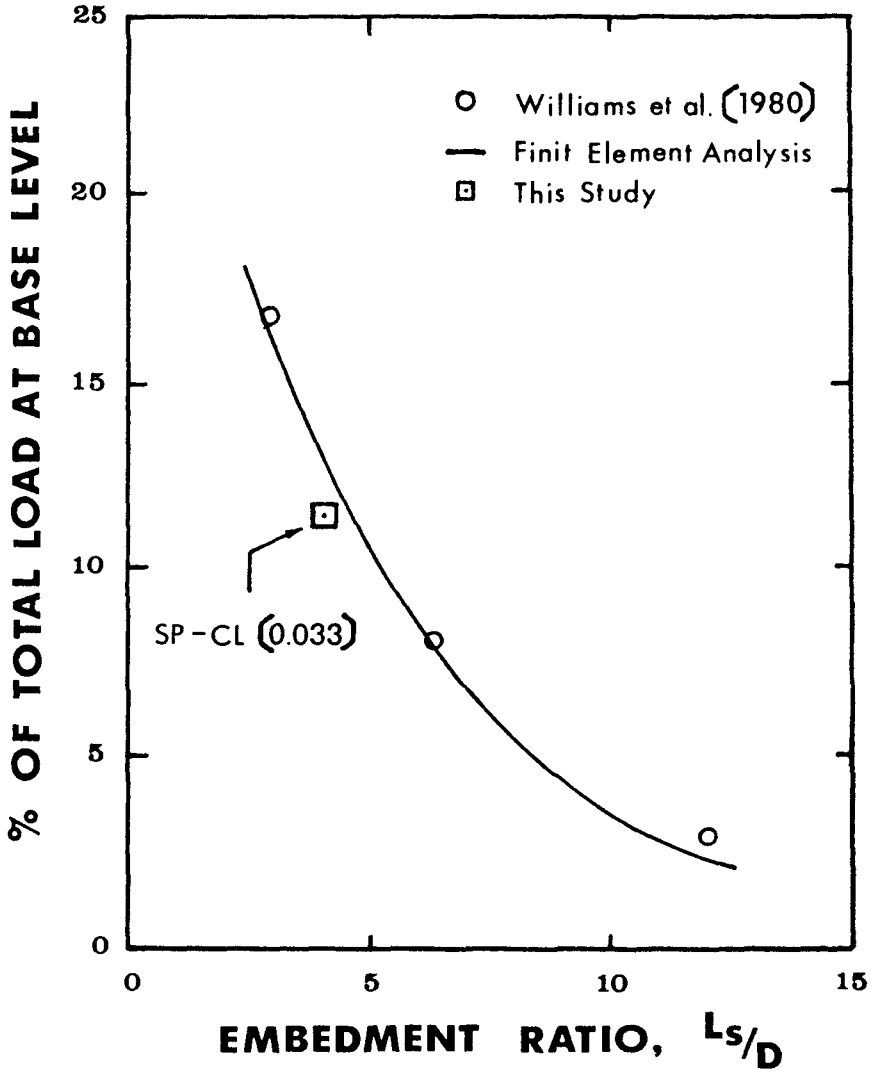

Fig. 7.3 The percentage of the total load reaching the pier base for various embedment ratios in the elastic range (after Williams et al. 1980).

TABLE 7.3 SUMMARY OF LOAD TRANSFER DATA FOR GROOVED MODEL CONCRETE PIER, CW-CS(0.303).

Applied Load Q_a (kN)	Base Load Q_b (kN)	Q_b/Q_a (%)
17.80	0.00	0.0
35.60	0.00	0.0
53.30	0.00	0.0
62.30*	0.00	0.0
71.20	0.89	1.3
89.00	1.78	2.0
106.80	3.42	3.2
124.50	6.23	5.0
142.30	10.67	7.5
160.10	26.74	16.7
169.00	42.76	25.3

* Elastic Loading Limit

sults for the grooved pier does not confirm to their analysis. This difference may be due to the lower sensitivity of the load measuring system used for determining base loads. The flat jacks used did not function as anticipated, therefore, the measured values of Q_b were not reliable.

CHAPTER 8

LONG-TERM TESTS ON CONVENTIONAL MODEL PIERS

8.1 GENERAL

Long-term loading tests were performed on two model steel piers, SP-SL(0.033) and SP-CL(0.033), and two concrete piers, CW-SL(0.025) and CW-CL(0.025), having relatively smooth socket walls.

The design loads for model piers were estimated using design charts developed for conventional piers (Horvath 1982) or from short-term loading tests. The loads used for testing were half of the estimated shaft failure load, Q_{sf}.

The time-dependent behaviour of the model piers with respect to displacement, load distribution and load transfer is presented and discussed in the following sections.

8.2 TIME-DISPLACEMENT BEHAVIOUR

8.2.1 Steel Piers

Two small model steel piers, D = 25.4 mm (1.0 in) and L_s = 101.6 mm (4.0 in), socketed into pseudo-rock were tested. It should be pointed out that the these tests were primarily done for preliminary information, to determine the procedures, feasibility of the research, etc.

The loading sequence for these piers are given in section 5.3.5.2 and 5.3.5.3. The elastic limit load for the piers with shaft resistance only and the combined shaft and end-bearing resistance were estimated and were found to be 2.22 kN (500.0 lb) and 5.34 kN (1,200.0 lb) respectively from load-displacement curves. The creep behaviour of the model steel piers during the period of sustained load testing are shown in Figs. 8.1 and 8.2.

Figure 8.1 indicates that significant creep movements did not occur as long as the total applied load was below the elastic limit, Q_E = 2.22 kN (500.0 lb). The rate of creep was found to be 0.0076 mm (0.0003 in) per log cycle of time at 2.22 kN (500.0 lb) for the test pier. The rate of creep increased with incerasing values of applied load. At 5.34 kN (1,200.0 lb), the pier exhibited an initial rate of creep of 0.102 mm (0.004 in) per log cycle of time. This rate of creep continued for about 4 days after which the rate of creep decreased to 0.0305 mm (0.0012 in) per log cycle of time. It must, however, be pointed out that this load of 5.34 kN (1,200.0 lb) was beyoned the limit of the elastic range of loading, Q_E = 2.22 kN (500.0 lb), for the test pier (Fig. 6.1). The test pier, therefore, showed a higher rate of creep settlement at this loading.

The test pier with combined shaft and end-bearing resistance, SP-CL(0.033), showed a comparatively smaller rate of creep, 0.0061 mm (0.0002 in) per log cycle of time (Fig. 8.2) even at 5.34 kN (1,200.0 lb).

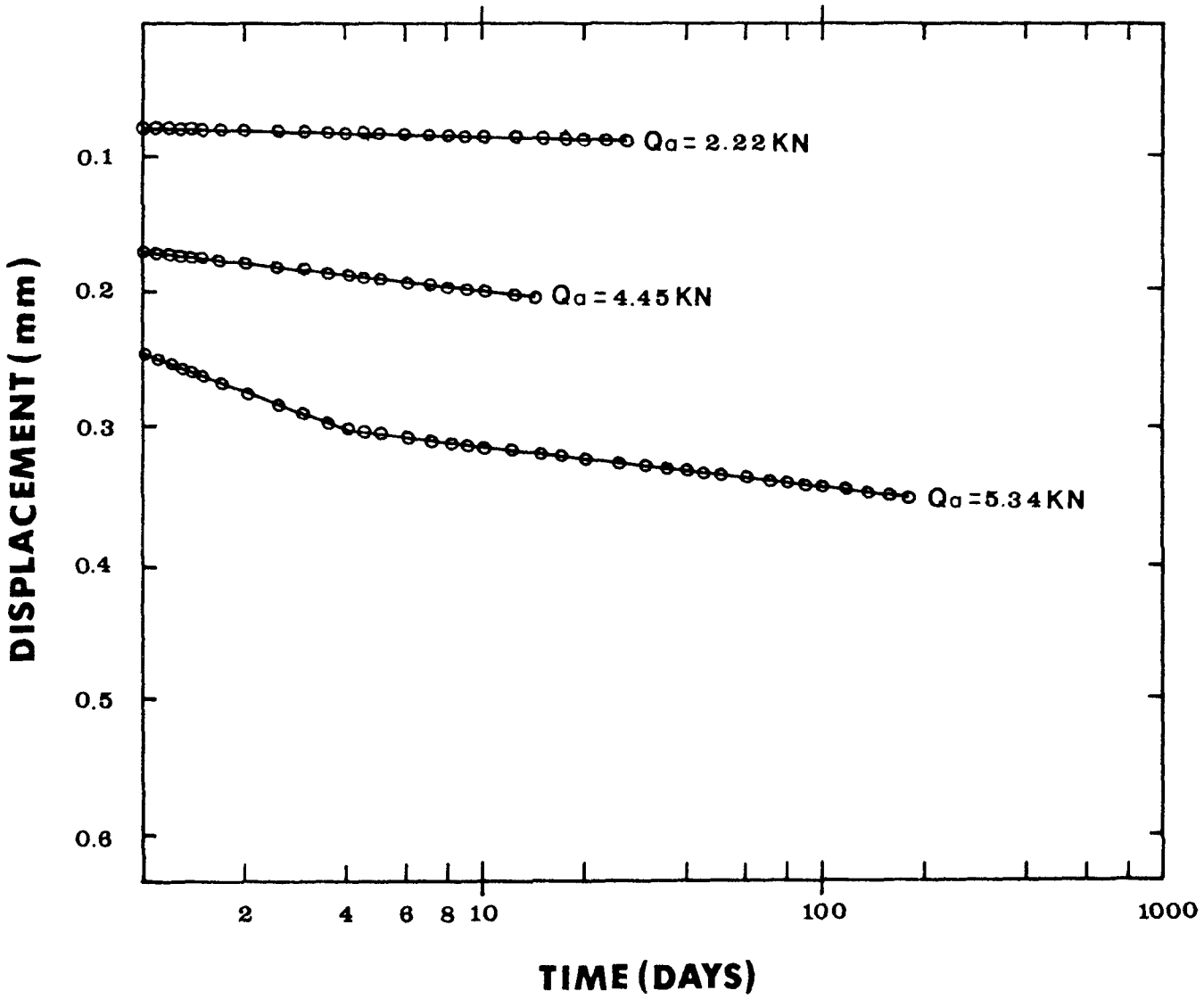

Fig. 8.1 Long-term (creep) behaviour for steel pier with shaft resistance only, SP-SL(0.033).

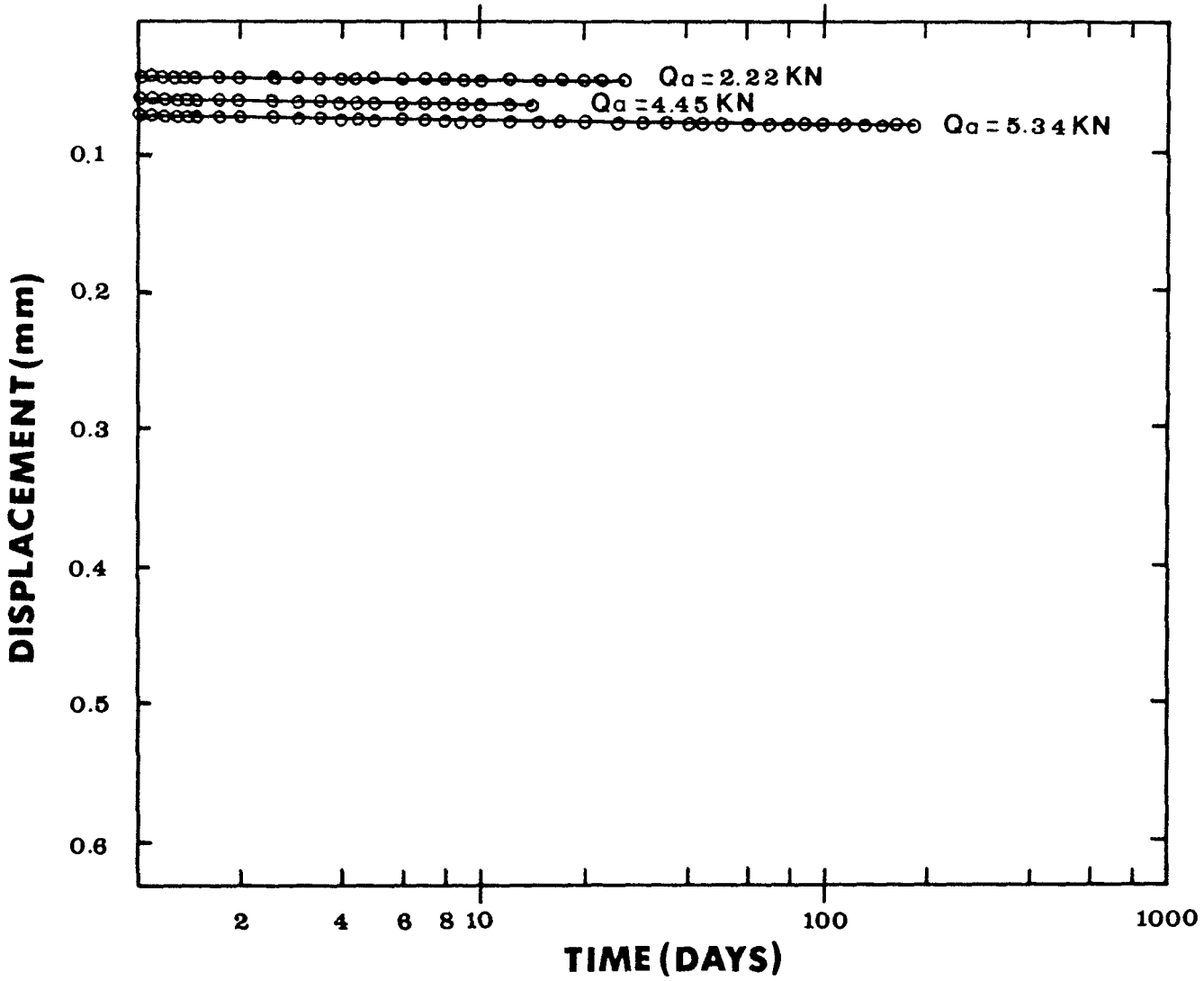

Fig. 8.2 Long-term (creep) behaviour for steel pier with combined shaft and end-bearing resistance, SP-CL(0.033).

The rate of creep for the various tests are summarized in Table 8.1.

8.2.2 Concrete piers

Two concrete model piers, D = 76.2 mm (3.0 in) and L_s = 152.4 mm (6.0 in), socketed into weak rock were tested. The test piers with shaft resistance only, CW-SL(0.025), and with combined shaft and end-bearing resistance, CW-CL(0.025), were subjected to the loads which were sustained.

The load-time-displacement behaviour of test piers, during the application of load are shown in Figs. 8.3 and 8.4.

The time-displacement data for 200 days for these piers are shown in Figs. 8.5 and 8.6. The displacement data has been replotted against the logarithm of time in Figs. 8.7 and 8.8.

It can be seen from Figs. 8.5 and 8.6, that most of the displacement for both model piers occurred within about 20 days.

The primary creep rate for the pier with shaft resistance only, CW-SL(0.025) was found to be 0.145 mm (0.0057 in) per log cycle of time. The creep rate decreased significantly to 0.031 mm (0.00012 in) per log cycle of time at the end of 120 days (Fig. 8.7).

The time-displacement behaviour of concrete test pier with combined shaft and end-bearing resistance, CW-CL(0.025), was similar to

TABLE 8.1 SUMMARY OF CREEP RATE FOR CONVENTIONAL MODEL STEEL PIERS IN PSEUDO-ROCK.

Test Pier	Support Condition	Applied Load Q_a (kN)	Q_a/Q_E (%)	Rate of Creep (mm/log cycle of time)	
				Primary, C_r	Secondary, C_{rs}
SP-SL(0.033)	S	2.22	100.0	0.0076	-
		4.45	200.0	0.0280	-
		5.34	240.0	0.1020	0.0305
SP-CL(0.033)	C	2.22	41.5	0.0038	-
		4.45	83.3	0.0051	-
		5.34	100.0	0.0061	-

S = Shaft Resistance Only

C = Combined Shaft and End-Bearing Resistance

Q_E= Elastic Limit Load

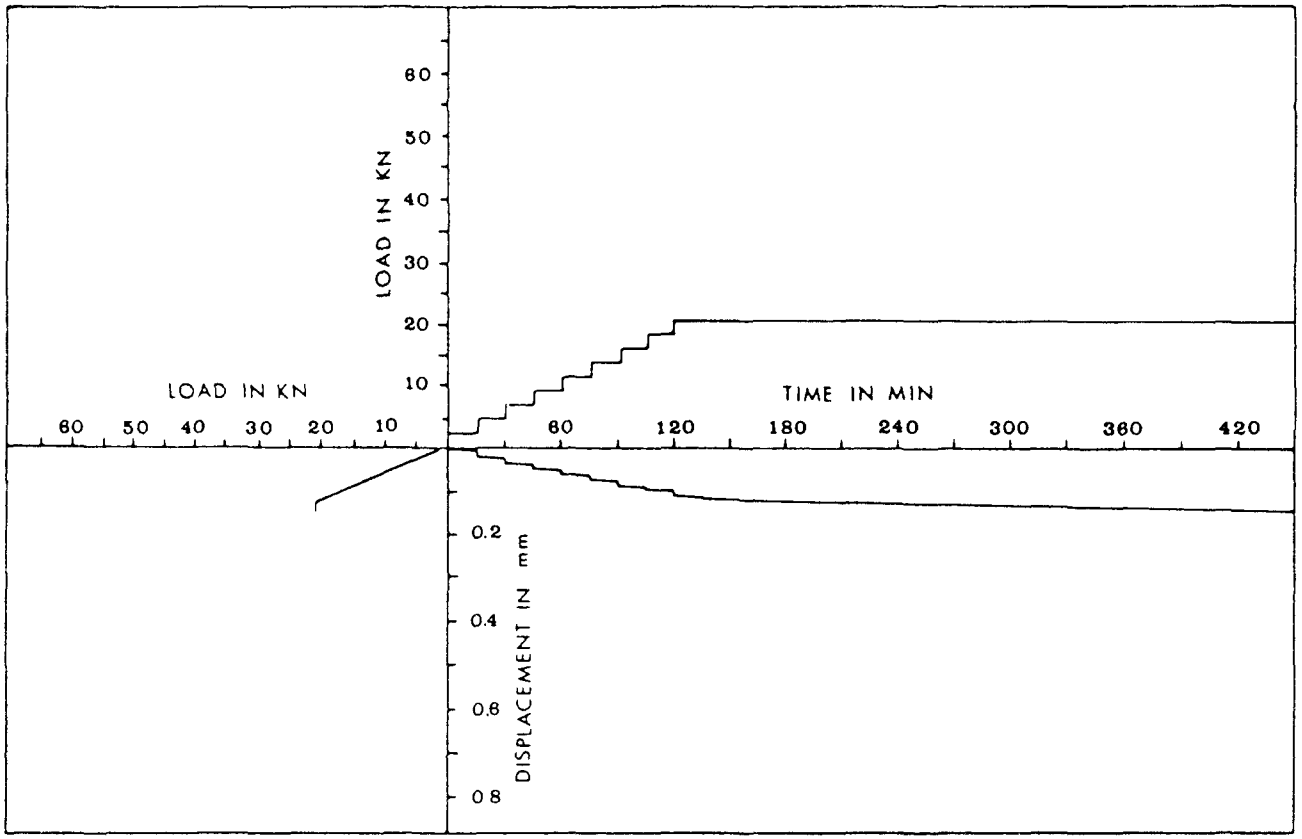

Fig. 8.3 Load-time-displacement behaviour for conventional concrete pier with shaft resistance only, CW-SL(0.025).

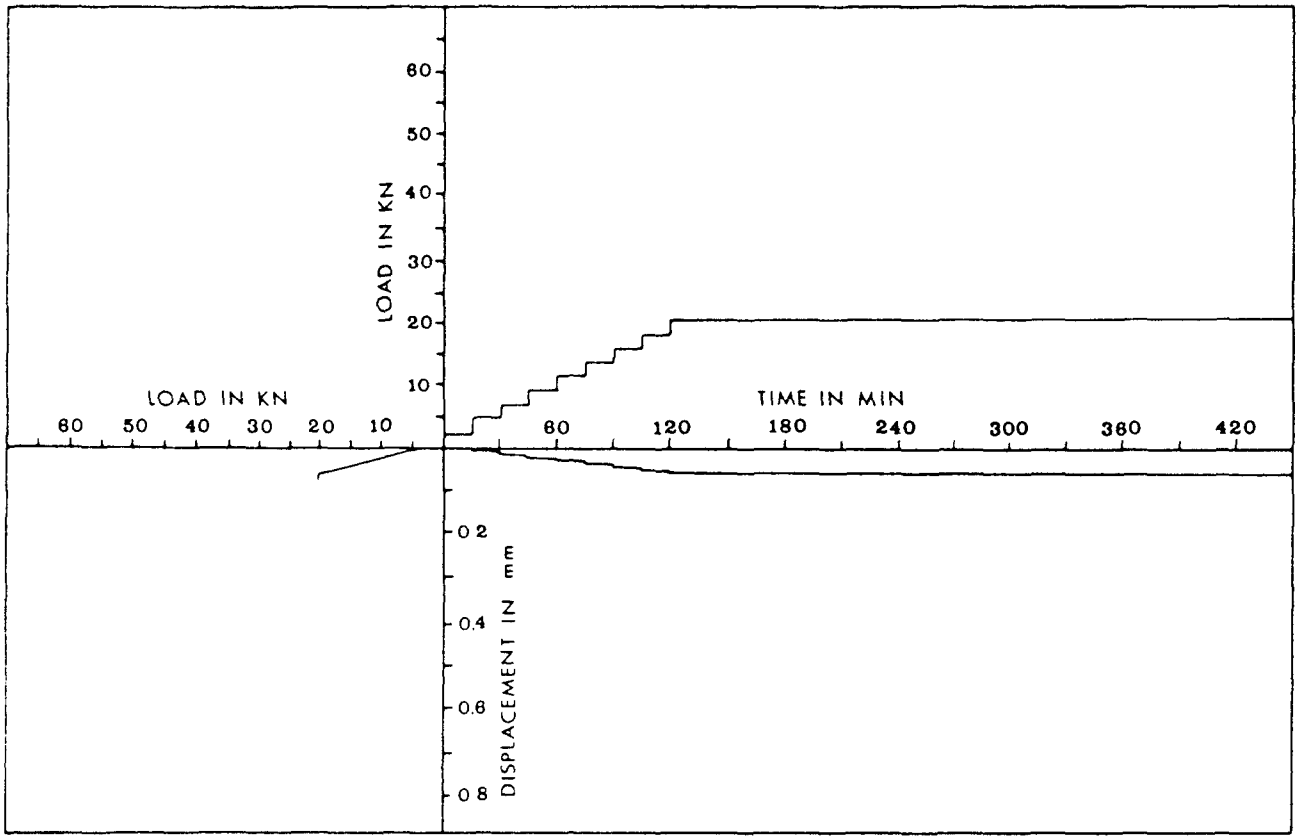

Fig. 8.4 Load-time-displacement behaviour for conventional concrete pier with combined shaft and end-bearing resistance, CW-CL(0.025).

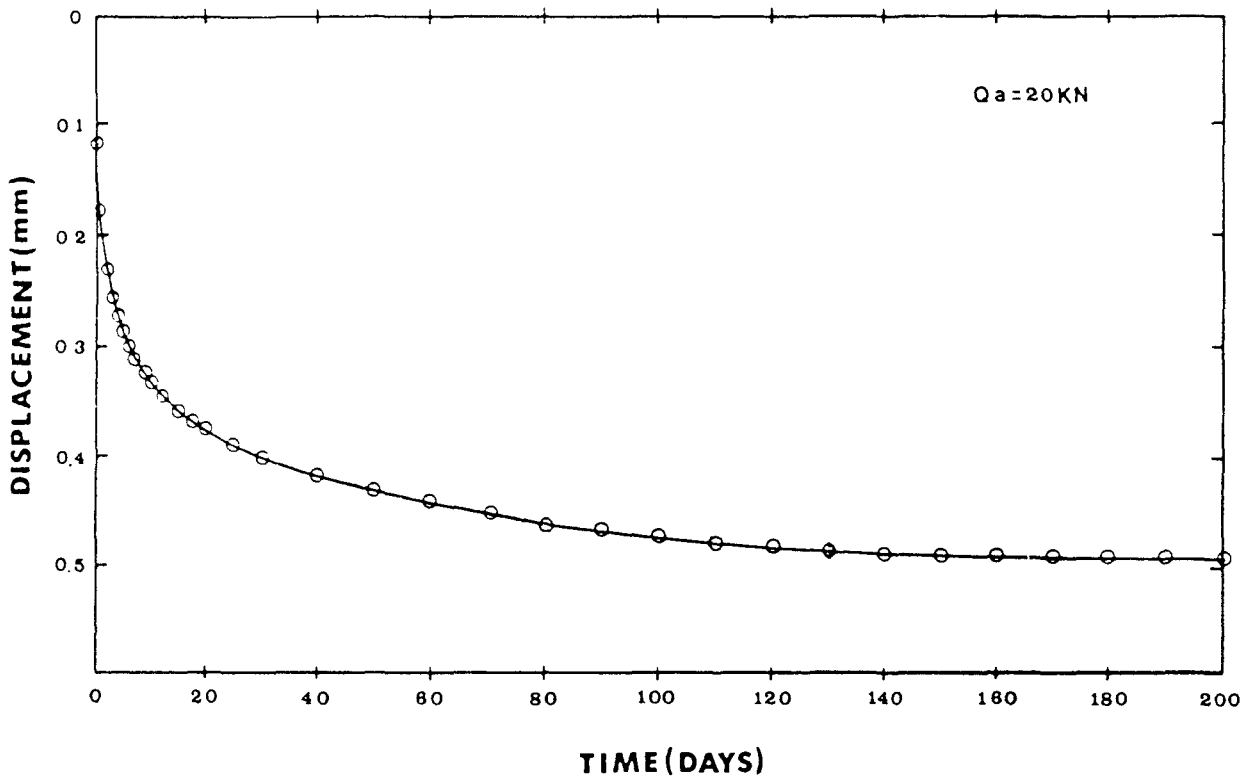

Fig. 8.5 Long-term behaviour of conventional concrete pier with shaft resistance only, CW-SL(0.025).

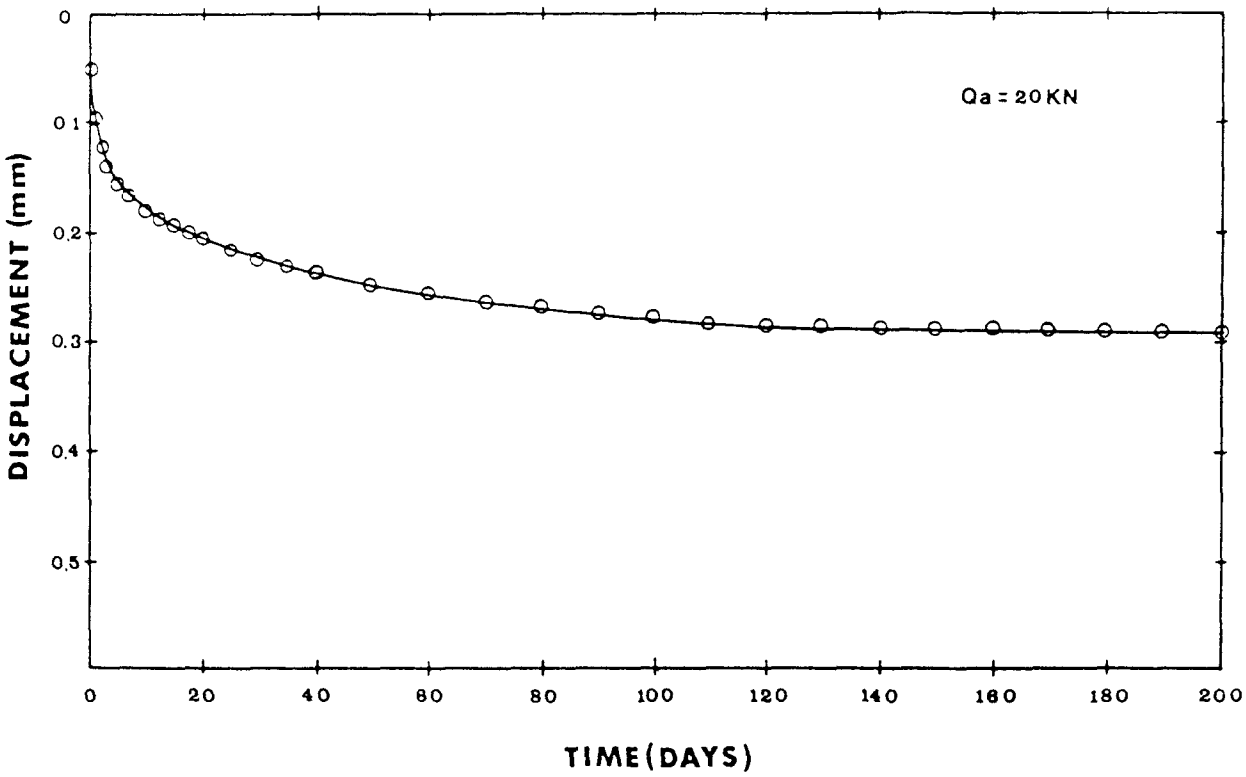

Fig. 8.6 Long-term behaviour of conventional concrete pier with combined shaft and end-bearing resistance, CW-CL(0.025).

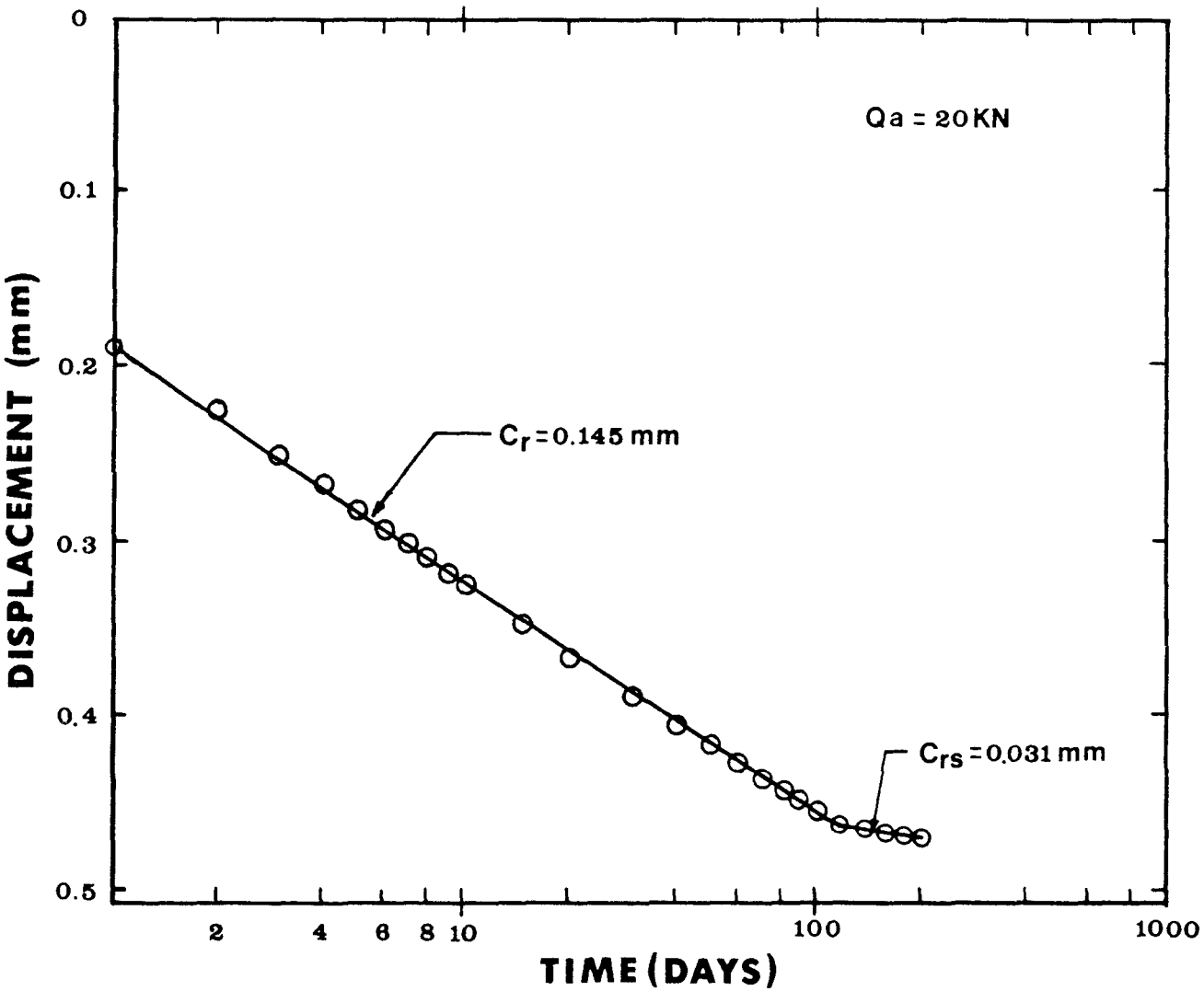

Fig. 8.7 Long-term (creep) behaviour of conventional concrete pier with shaft resistance only, CW-SL(0.025).

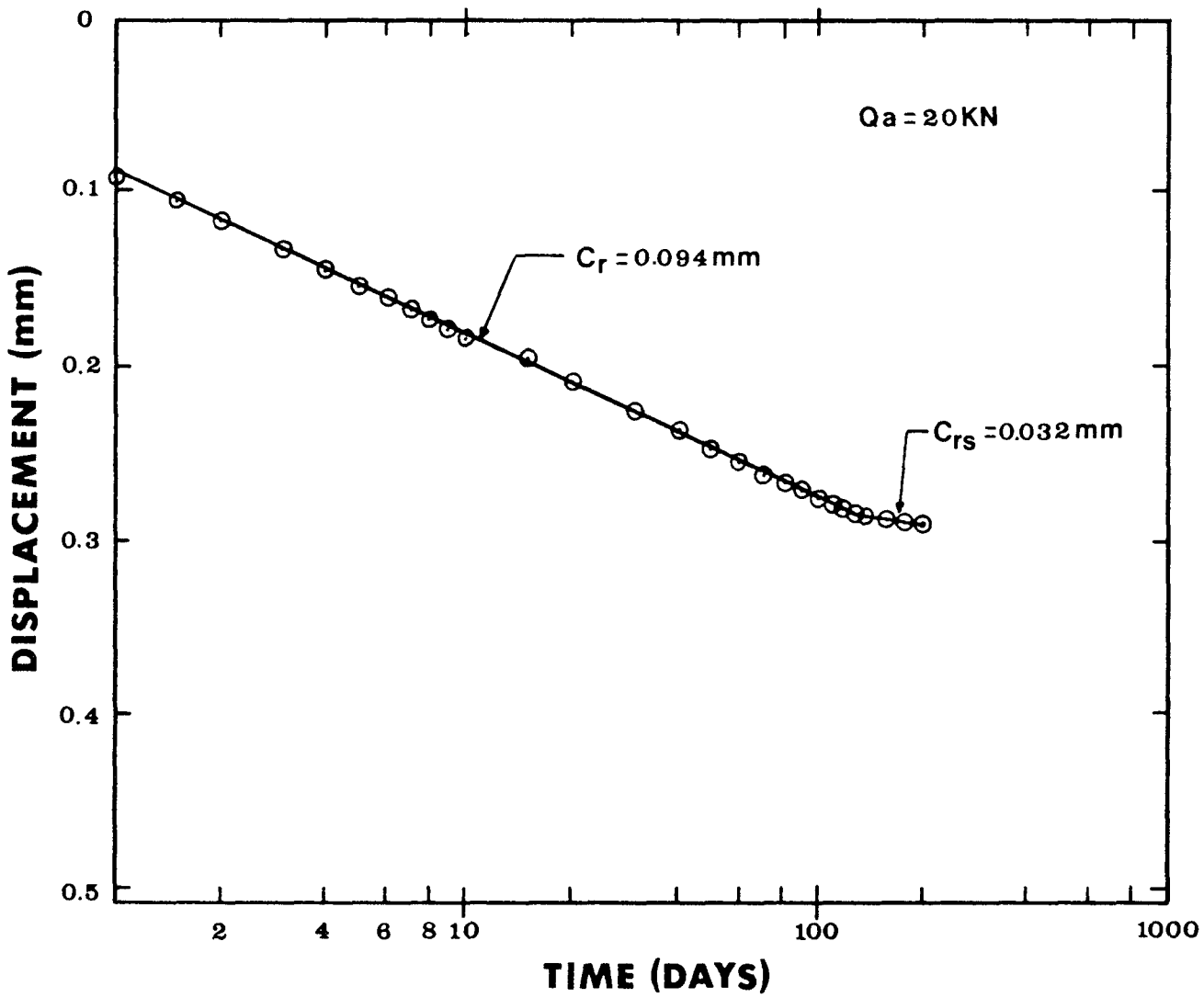

Fig. 8.8 Long-term (creep) behaviour of conventional concrete pier with combined shaft and end-bearing resistance, CW-CL(0.025).

that exhibited by the pier with shaft resistance only, CW-SL(0.025). The rate of creep was found to be 0.094 mm (0.0037 in) per log cycle of time, which was smaller than 0.145 mm (0.0057 in) per log cycle of time observed in case of test pier with shaft resistance only, CW-SL(0.025).

The concrete pier with combined shaft and end-bearing resistance, CW-CL(0.025), also showed a similar abrupt change in around 130 days (Fig. 8.8).

Table 8.2 summarized the creep rate behaviour for these model piers

8.3 LOAD DISTRIBUTION

The changes in load distributions along the length of model piers during the period of sustained loading are shown in Figs. 8.9 and 8.10.

The long-term test indicated that additional shaft resistance was mobilized along the lower portion of the pier with time. This mobilization of the shaft resistance is believed to be due to the slip along pier-rock interface during the course of the sustained loading. The hatched areas shown in Figs. 8.9 and 8.10 indicate this change in the load distribution under sustained load.

The comparison of test piers show that pier with combined shaft and end-bearing resistance, SP-CL(0.033), underwent relatively smaller changes in the load distribution as compared to the pier with shaft resistance only, SP-SL(0.033).

TABLE 8.2 SUMMARY OF CREEP RATE FOR CONVENTIONAL CONCRETE MODEL PIERS IN WEAK ROCK.

Socket Type	Test Pier	Applied Load Q_a (kN)	Q_a/Q_E (%)	Rate of Creep (mm/log cycle of time)		Time to End of Primary Creep t_p (Days)
				Primary C_r	Secondary C_{rs}	
Conventional	CW-SL(0.025)	20.0	100.0	0.145	0.031	120
	CW-CL(0.025)	20.0	85.0	0.094	0.032	130

Q_E = Elastic Limit Load

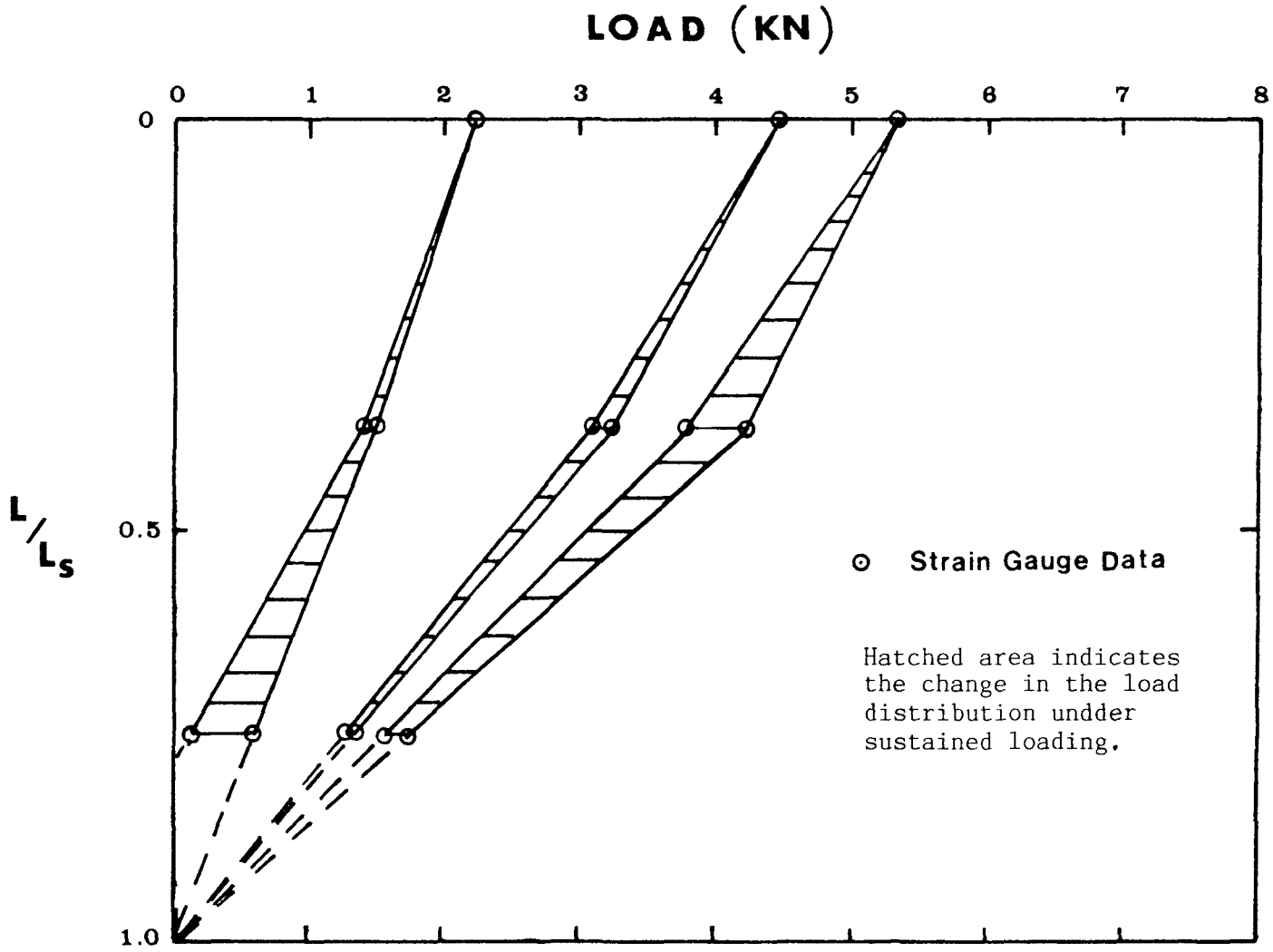

Fig. 8.9 Time effects on load distribution curves for steel pier with shaft resistance only, SP-SL(0.033), under sustained load.

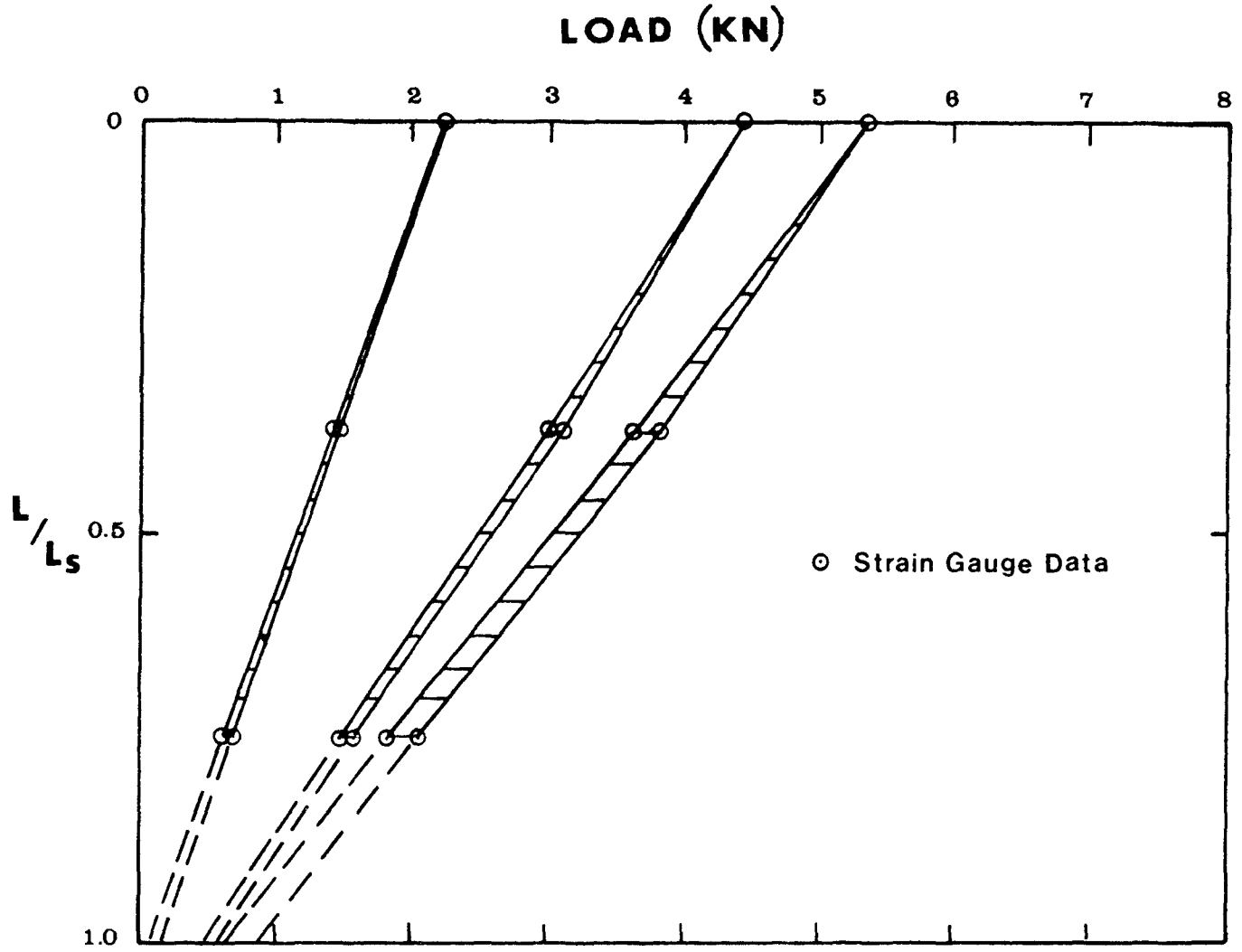

Fig. 8.10 Time effects on load distribution curves for steel pier with combined shaft and end-bearing resistance, SP-CL(0.033), under sustained load.

8.4 LOAD TRANSFER

8.4.1 Steel Pier

The estimated increase in the load transferred to end-bearing support at the base, SP-CL(0.033), with time for sustained loading are shown in Fig. 8.10.

The test pier showed increase in the load transfer when the pier was subjected to a sustained loading. The portion of the load transferred to the base was found to increase with time (See Fig. 8.10 and Table 8.3). The test result showed an average increase in base load of about 3.0 % of applied load, Q_a, during the course of the sustained loading.

8.4.2 Concrete Pier

The increase in load transfer to the base of the concrete pier, CW-CL(0.025), is shown in Fig. 8.11. About 4.5 % of the total applied load, Q_a = 20.0 kN (4,500.0 lb), was transferred to the base immediately after the load applied. The load supported by end-bearing increased with time when the applied load was maintained constant (Fig. 8.11). About 14.0 % of the total applied load was found to have been transferred to the base at the end of 200 days.

TABLE 8.3 SUMMARY OF LOAD TRANSFER DATA FOR CONVENTIONAL STEEL MODEL PIER, SP-CL(0.033), SOCKETED IN PSEUDO-ROCK.

Applied Load Q_a (kN)	Q_a/Q_E	% Load Transferred to the Base $(Q_b/Q_a) \times 100$		Difference	Average
		Short-Term	Long-Term		
2.22	0.4	5.0	8.0	3.0	
4.45	0.8	10.0	12.1	2.1	2.9
5.34*	1.0	11.3	14.9	3.6	

* = Elastic Loading Range

Q_E = Elastic Limit Load

Q_b = Base Load

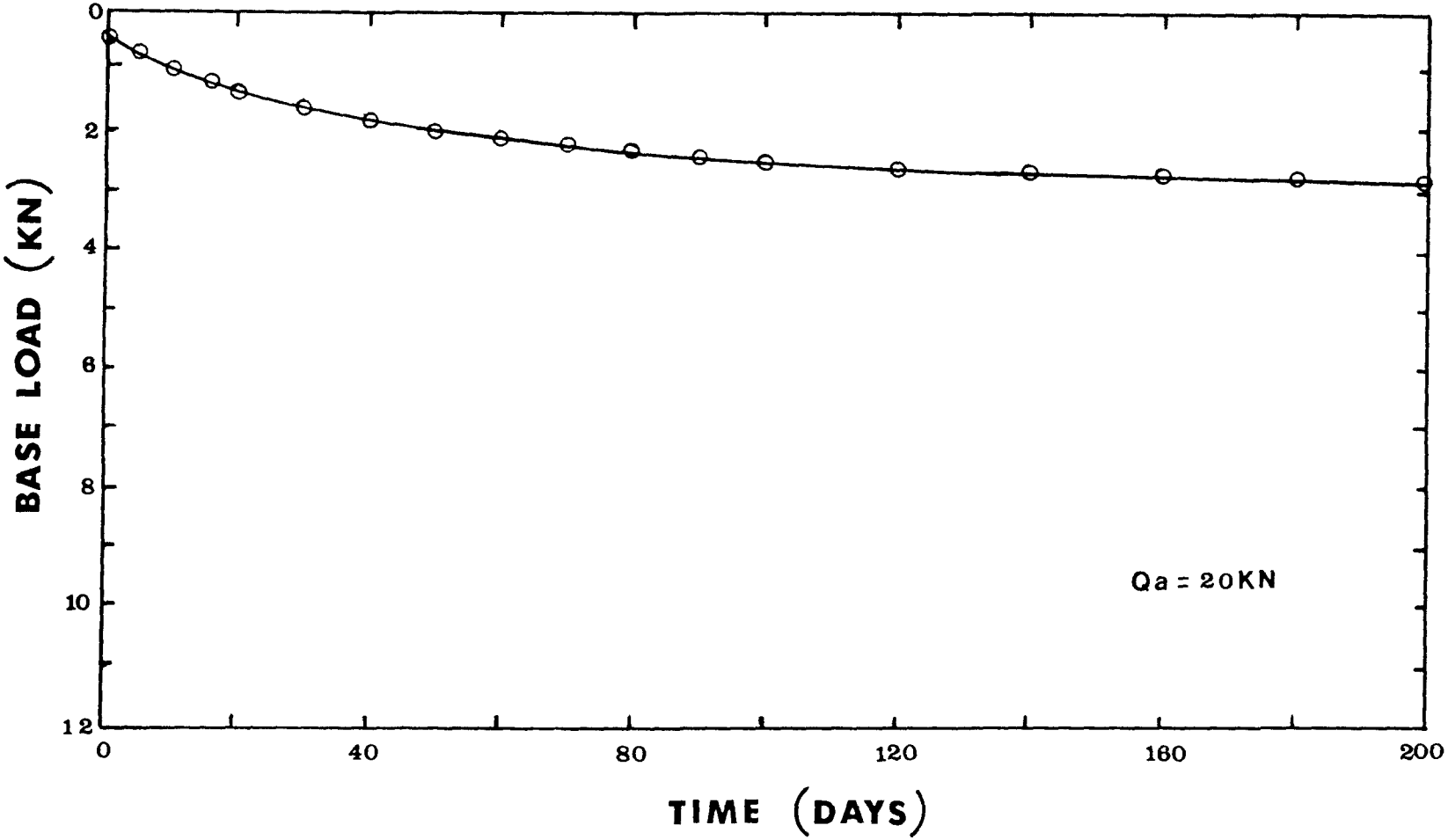

Fig. 8.11 Base load versus time for conventional concrete pier with combined shaft and end-bearing resistance, CW-CL(0.025).

CHAPTER 9

LONG-TERM TESTS ON GROOVED MODEL PIERS

9.1 GENERAL

A total of three grooved concrete model piers, D = 76.2 mm (3.0 in) and L_s = 152.4 mm (6.0 in), were tested under long-term conditions. These piers had different values of shaft roughness and were cast in weak rock. One pier had a load cell at the base, CW-CL(0.303), so that end-bearing resistance was measured and the other two had a void at their base, CW-SL(0.081) and CW-SL(0.303).

The load test results are presented and discussed in the following sections.

9.2 TIME-DISPLACEMENT BEHAVIOUR

The load-displacement-time behaviours for the model piers are shown in Figs. 9.1 to 9.3. A 15 minute loading increment was used for all grooved socketed piers up to the sustained working loads. The time-displacement behaviours of the test piers under the sustained loading conditions are shown in Figs. 9.4 to 9.9.

The time-displacement behaviour as presented in Figs. 9.4 to 9.6 show the typical response of the model piers subjected to sustained loading. Most of the settlement occurred during the first 30 days.

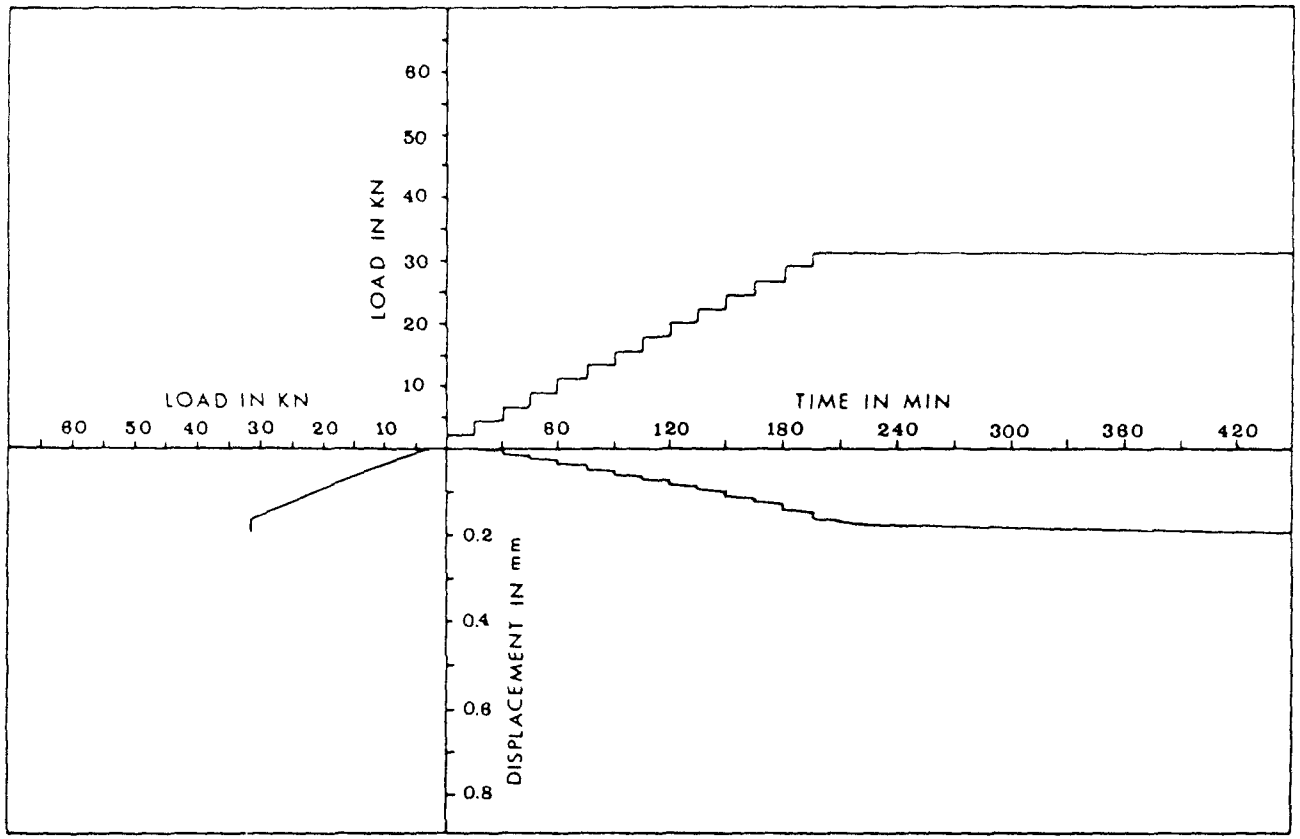

Fig. 9.1 Load-time-displacement behaviour for grooved concrete pier with shaft resistance only, CW-SL(0.081).

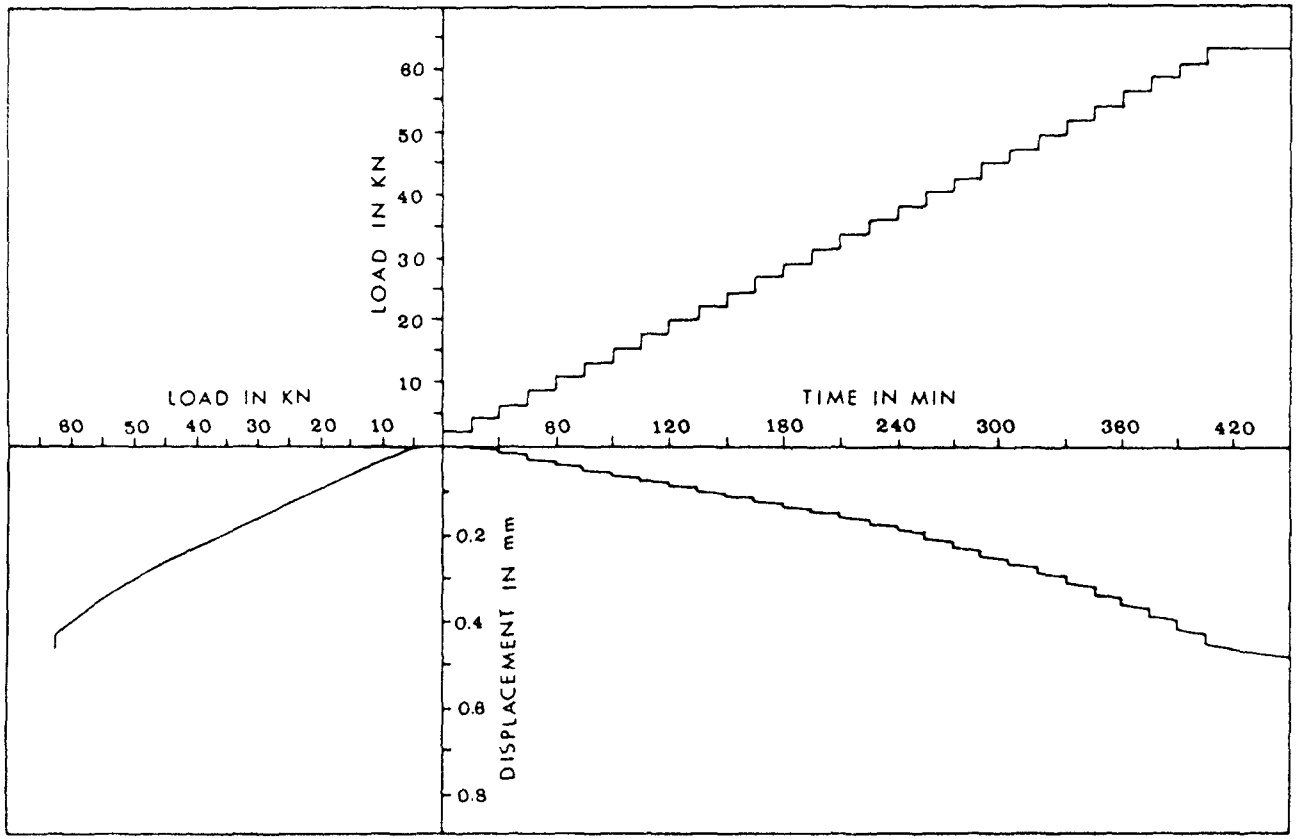

Fig. 9.2 Load-time-displacement behaviour for grooved concrete pier with shaft resistance only, CW-SL(0.303).

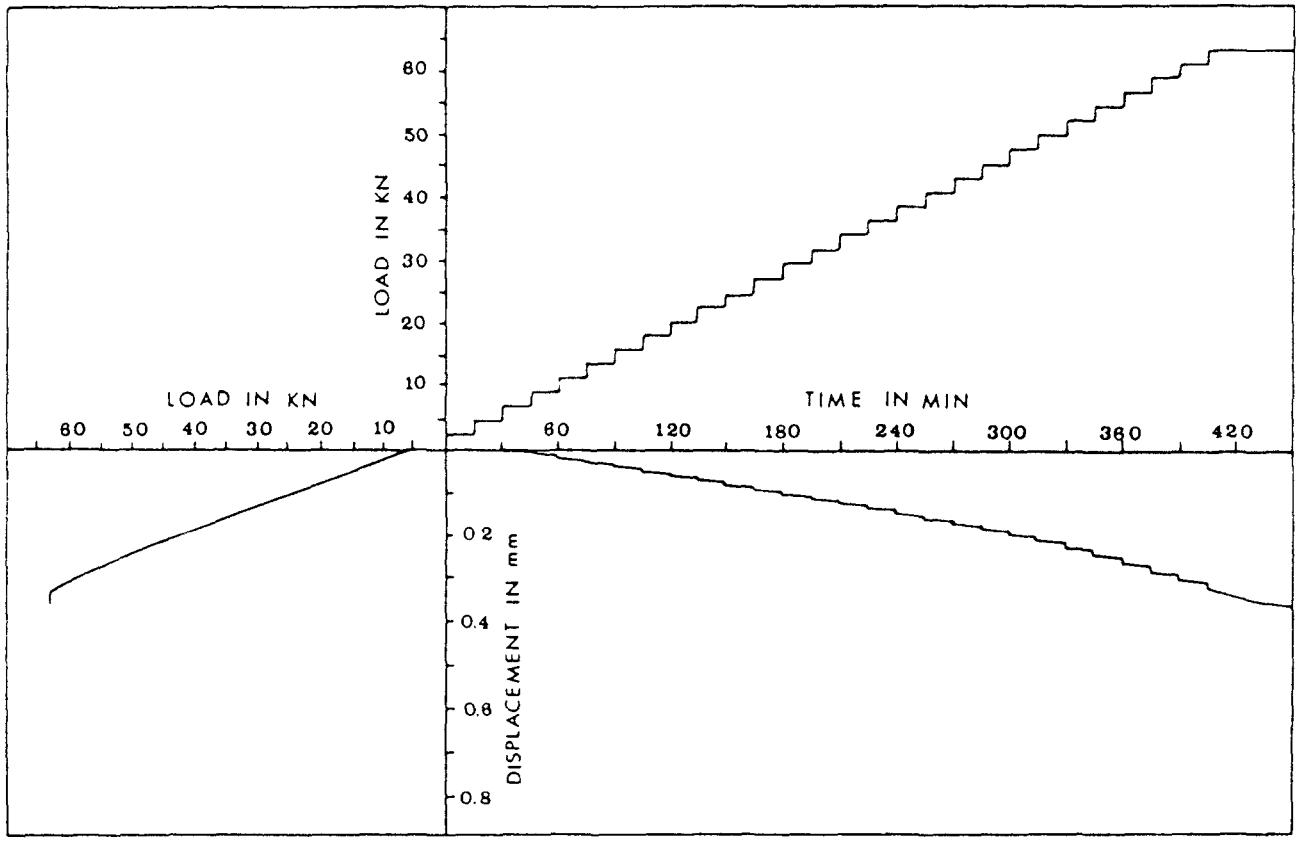

Fig. 9.3 Load-time-displacement behaviour for grooved concrete pier with combined shaft and end-bearing resistance, CW-CL(0.303).

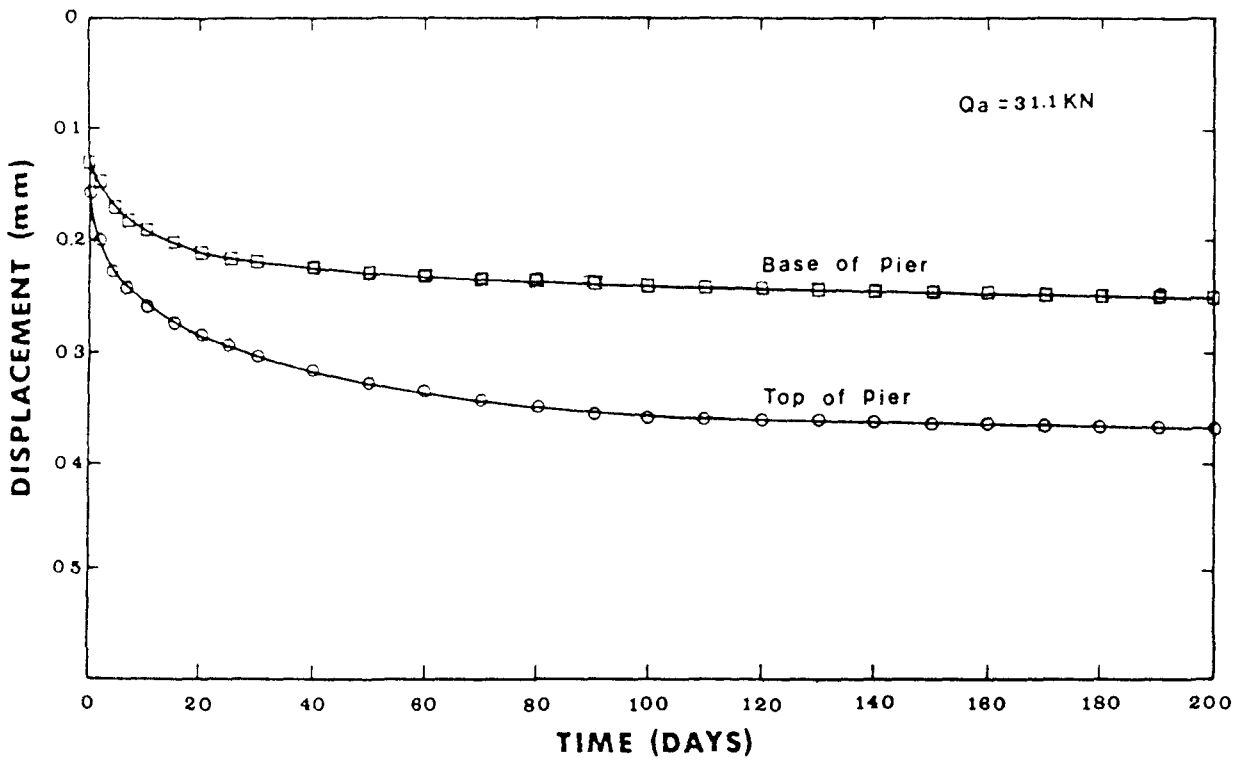

Fig. 9.4 Long-term behaviour of grooved concrete pier with shaft resistance only, CW-SL(0.081).

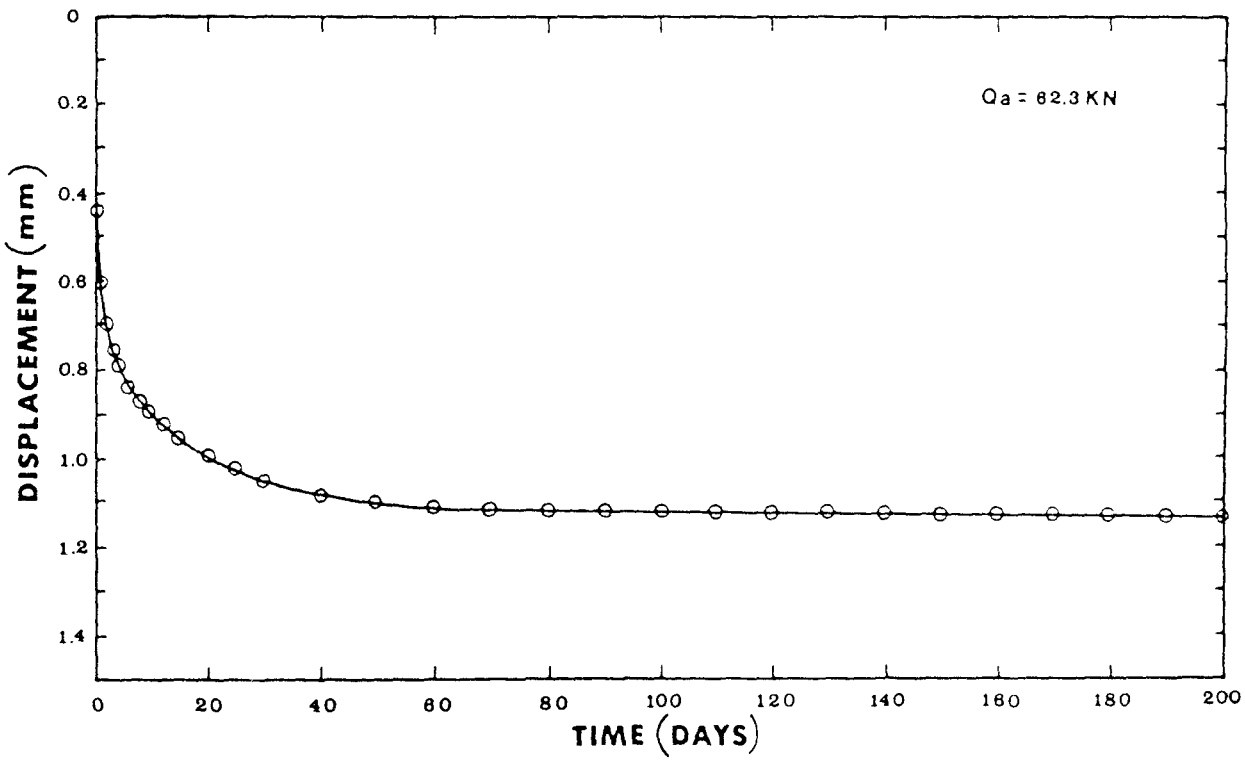

Fig. 9.5 Long-term behaviour of grooved concrete pier with shaft resistance only CW-SL(0.303).

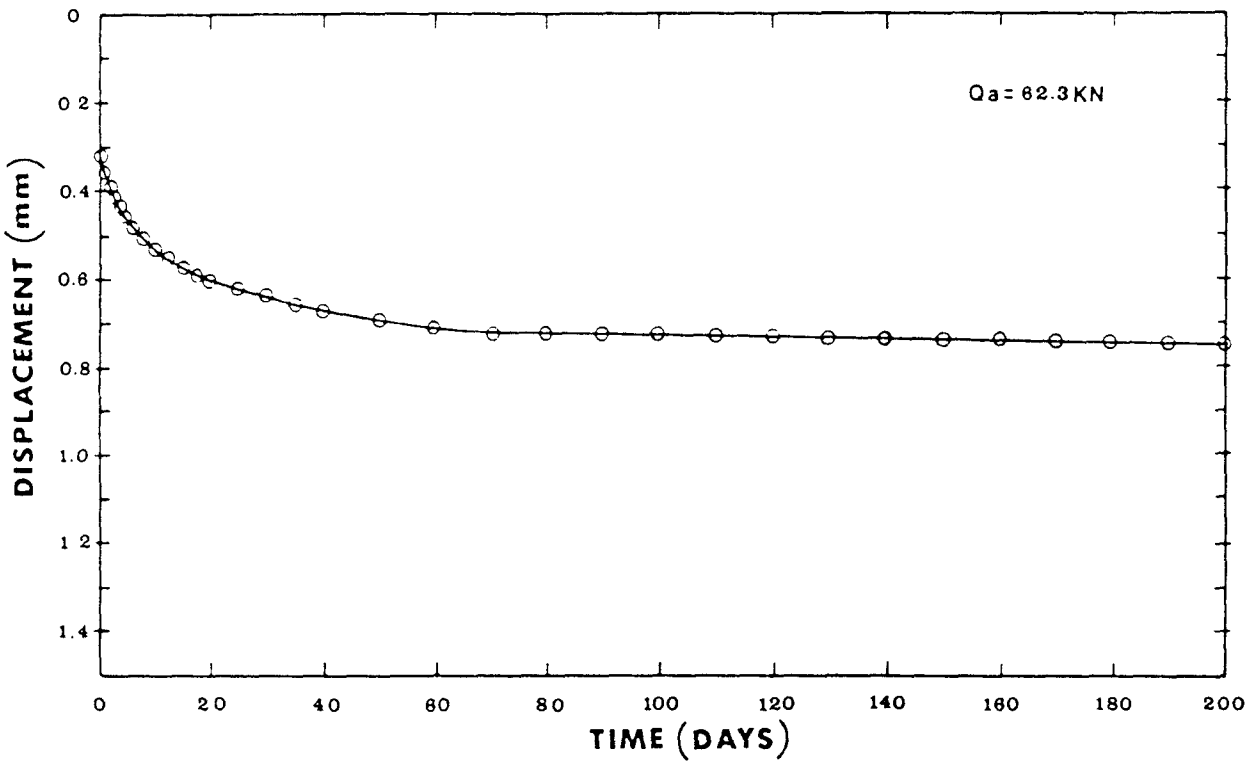

Fig. 9.6 Long-term behaviour of grooved concrete pier with combined shaft and end-bearing resistance, CW-CL(0.303).

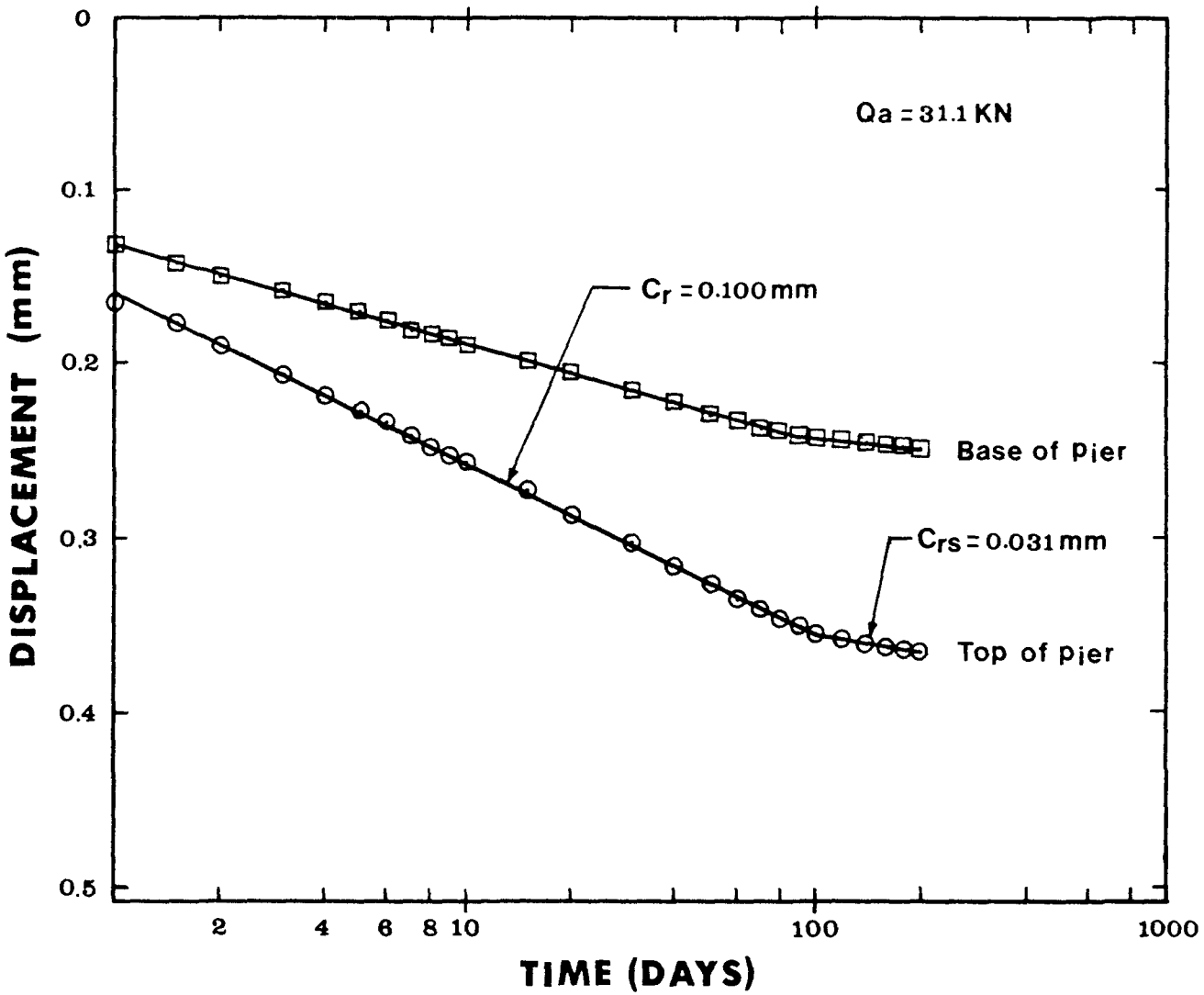

Fig. 9.7 Long-term (creep) behaviour of grooved concrete pier with shaft resistance only, CW-SL(0.081).

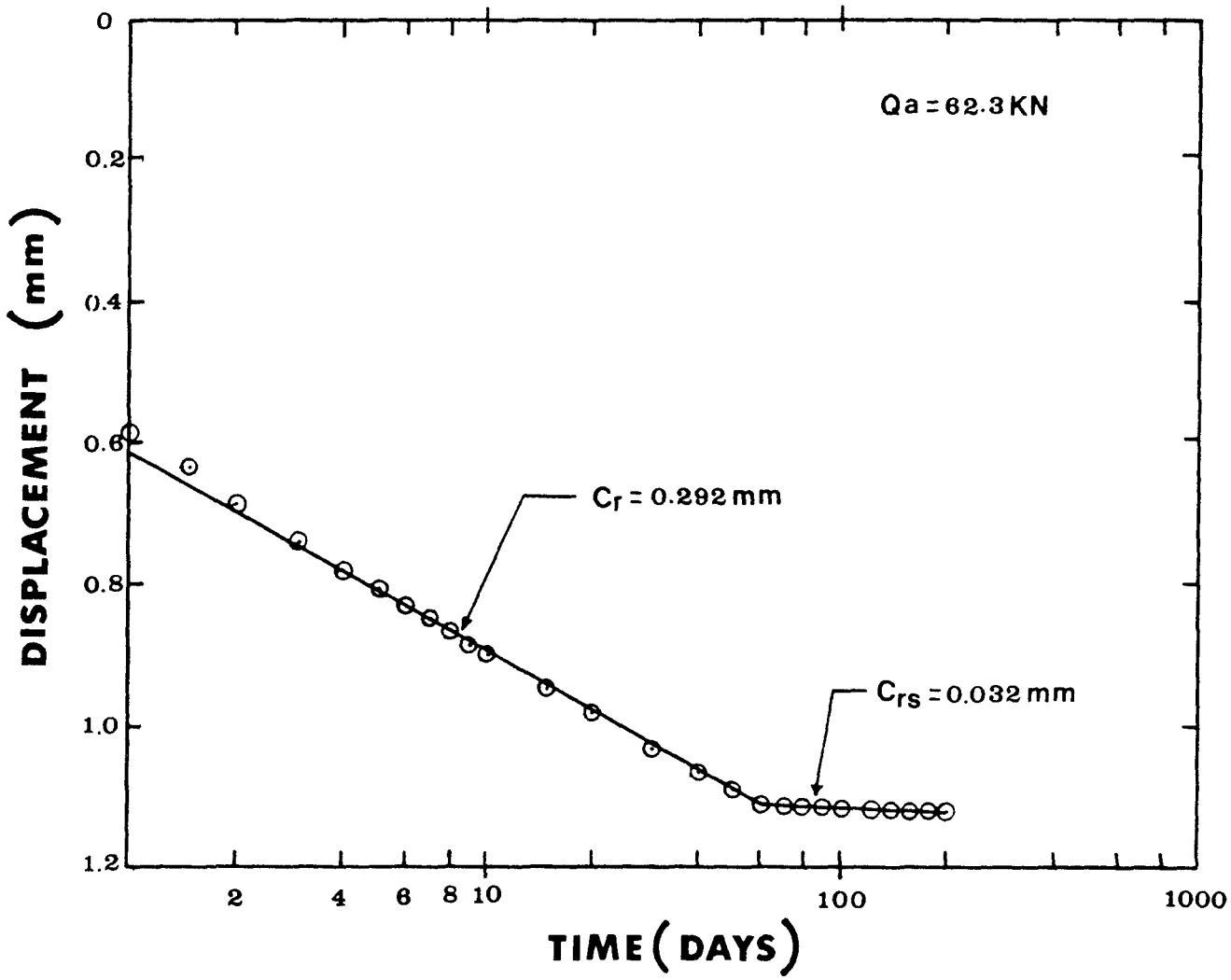

Fig. 9.8 Long-term (creep) behaviour of grooved concrete pier with shaft resistance only, CW-SL(0.303).

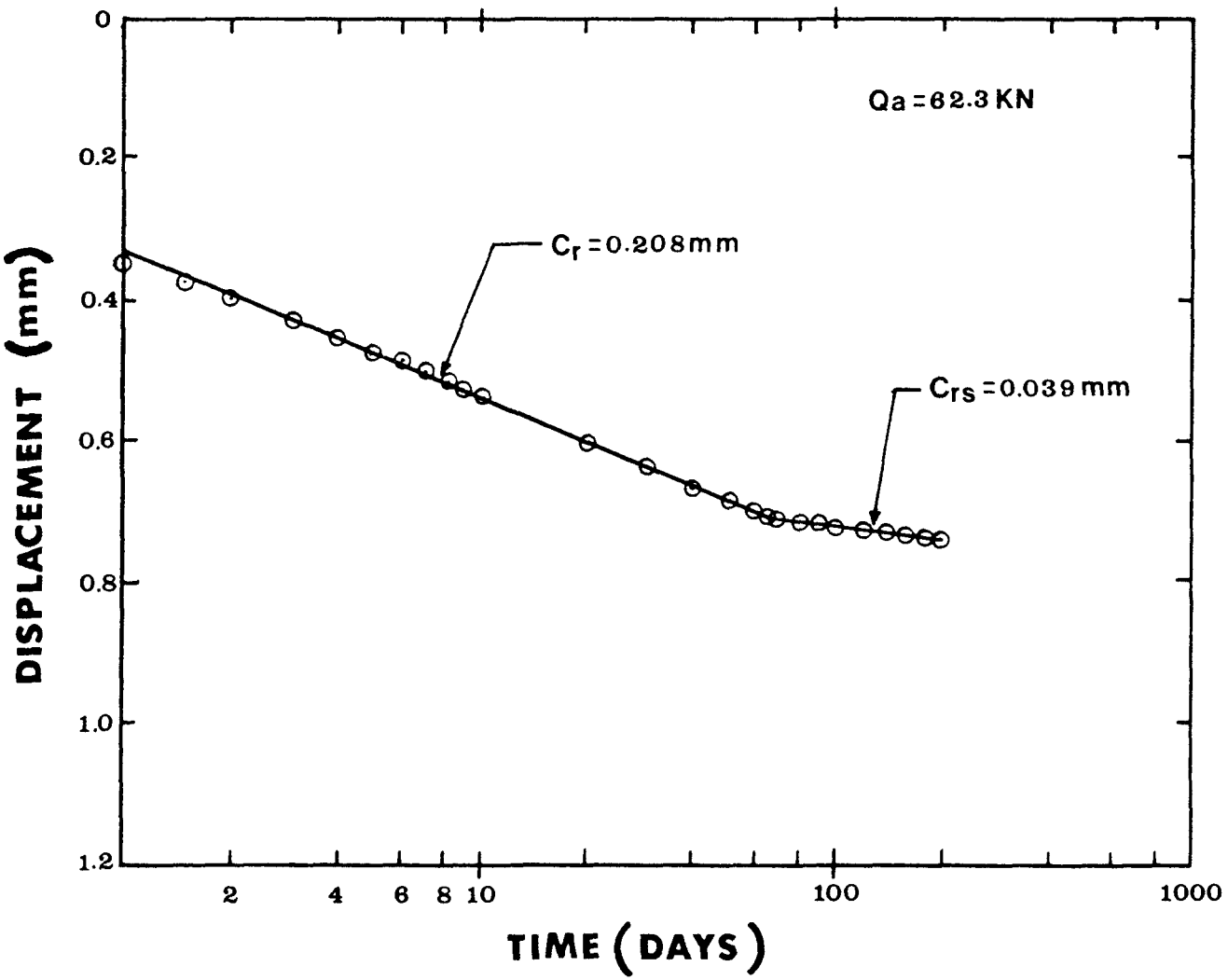

Fig. 9.9 Long-term (creep) behaviour of grooved concrete pier with combined shaft and end-bearing resistance, CW-CL(0.303).

The reuslts showed that the grooved pier with shaft resistance only, CW-SL(0.303), had a higher creep rate, 0.292 mm (0.0115 in) per log cycle of time, (Fig. 9.8) than the pier with combined shaft and end-bearing resistance, CW-CL(0.303), 0.208 mm (0.0082 in) per log cycle of time (Fig. 9.9).

Displacements of model pier, CW-SL(0.081), was measured at the top as well as the base of the pier (See Fig. 5.7). As expected, the rate of creep was found to be different at the top and at the base of pier (0.1 mm (0.0039 in) vs 0.056 mm (0.0022 in) per log cycle of time).

The secondary creep rate, C_{rs}, for all concrete model piers tested were found to be lie within a very narrow range and averaged 0.033 mm (0.0013) per log cycle of time (Table 9.1). It should be pointed out that the stress levels, the socket geometry and the compressive strength of weak rock for the piers in Table 9.1 were all different. The creep rate for these piers are, therefore, not discussed at this time. A detailed discussion on the creep rate is included in section 9.4.

Long-term one-dimensional consolidation tests were perfomed on 61.98 mm (2.44 in) diameter x 27.94 mm (1.1 in) high shale samples at a vertical stress of 67.9 kPa (468.14 psi) which was approximately equal to one-half the average undrained strength of shale. It is interesting to note that the average primary creep rate, 0.034 mm (0.00134 in) per log cycle of time, observed in one-dimensional consolidation test (Fig. 9.10) was very close to the average secondary creep rate, 0.033 mm

TABLE 9.1 SUMMARY OF CREEP RATE FOR CONCRETE MODEL PIERS IN WEAK ROCK.

Socket Type	Test Pier	Applied Load Q_a (kN)	Q_a/Q_E (%)	Rate of Creep (mm/log cycle of time)		Time to End of Primary Creep t_p (Days)
				Primary C_r	Secondary C_{rs}	
Conventional	CW-SL(0.025)	20.0	100.0	0.145	0.031	120
	CW-CL(0.025)	20.0	85.0	0.094	0.032	130
Grooved	CW-SL(0.081)	31.1	111.2	0.100	0.031	100
	CW-SL(0.303)	62.3	141.0	0.292	0.032	60
	CW-CL(0.303)	62.3	125.2	0.208	0.039	66

Q_E = Elastic Limit Load

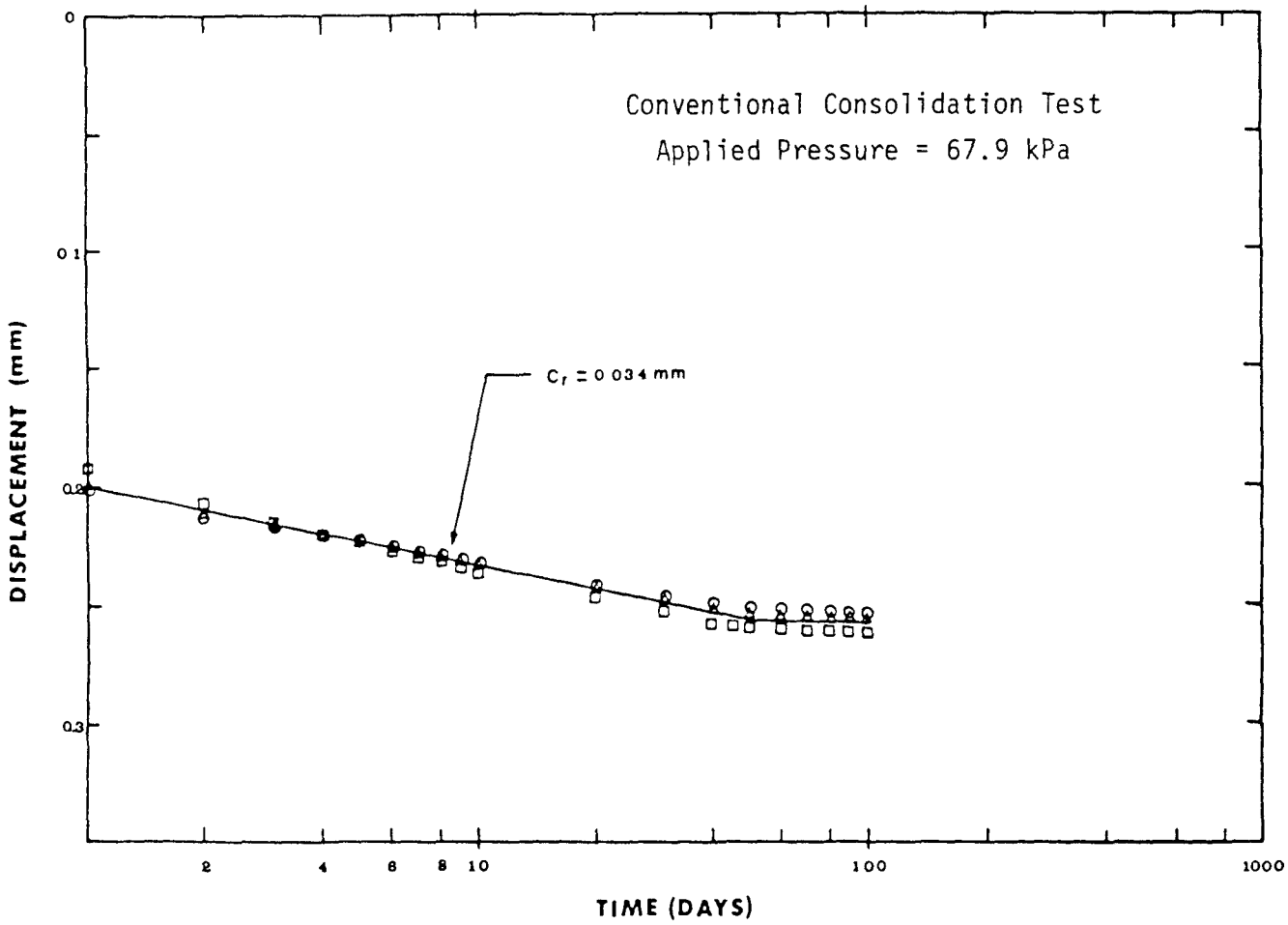

Fig. 9.10 Time versus displacement behaviour for Queenston Shale.

(0.013 in), observed in the model socketed piers in weak rock (Table 9.1).

9.3 LOAD TRANSFER TO THE BASE

The time versus load transfer data for the grooved pier with combined shaft and end-bearing resistance, CW-CL(0.303), tested using the long-term test is shown in Fig. 9.11.

Figure 9.11 shows that only 0.3 % of the total applied load was transferred to the base immediately after the application of the load 62.4 kN (14,000.0 lb). This value of 0.3 % is significantly less than the value estimated from elastic solutions proposed by Donald et al. (1980) and Pells and Turner (1979).

Figure 9.11 also shows that the load transfer gradually increased with time for the first 100 days. The rate of change was steadly decreasing and reached almost a steady-state at around 160 days. The load transferred to the base at this point was found to be about 6.8 % of the applied load of 62.4 kN (14,000.0 lb). This value of 6.8 % is below the value of 20.0 % as estimated by the elastic solutions (Donald et al. 1980; Pells and Turner 1979). This discrepancy may be due to difficulties with the base load measuring system.

In order to compare the conventional and grooved piers, the base load, Q_b, as a percentage of the applied load, Q_a, has been plotted against the log time (Fig. 9.12). Figure 9.12 shows that the base load transfer at the end of 200 days was larger for the conventional pier

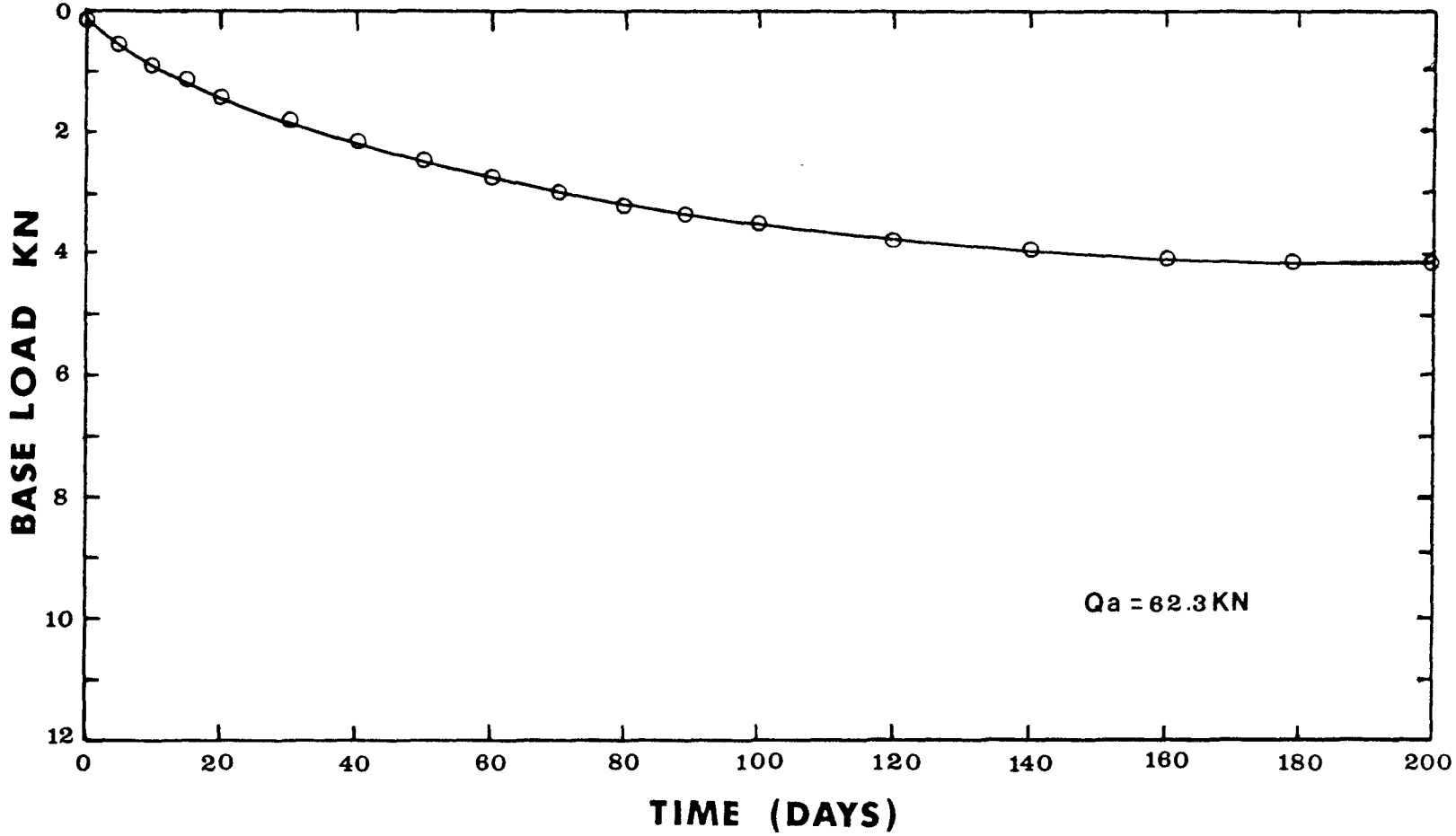

Fig. 9.11 Base load versus time for grooved concrete pier with combined shaft and end-bearing resistance, CW-CL(0.303).

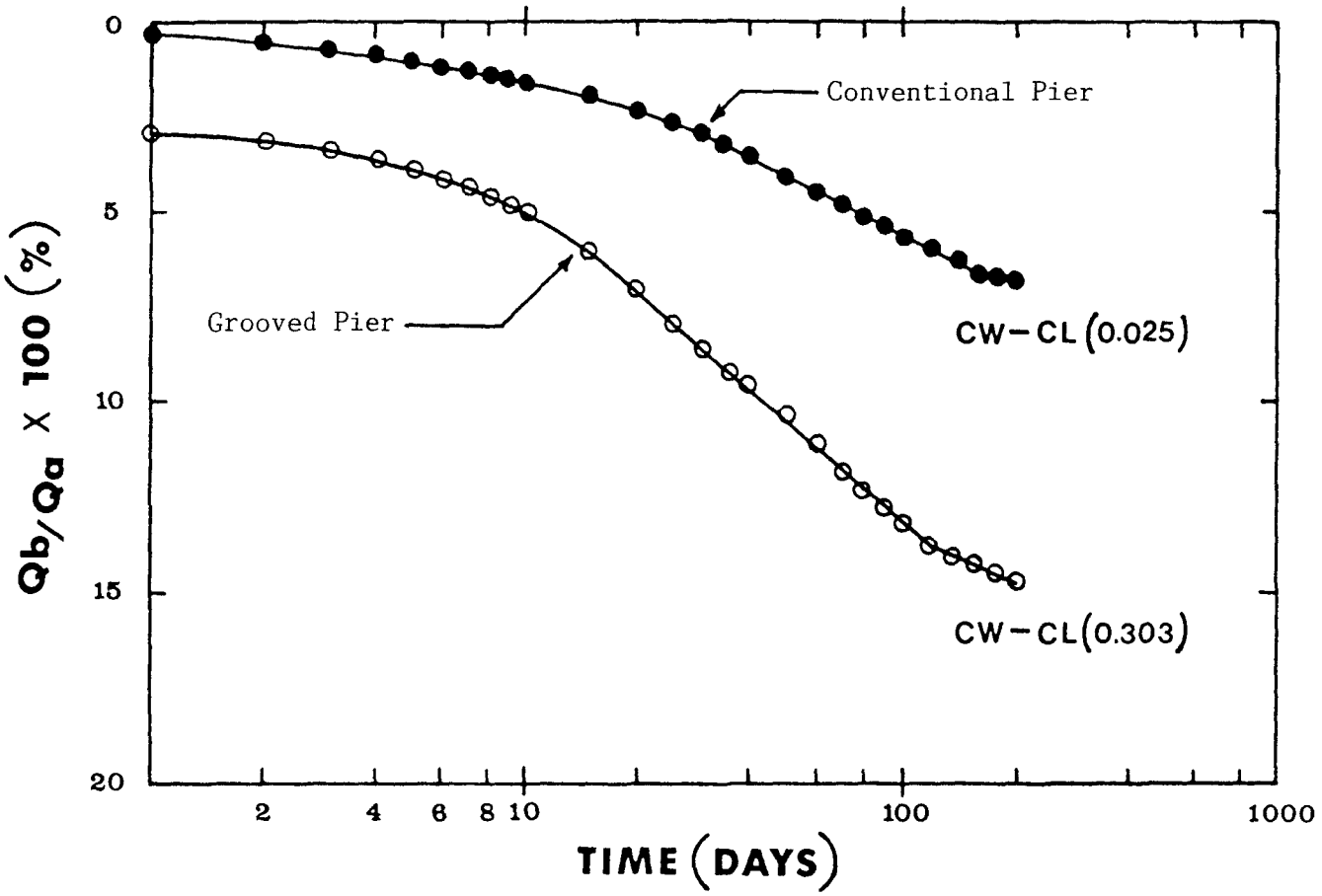

Fig. 9.12 Comparison of load transfer behaviour for conventional and grooved concrete pier.

(14.8 %) than for the grooved piers (6.8 %). This data suggests that creep along the pier-rock interface is greater for conventional (smooth) piers than for grooved (rough) piers.

9.4 COMPARISON OF CONVENTIONAL AND GROOVED PIERS

9.4.1 Time-Displacement Behaviour

In order to compare the behaviour of conventional and grooved piers, the normalized displacements are plotted against the log time in Figs. 9.13 and 9.14.

Normalized displacement, S_N, has been defined as:

$$(9.1) \quad S_N = \frac{E_s \ r_s}{Q_a} \ S$$

where E_s is secant Young's modulus of weak rock,

r_s is radius of socket,

Q_a is applied load, and

S is measured displacement.

Based on the normalized displacement, S_N, the results indicate that the initial displacement as well as the rate of creep are dependent on the relative roughness of the interface as measured by Roughness Factor (RF). The initial displacement and the creep rate increased with decreasing Roughness Factor (RF). These results are summarized in Table 9.2 and show that the relative roughness of the pier-rock interface has a significant influence on the long-term displacement behaviour of rock

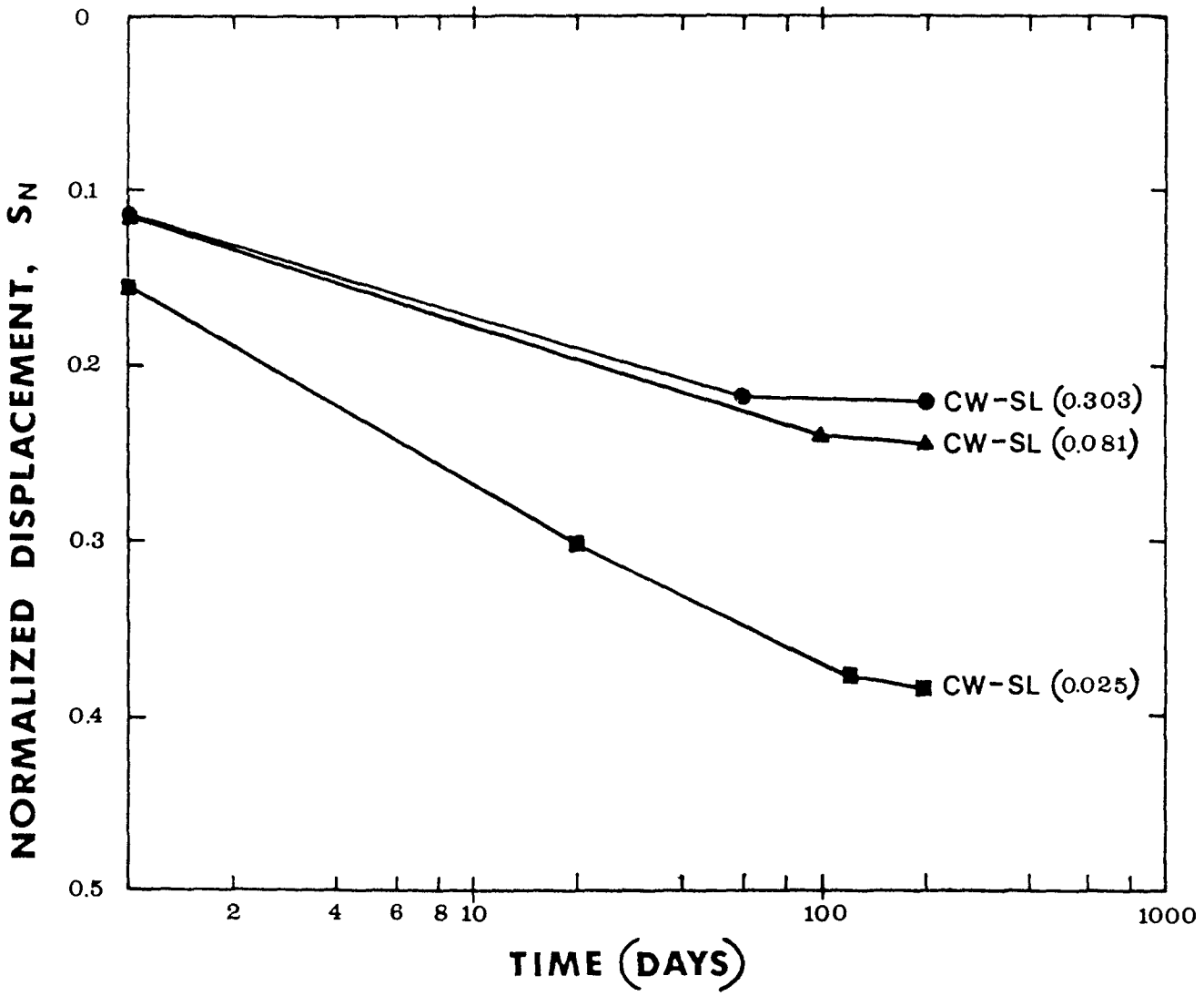

Fig. 9.13 Comparison of long-term (creep) behaviour of conventional and grooved concrete piers with shaft resistance only.

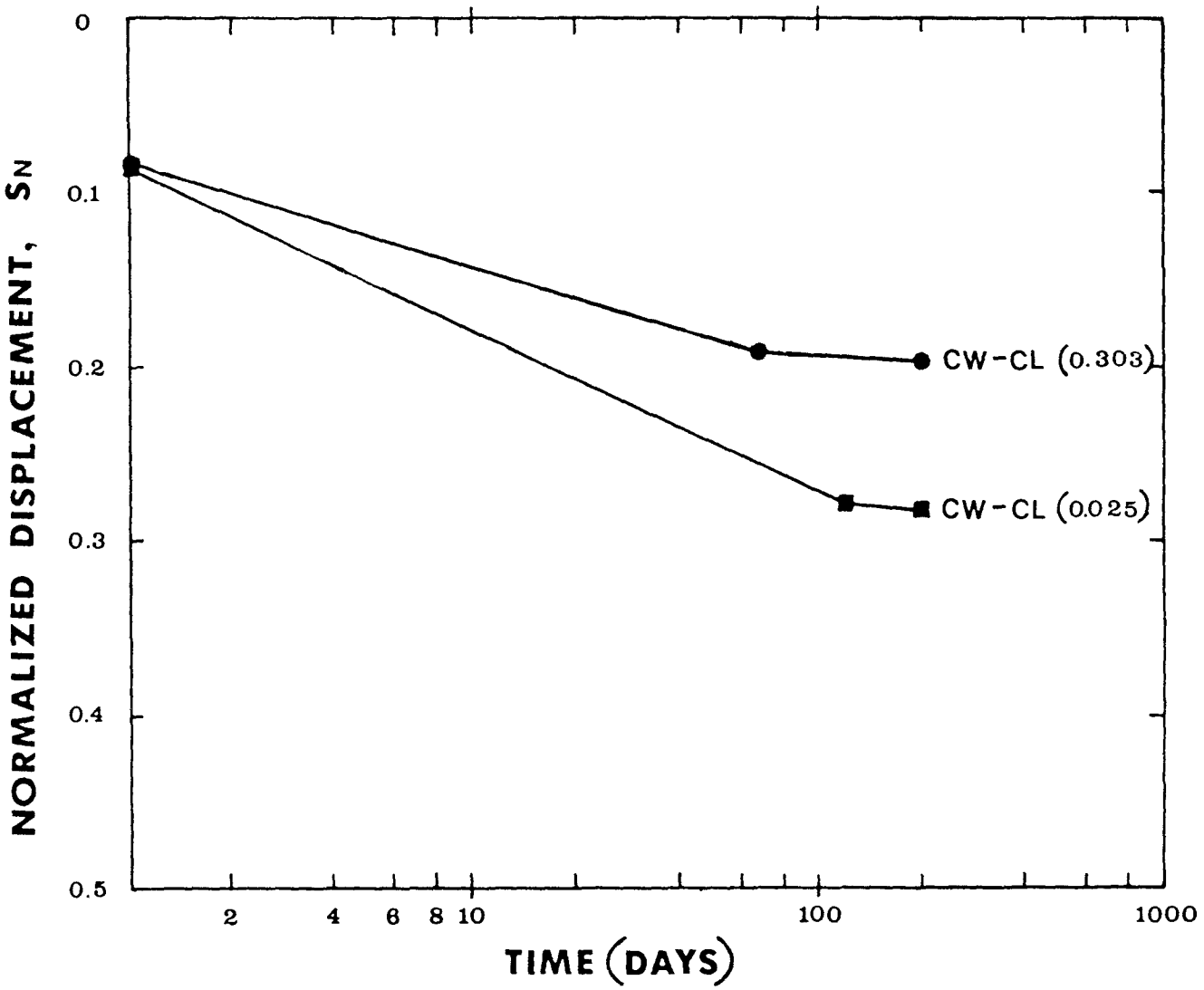

Fig. 9.14 Comparison of long-term (creep) behaviour of conventional and grooved concrete pier with combined shaft and end-bearing resistance.

TABLE 9.2 COMPARISON OF ROUGHNESS FACTOR (RF) WITH RATE OF CREEP BASED ON NORMALIZED DISPLACEMENT, S_N.

Pier Type	Pier Material	RF	Support Condition	Applied Load Q_a (kN)	Rate of Creep based on S_N	
					Primary	Secondary
Conventional	Concret	0.025	S	20.0	0.116	0.033
	Concret	0.025	C	20.0	0.094	0.025
Grooved	Concrete	0.081	S	31.1	0.064	0.012
	Concrete	0.303	S	62.3	0.058	0.008
	Concrete	0.303	C	62.3	0.061	0.010

S = Shaft Resistance Only

C = Combined Shaft ans End-Bearing Resistance

socketed pier foundations.

9.4.2 Transition to Secondary Creep

The results of the tests on the concrete model piers indicated that the rate of creep decreased significantly after a certain period of time. The time required to reach secondary creep was found to be strongly influenced by the shaft roughness. It can be seen from Figs. 9.13 and 9.14, that the time to secondary creep increased as the roughness factor decreased (Table 9.2).

This behaviour is comparable to the primary creep behaviour of short-bored piles in typical London clay soils reported by Green (1961). He observed that the end of the primary creep occured after 90 days and practically no movement was observed after 3 years.

Based on the present results, correlations between the Roughness Factor (RF) and time for the end of primary creep have been developed and plotted (Fig. 9.15).

It appears, therefore, that the relative roughness of the pier-rock interface has a significant influence on the time to the end of the primary creep behaviour of rock socketed pier foundations.

9.5 COMPARISON WITH FULL-SCALE AND SMALL-SCALE PIERS

The creep rate for the model piers tested are compared with the available published test data on full-scale and small-scale socketed piers in Table 9.3 and 9.4. The creep rate were calculated based on the

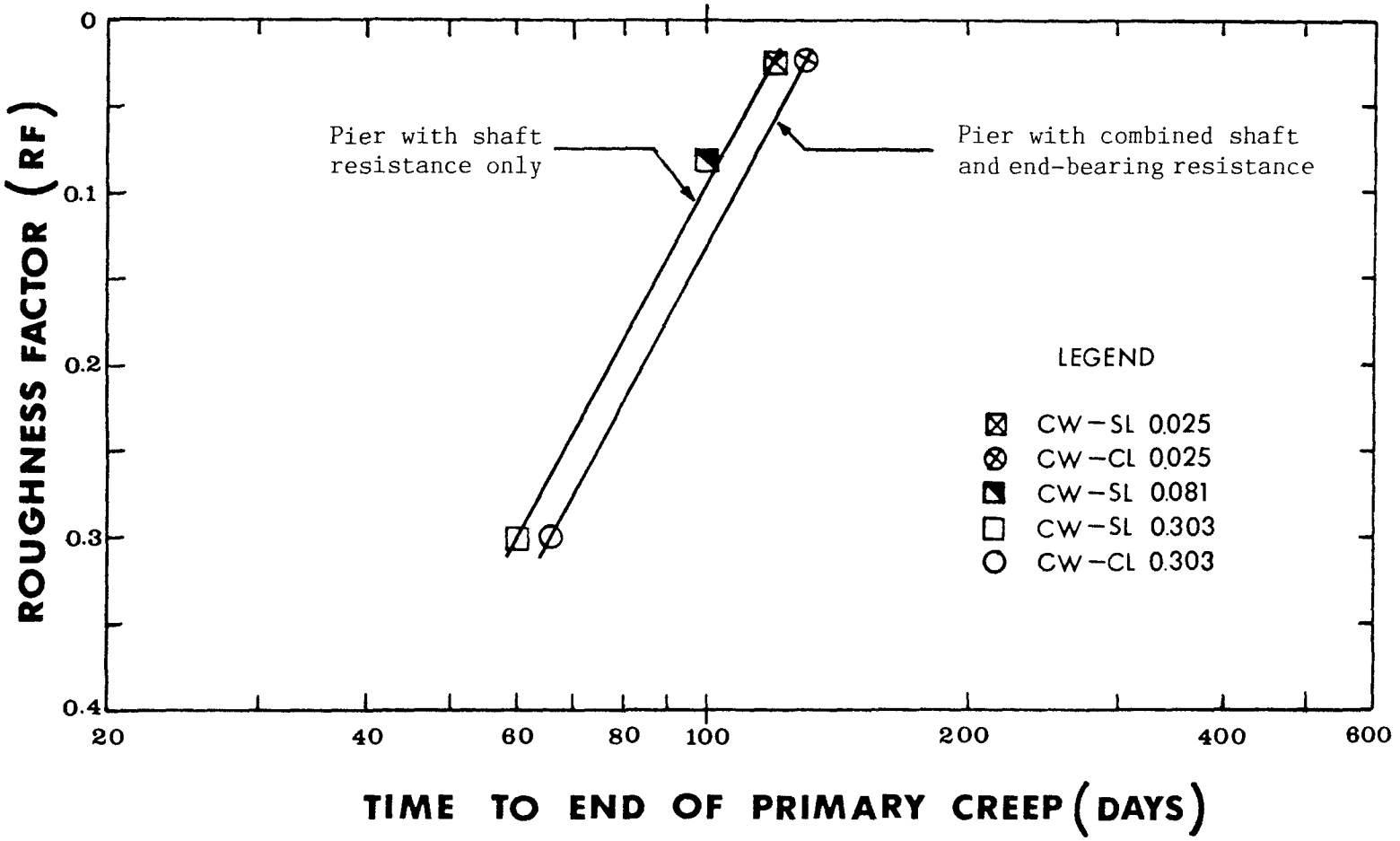

Fig. 9.15 Roughness factor versus time to end of primary creep behaviour for model concrete piers socketed in Queenston Shale

TABLE 9.3 COMPARISON OF CREEP RATE, C_r, FOR CONVENTIONAL SOCKETED PIERS.

Pier No	Socket Diameter D (mm)	Socket Length L_s (mm)	RF	Support Condition	Applied Load Q_s (kN)	Q_s/Q_E	Rock Type	Compressive Strength of Rock σ_c (MPa)	Duration of Testing Time t (Days)	Creep Rate C_r (mm/log cycle of time)	Normalised Creep Rate C_{rn} (mm/log cycle of time)	References
S5	1170	2510	0.008	S	4090	2.05	Mudstone*	0.59	0.042	1.0	0.489	Williams (1980)
S12	335	900	—	S	350	1.10	Mudstone*	0.58	0.021	0.353	0.328	Williams (1980)
S15	395	810	—	S	300	1.30	Mudstone*	0.58	0.021	0.411	0.316	Williams (1980)
M1	1220	2000	0.013	S	3390	2.11	Mudstone**	2.50	0.083	0.667	0.314	Williams (1980)
M2	1300	2000	0.032	S	3620	1.38	Mudstone**	2.30	0.083	0.333	0.241	Williams (1980)
P2	710	1170	0.025	C	6450	1.94	Queenston Shale	11.10	1.583	1.900	0.940	Horvath (1982)
CW-SL(0.025)	76.2	152.4	0.025	S	20	1.0	Queenston Shale	6.30	200.0	0.145	0.145	This Study
CW-CL(0.025)	76.2	152.4	0.025	C	20	0.85	Queenston Shale	7.50	200.0	0.094	0.110	This Study
SP-SL(0.033)	25.4	101.6	0.033	S	4.45	2.00	Pseudo Rock	16.20	14.0	0.028	0.019	This Study
SP-CL(0.033)	25.4	101.6	0.033	C	5.34	1.0	Pseudo Rock	16.20	180.0	0.006	0.006	This Study

S = Shaft Resistance Only

C = Combined Shaft and End-Bearing Resistance

* Highly Weathered

** Moderately Weathered

TABLE 9.4 COMPARISON OF CREEP RATE, C_r, FOR GROOVED PIERS.

Pier No	Socket Diameter D (mm)	Socket Length L_s (mm)	RF	Support Condition	Applied Load Q_s (kN)	Q_s/Q_E	Rock Type	Compressive Strength of Rock σ_c (MPa)	Duration of Testing Time t (Days)	Creep Rate C_r (mm/log cycle of time)	Normalised Creep Rate C_{rn} (mm/log cycle of time)	References
P4	710	1370	0.081	C	4450	1.93	Queenston Shale	5.53	1.75	0.490	0.253	Horvath (1982)
WC303/2	1580	2000	0.07	S	6000	1.33	Mudstone*	3.49	0.083	0.310	0.233	Williams (1980)
West Socket	610	1397	0.12	C	8896	2.0	Sandstone**	8.36	0.500	0.230	0.115	Glos and Briggs (1983)
CW-SL(0.081)	76.2	152.4	0.081	S	31.1	1.11	Queenston Shale	7.78	200.0	0.100	0.090	This Study
CW-SL(0.303)	76.2	152.4	0.303	S	62.3	1.41	Queenston Shale	4.00	200.0	0.292	0.207	This Study
CW-CL(0.303)	76.2	152.4	0.303	C	62.3	1.25	Queenston Shale	5.60	200.0	0.208	0.166	This Study

S = Shaft Resistance Only

C = Combined Shaft and End-Bearing Resistance

* Moderately to Slightly Weathered

** Soft Shaley

author's interpretation of published time-displacement data.

It can be seen from these comparisons that creep rate for the full-scale and small-scale piers vary widely. It is believed that this variation may be primarily due to the difference in the loading conditions which may be expressed in terms of the ratio Q_a/Q_E (where Q_a is the applied load and Q_E is the elastic load limit of the test pier), compressive strength of the weak rock, shaft roughness and time durations, t, employed for various tests (Table 9.3 and 9.4).

It should also be pointed out that the creep rate calculations on data by others were based on short duration tests and may not accuately reflect the true long-term behaviour.

It can be seen from Table 8.1, that the rate of creep increased with the increase in ratio Q_a/Q_E. This dependence of creep on the applied stress has been reported by Al-Shaikh-Ali and Davis (1975) and Wooley and Reese (1974). Normalized creep rate, C_{rn}, has, therefore, been used in this study which is defined as:

$$C_{rn} = \frac{Q_E}{Q_a} C_r \qquad (9.2)$$

where Q_E is load at linear elastic limit,

Q_a is applied load, and

C_r is measured creep rate.

The values of C_{rn} for the model socketed pier tests of the present study are given in Tables 9.3 and 9.4. The rate of creep data for the full-scale and small-scale tests reported in literature have been similarly treated and included in the Tables 9.3 and 9.4 for comparison.

9.6 COMPARISON OF SHORT-TERM AND LONG-TERM SETTLEMENTS

The results of the tests on the model socketed piers of the present study indicated that the settlement is significantly influenced by the relative roughness of pier-rock interface. The average ratio of long-term and short-term settlements was found to be about 3.3 for conventional socketed piers and 2.3 for grooved socketed piers. A summary of these short-term and long-term settlements are given in Table 9.5.

It can be seen from Table 9.5, that the ratio of long-term and short-term settlements of grooved piers was smaller than for conventional piers. This trend is believed to be due to the fact that while conventional piers derive the load capacity primarily through the bond and friction between the piers and the surrounding weak rock, the load capacity of the grooved piers is mainly due to shear strength of the weak rock material. The grooved piers, therefore, have larger resistance to settlements.

Similar trend regarding the increase in settlement due to sustained loading was reported for friction piles in clay soil, where the long-term and short-term settlements observed to be arround 2.8. For clays, the increase in the total settlement may be largely due to the

TABLE 9.5 COMPARISON OF SHORT-TERM AND LONG-TERM SETTLEMENTS.

Test Pier	Observed Settlement (% of D)			Normalized Settlement		
	Short-Term* S_s	Long-Term** S_L	S_L/S_s	Short-Term* S_{sn}	Long-Term** S_{Ln}	S_{Ln}/S_{sn}
CW-SL(0.025)	0.19	0.61	3.21	0.120	0.385	3.21
CW-CL(0.025)	0.11	0.38	3.45	0.081	0.281	3.45
CW-SL(0.081)	0.22	0.48	2.18	0.112	0.244	2.18
CW-SL(0.303)	0.59	1.45	2.37	0.093	0.220	2.37
CW-CL(0.303)	0.42	0.97	2.26	0.088	0.198	2.26

* Settlement measured 15 minute after applied design load

** Settlement measured 200 days after applied design load

consolidation of the soil (Eide et al. 1961).

The increase in total settlement due to sustained loading is generally believed to be due to the phenomenon called "load-shedding" (O'Neill and Reese 1970; Peck 1965; Wooley and Reese 1974). The "load-shedding" is a mechanism by which a slow and gradual transfer of the load along the length of the piers takes place as the top of the piers is maintained constant. This load transfer, in general, induces more settlement. However, in-case of piers with combined shaft and end-bearing resistance support, the load-shedding would also increase the base load which may in turn result in an increased settlement.

The results of the present study indicate that for design purpose, the long-term settlement for the conventional piers with relatively smooth socket (RF = 0.025) can be as much as 4 times the short-term settlement, whereas this ratio is less than 3 for piers with rough socket walls ($RF \geq 0.081$) (Table 9.5).

CHAPTER 10

ANALYSIS OF LONG-TERM (CREEP) SETTLEMENT IN SOCKETED PIERS

10.1 GENERAL

Weak rock is not an ideal elastic material and may experience creep even at normal working loads ($Q_a \leqq Q_{u/2}$). Field test on full and small-scale socketed piers indicated that the time-dependent deformation may be significant (Al-Shaikh-Ali 1977; Al-Shaikh-Ali and Davis 1975; Cole and Stroud 1977; Horvath 1982).

Booker and Poulos (1976) have presented an analytical method for predicting the long-term settlement of pile foundations in clay based on viscoelastic behaviour. This method has been adapted to the problem of long-term behaviour of socketed piers in weak rock. An outline of the method proposed by Booker and Poulos is given in section 10.2 and the suggested method for the estimating for weak rock in section 10.4.

10.2 VISCOELASTIC ANALYSIS FOR CREEP IN PILE FOUNDATIONS

A linear viscoelastic model for soil can be obtained by considering the spring and dashpot system given in Fig. 10.1. The stress-strain law for this model can be expressed by the differential equation:

$$(10.1)\quad \frac{\eta_2}{E_3}\dot{\sigma} + \left(1 + \frac{E_1}{E_3}\right)\sigma = E_1\varepsilon + \eta_2\dot{\varepsilon}$$

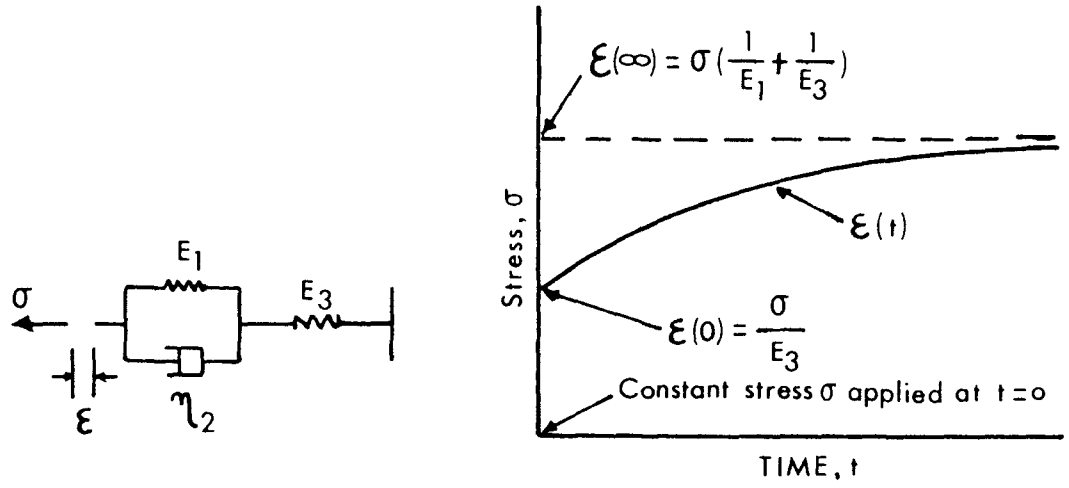

a) Three Element Model of a Visco-Elastic Material

b) Response Under Constant Stress

Fig. 10.1 Viscoelastic material response (after Booker and Poulos 1976).

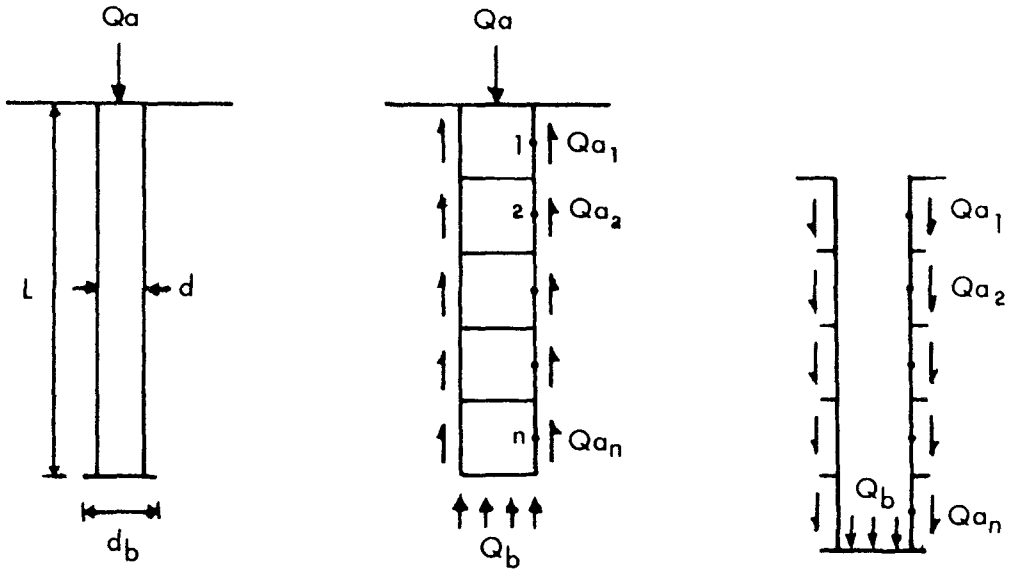

Pile Geometry

Stresses Acting on Pile

Stresses Acting on Soil

Fig. 10.2 Assumed stress conditions in and around the pile (after Booker and Poulos 1976).

where E_1, E_3 is spring stiffnesses for viscoelastic model,

σ is uniaxial stress,

ε is uniaxial strain, and

η_2 is dashpot viscosity.

Under condition of constant stress, σ_0, the strain as a function of time, is given by Booker and Poulos as:

$$\varepsilon(t) = \sigma_0 J(t) \tag{10.2}$$

where the creep function, J(t), is given by

$$J(t) = \frac{1}{E_3} + \frac{1}{E_1}\left\{1 - \exp\left(-\frac{E_1 t}{\eta_2}\right)\right\} \tag{10.3}$$

and is of form

$$J(t) = A + Be^{-\alpha t} \tag{10.4}$$

In addition they proposed a creep function of the form

$$J(t) = A + B \log (1 + \alpha t) \tag{10.5}$$

for soils that appear to creep indefinitely, where A, B and α are experimentaly define parameters.

Booker and Poulos indicated how the application of a Laplace transform converts a viscoelastic problem to an equivalent elastic problem. If it is possible to find an explicit solution of this trans-

form, the solution of the viscoelastic problem may be found by inversion of the Laplace transform, via the correspondence principle. They solved the pile problem (Fig. 10.2) using the method of influence coefficients or Boundary Element Method in Laplace transform space. They then invert the solution into real time to obtain engineering quantities of interest.

Booker and Poulos proposed solutions for the soil model in Fig. 10.1. The creep function for the soil is given by equation 10.5.

For a creep function of the general form of equation 10.4. Booker and Poulos stated that "larger settlements occur for the more compressible piles (smaller E_c/E_0), but the rate of increase of settlement with time does not appear to be sensitive to E_c/E_0. The proportion of load transferred to the base increase as E_c/E_0 increase, and that for a given E_c/E_0, this proportion increases with time, i,e., a gradual transfer of load occurs from the shaft to the base due to creep." Where E_c is Young's modulus of concrete and E_0 is the instantaneous Young's modulus of soil.

When the creep function was taken to be of the form of equation 10.5, Booker and Poulos noted that "the settlement of a pile in such a soil increases indefinitely while the proportion of base load and the stress distribution along the pile asymptotes to that for a rigid pile in an elastic soil."

Furthermore it was observed that the total settlement, S(t), at any time, t, of the pile in such a soil can be simply written as:

$$(10.6)\quad S(t) = \frac{Q_a}{d} I\, J(t)$$

where Q_a is applied load,

d is pile diameter, and

I is settlement influence factor for rigid pile in elastic soil (See Mattes 1969; Mattes and Poulos 1969).

"Because, with the soil model considered here, the settlement eventually increases linearly with log time, it is useful to characterize the creep settlement behaviour by the logarithmic creep settlement rate, C_r, i.e., the slope of the settlement versus (natural) log time relationship."

From equations 10.5 and 10.6

$$(10.7)\quad C_r = \frac{dS}{d(\log t)} = \frac{Q_a I B}{d}$$

Equations 10.6 and 10.7 can be used to estimate the time-dependent settlements. The parameters in the equations can be determined from tests. Booker and Poulos suggest the following procedure for determining the parameters, A, B and α:

1) The Parameter "A" maybe determined as:

$$(10.8)\quad A = \frac{1}{E'}$$

where E' is drained Young's modulus.

2) The parameter "B" can be determined from the logarithmic creep rate obtained from field test on the pile using equation 10.9.

$$B = \frac{C_r \, d}{Q_a \, I} \qquad (10.9)$$

3) The parameter "α" may be estimated with sufficient accuracy as:

$$\alpha = \frac{1}{t_\alpha} \qquad (10.10)$$

where t_α is the time obtained by extrapolating the linear portion of the settlement versus log time curve back to the horizontal line representing the sum of the immediate and consolidation settlements.

10.3 ADAPTION OF VISCOELASTIC ANALYSIS TO CREEP IN SOCKETED PIERS

The observed settlement versus log time curves were found to be linear for the model test piers (Figs. 10.3 to 10.7), an attempt is, therefore, made here to apply the results of the logarithmic creep function to long-term behaviour of socketed piers in weak rock.

The following important aspects were taken into account:

The calculation of parameters A, B and α for this case was done as follows.

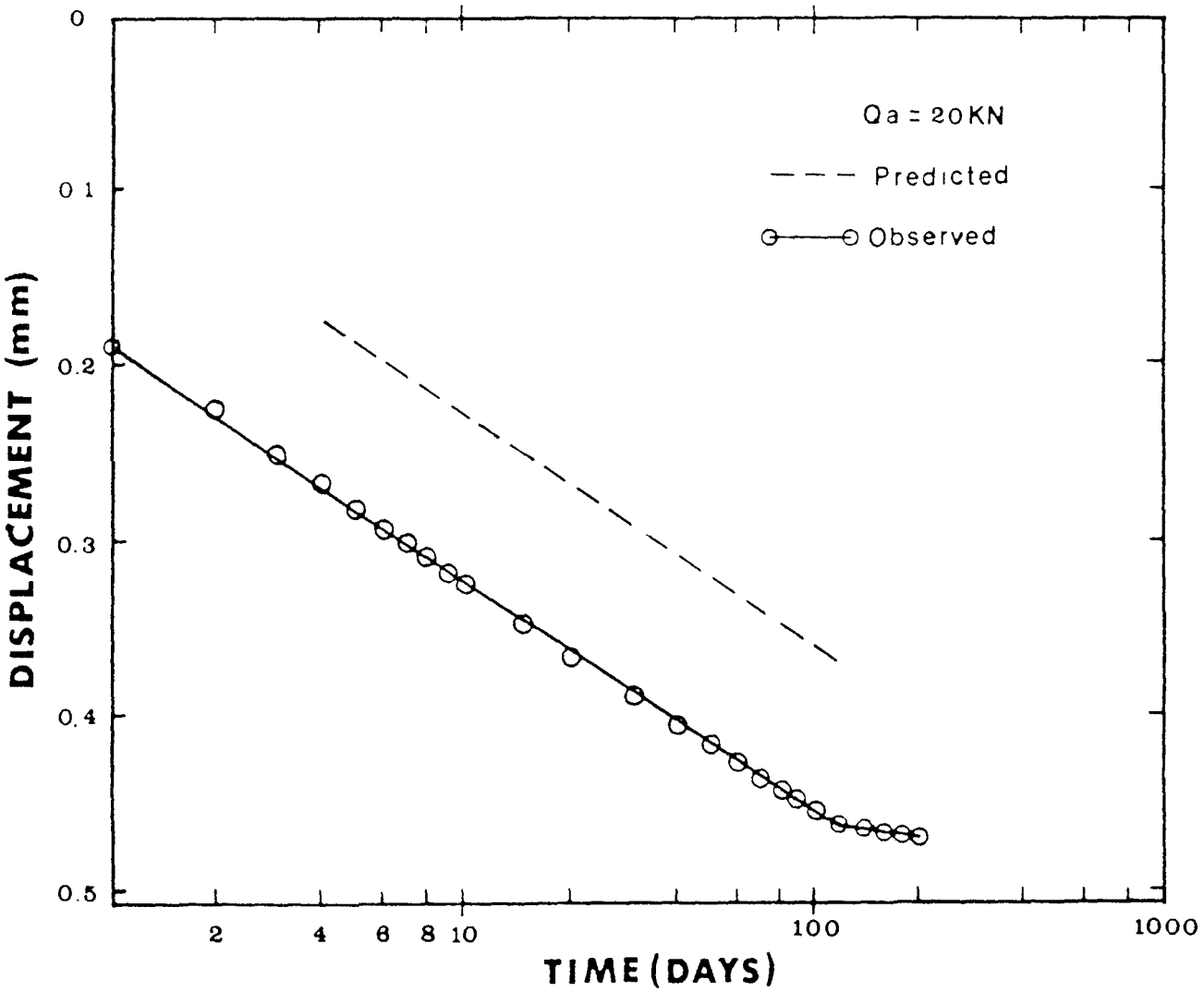

Fig. 10.3 Comparison of predicted and observed settlement for test pier with shaft resistance only, CW-SL(0.025).

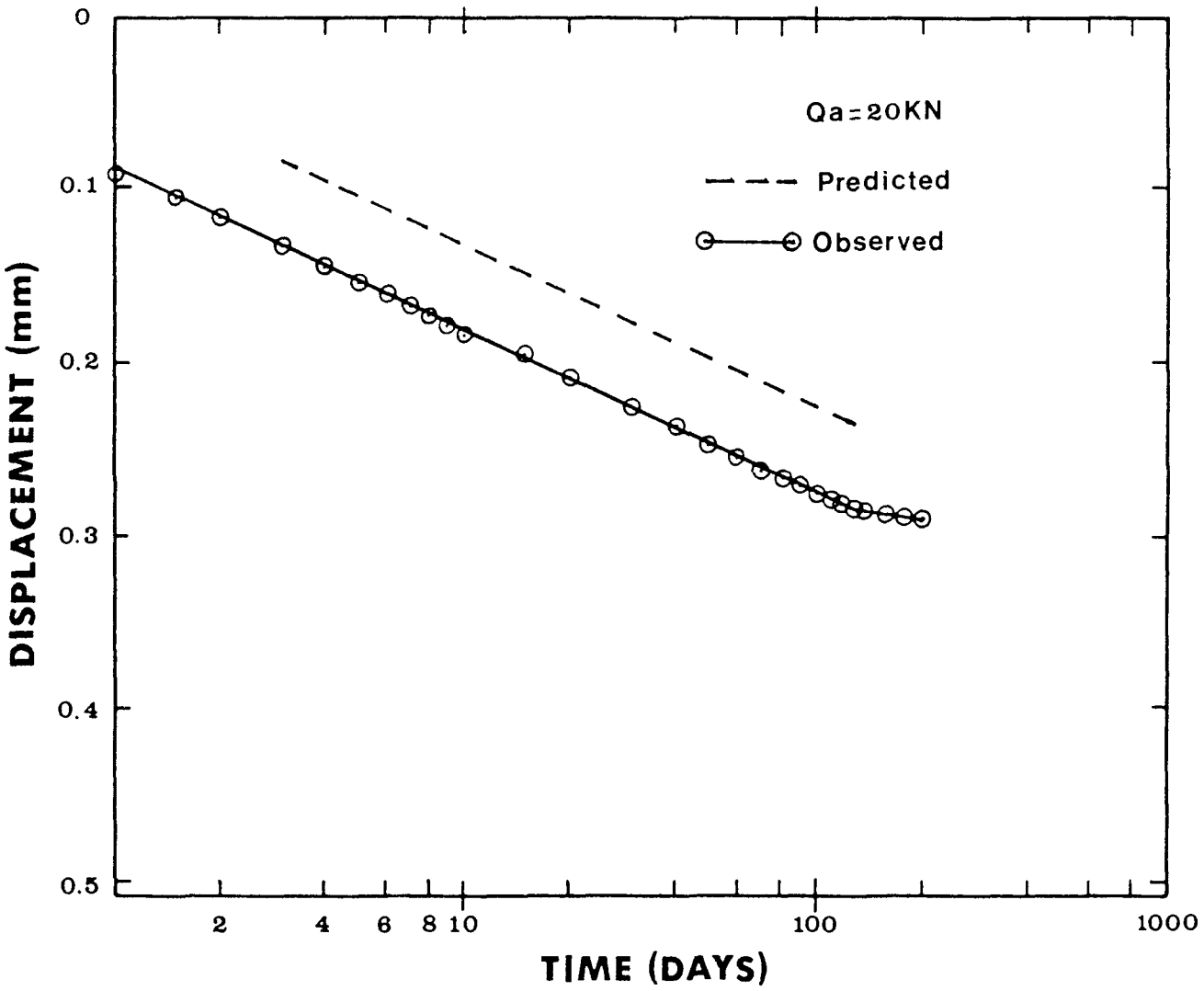

Fig. 10.4 Comparison of predicted and observed settlement for test pier with combined shaft and end-bearing resistance, CW-CL(0.025).

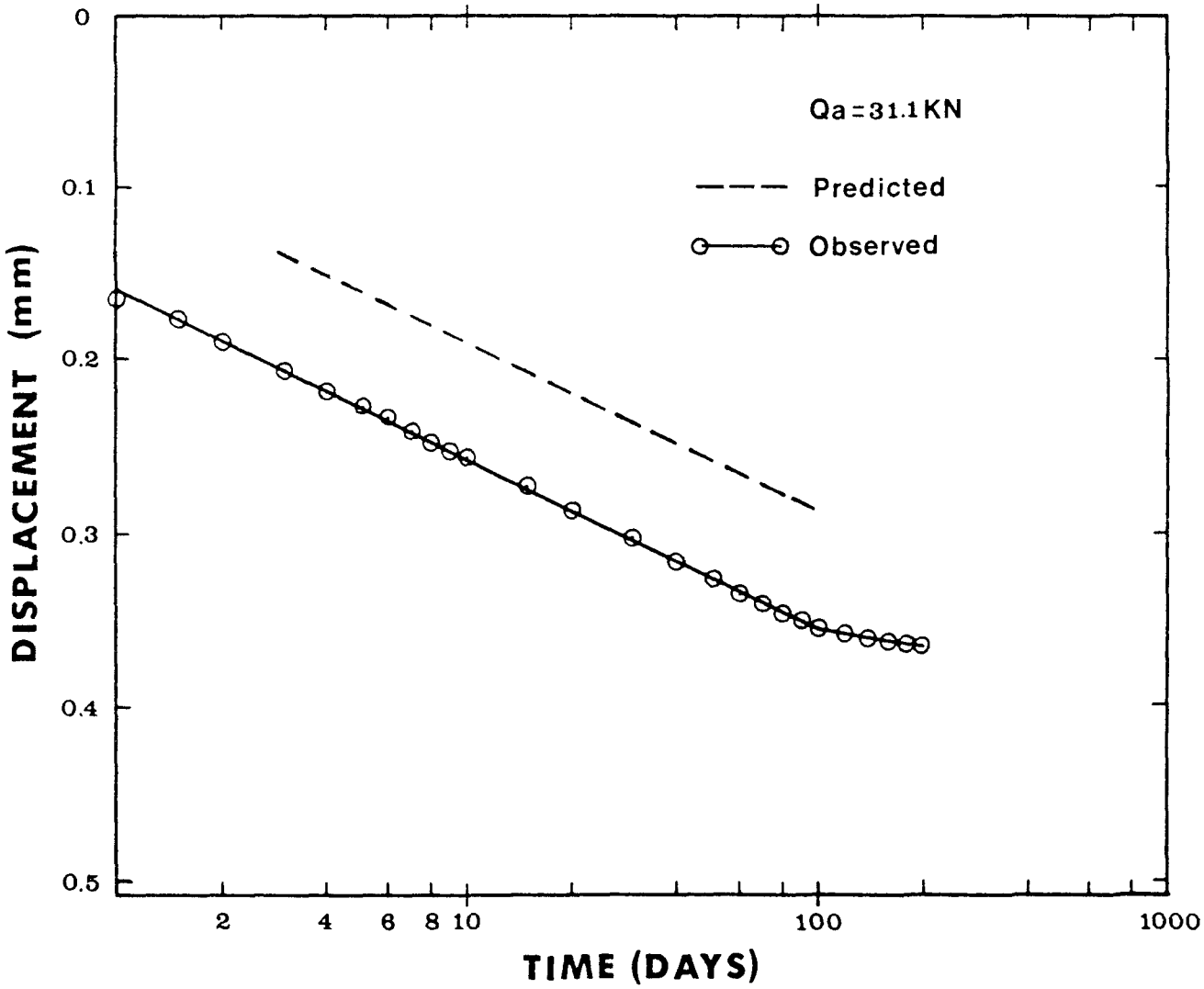

Fig. 10.5 Comparison of predicted and observed settlement for test pier with shaft resistance only, CW-SL(0.081).

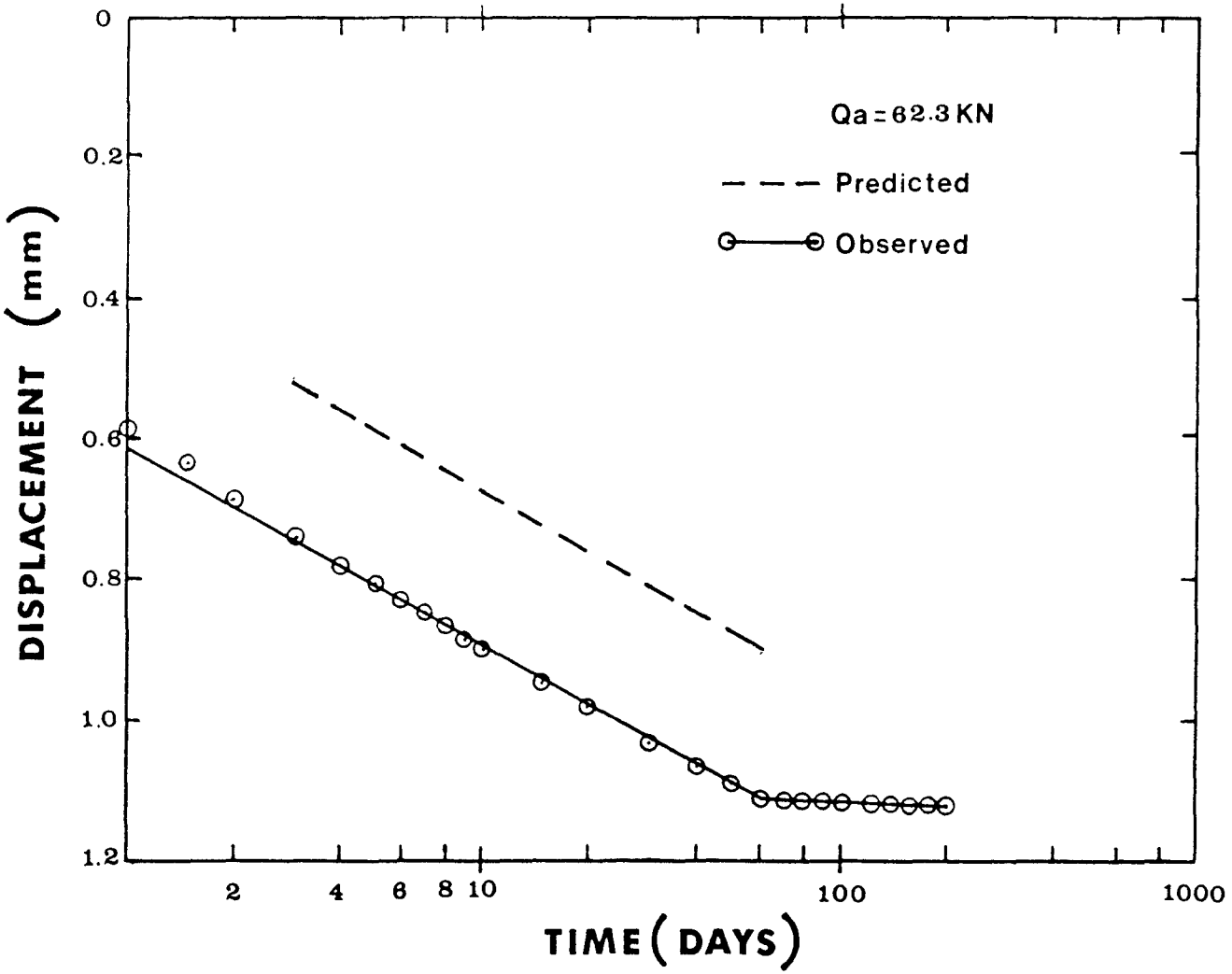

Fig. 10.6 Comparison of predicted and observed settlement for test pier with shaft resistance only, CW-SL(0.303).

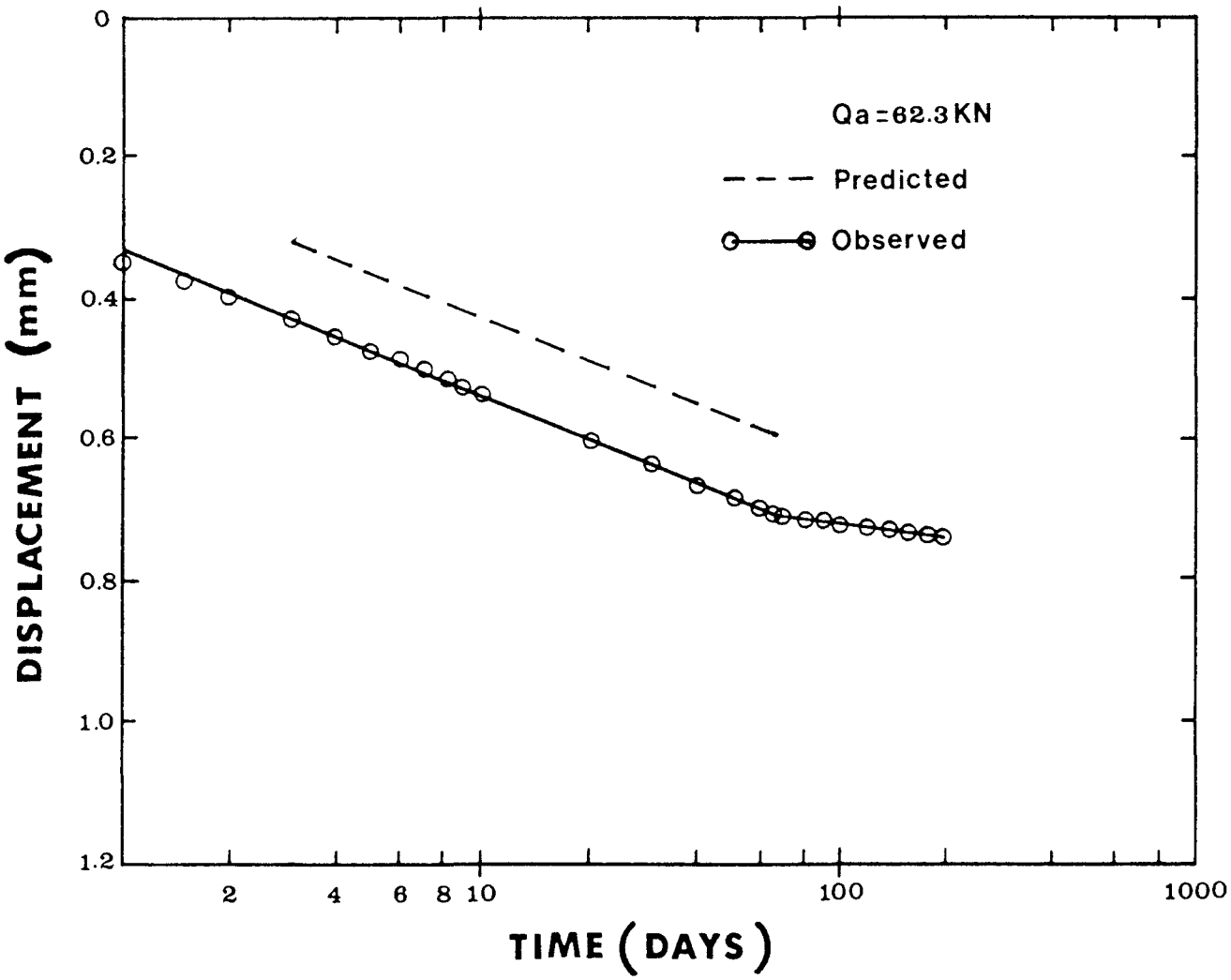

Fig. 10.7 Comparison of predicted and observed settlement for test pier with combined shaft and end-bearing resistance, CW-CL(0.303).

$$A = \frac{1}{E_r} \tag{10.11}$$

where E_r is the Young's modulus for weak rock back calculated from the pier load test as per Pells and Turner (1979).

$$B = \frac{C_r\ D}{Q_a\ I_s} \tag{10.12}$$

as in equation 10.9 but the settlement influence factor, I_s, as given by Pells and Turner (1979) was used (Figs. 10.8 and 10.9).

$$\alpha = \frac{1}{t_\alpha} \tag{10.13}$$

was calculated for each pier from the settlement versus log time plots as in equation 10.10.

Table 10.1 summarizes the value of creep parameters determined for each test pier. Settlement were calculated for each test pier using equation 10.6

It can be seen that the predicted settlement-log time curves (Figs. 10.3 to 10.7), are above but approximately parallel to the observed values. In addition the test piers show a secondary creep curve which is not predicted by equation 10.5.

The following modifications were introduced to adjust the predicted settlements to the observed values. Modified creep function,

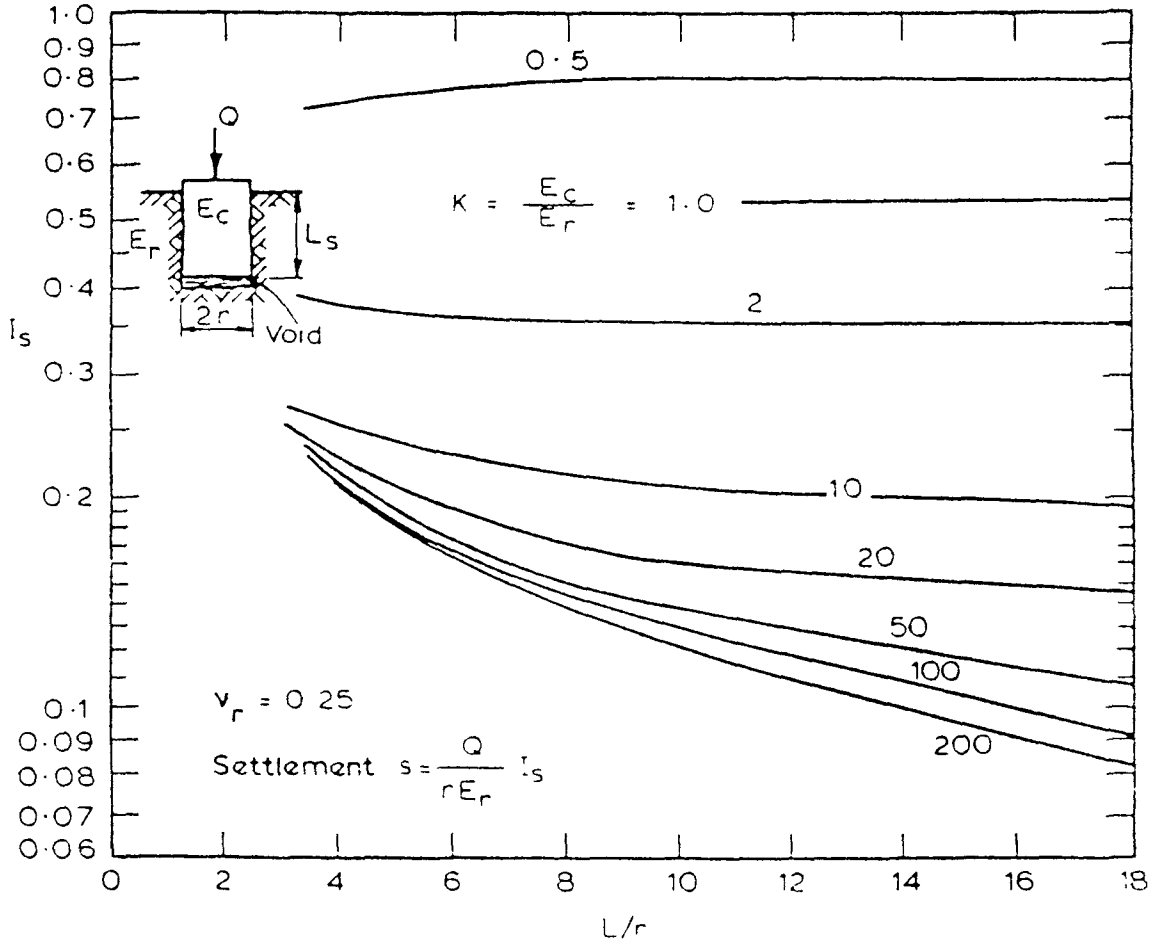

Fig. 10.8 Elastic settlement of a shear socket (after Pells and Turner 1979).

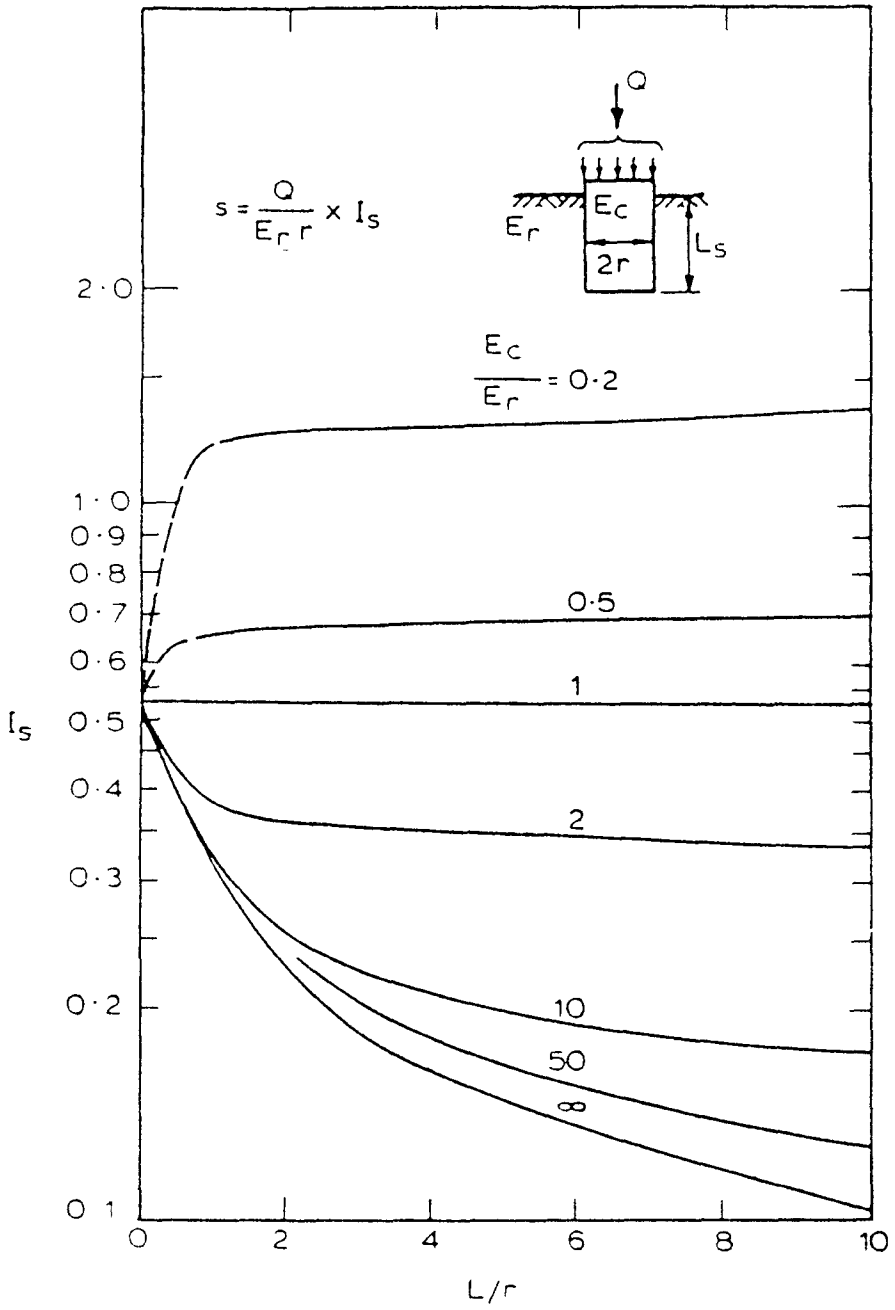

Fig. 10.9 Elastic settlement of a complete rock socket (after Pells and Turner 1979).

TABLE 10.1 SUMMARY OF CREEP FUNCTION, J(t), PARAMETERS FOR TEST PIERS IN QUEENSTON SHALE.

Pier No.	Diameter D (mm)	Length L_s (mm)	L_s/D	E_c (GPa)	E_r (MPa)	E_c/E_r	Creep Function Parameter A (mm^2/kN)	Creep Function Parameter B (mm^2/kN)	Creep Function Parameter α (1/t)	Factor n	References
CW-SL(0.025)	76.2	152.4	2.0	31.9	879	36.3	1.1377×10^{-6}	2.4553×10^{-6}	1.0	2.50	This Study
CW-CL(0.025)	76.2	152.4	2.0	31.9	1573	20.3	6.3570×10^{-7}	1.7470×10^{-6}	1.0	2.35	This Study
CW-SL(0.081)	76.2	152.4	2.0	31.9	1116	28.6	8.9610×10^{-7}	1.0890×10^{-6}	1.0	1.85	This Study
CW-SL(0.303)	76.2	152.4	2.0	31.9	830	38.4	1.2048×10^{-6}	1.5873×10^{-6}	3.3	1.70	This Study
CW-CL(0.303)	76.2	152.4	2.0	31.9	800	39.8	1.2500×10^{-6}	1.3390×10^{-6}	1.0	1.62	This Study
P2(0.025)	710	1370	1.9	41.4	290	146.9	3.4483×10^{-6}	1.68410×10^{-6}	2.5	2.43	Horvath (1982)
P4(0.081)	710	1370	1.9	41.4	310	133.5	3.2258×10^{-6}	4.43200×10^{-7}	1.0	1.70	Horvath (1982)

E_c = Concrete Pier Young's Modulus

E_r = Back-Calculated Rock Young's Modulus

$J(t)^*$, is given by:

(10.14) $$J(t)^* = nA + B \log (1 + \alpha t)$$

and the settlement time relationship is given by:

(10.15) $$S(t) = \frac{Q_a}{D} I_s J(t)^* \qquad \text{for } t < t_p$$

It may be point out that the settlement - log time behaviour of socketed piers is composed of two parts: primary and secondary. Figures (10.3 to 10.7) indicate that secondary creep rate is significantly lower than the primary creep rate. Disregarding this break in the settlement-log time curve would, therefore, lead to a gross overestimation of the prediction of long-term settlements. The average secondary creep rate for Queenston Shale has been found to be 0.033 mm (0.0013 in) per log cycle of time (Table 9.1), while primary creep rate varies between 0.1 mm (0.0039 in) per log cycle of time to 0.292 mm (0.0115 in) per log cycle of time. The following equation is now proposed to take this into account:

(10.16) $$S(t) = \frac{Q_a}{D} I_s J(t)^* + 0.033 (\log t - \log t_p)$$

$$\text{for } t > t_p$$

where t_p is the time of termination of primary creep in days. For test piers of the study t_p is given in Table 9.1.

The factor, n, introduced in equation 10.14 is found to vary between 1.62 to 2.50 and is given in Table 10.1. The factor, n, appeared

to be a function of the Roughness Factor (RF) and is plotted against RF in Fig. 10.10.

To conclude, from the results of model test, the creep function parameters A, B and α were calculated from test data. It was found that test results could be reasonably predicted using equations 10.15 and 10.16.

10.4 SUGGESTED METHOD FOR ESTIMATING LONG-TERM SETTLEMENTS IN SOCKETED PIERS

Data from a variety of field and laboratory test may be used to provide useful informations of long-term settlements in the field. Since socketed piers are constructed in different types of weak rock, the creep rate is affected by many factors, the most important of which are stress level, pier-rock interface and rock material properties. In order to account for these variation of properties, creep rates determined from published data as well as model test were normalized as per equation 9.2. This normalized creep rate, C_{rn}, is plotted as a function of the compressive strength of weak rock in Fig. 10.11 and Table 9.3 and 9.4

The following method is suggested for estimating long-term settlement of weak rock in practice.

1) Determine the Young's modulus of weak rock, E_r, back figured from pier load test as per Pells and Turner (1979). The value of "A" can be calculated using equation 10.11.

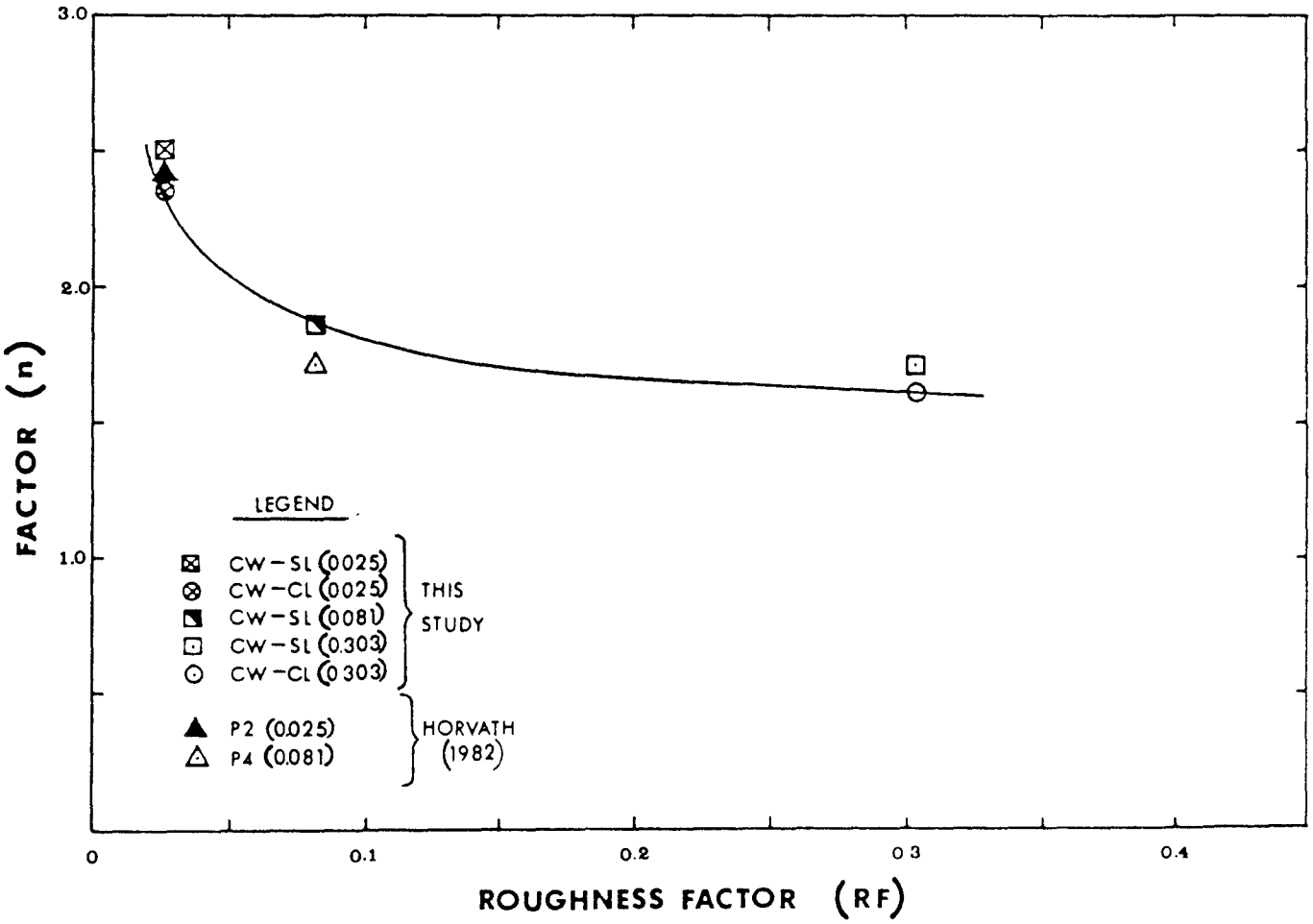

Fig. 10.10 Factor, n, versus Roughness Factor (RF) for test piers in weak rock (Queenston Shale).

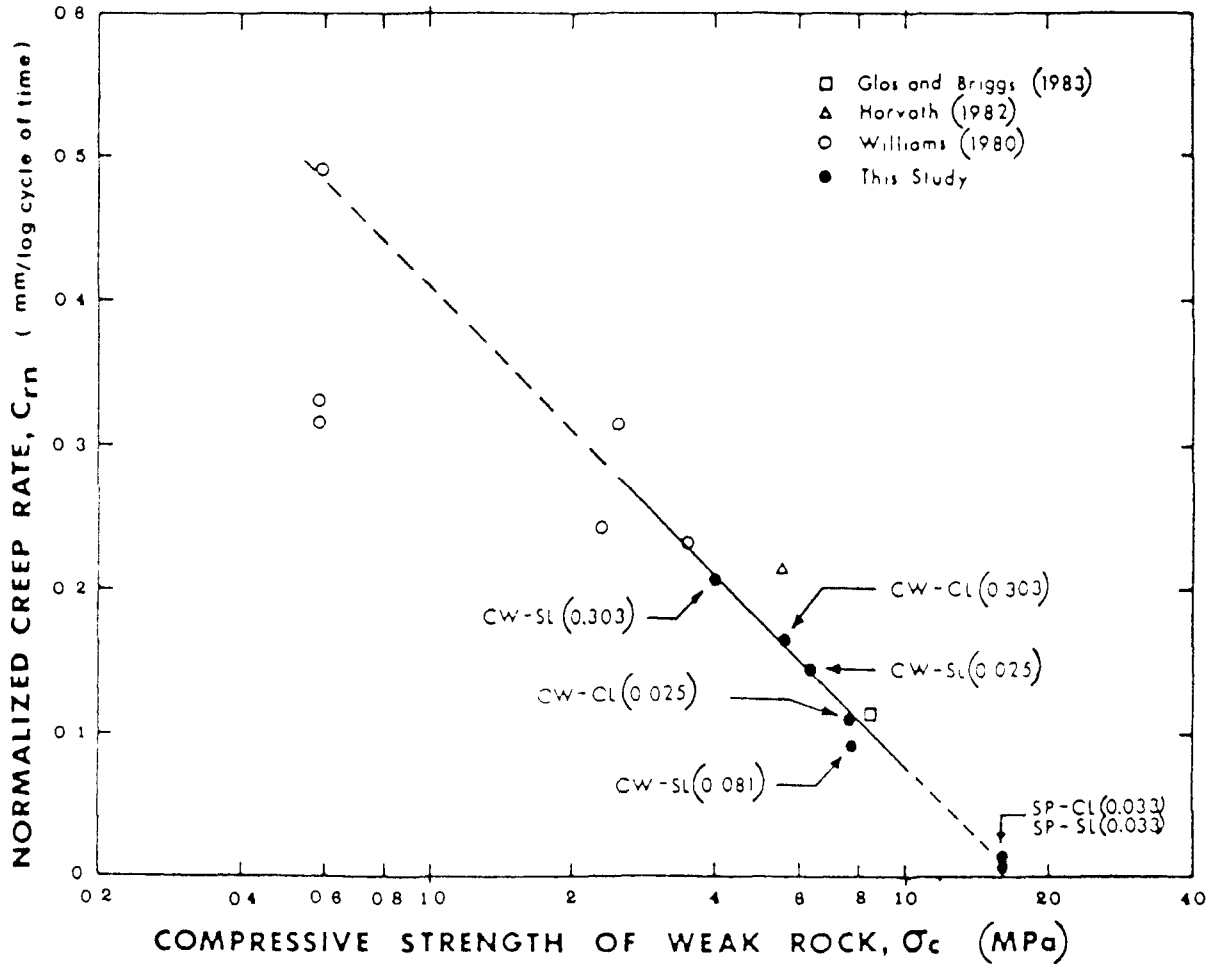

Fig. 10.11 Normalized creep rate, C_{rn}, versus compressive strength of weak rock, σ_c, for piers in weak rock.

$$A = \frac{1}{E_r}$$

2) Dependant on the compressive strength of weak rock, a normalized creep rate, C_{rn}, is obtained from Fig. 10.11. Calculate "B" using C_{rn} in equation 10.12, the parameter "B" is, therefore, calculated as per the following relation:

$$B = \frac{C_{rn}\, D}{Q_E\ I_s} \qquad (10.17)$$

3) The value of parameter "α" may be determined from the settlement versus log time curves as:

$$\alpha = \frac{1}{t_\alpha}$$

The model tests of present study indicated that for the weak rock (Queenston Shale), the value of α can be taken as 1.0 (Table 10.1).

4) The factor, n, for use in equation 10.14 can be estimated from Fig. 10.10. Roughness Factor (RF) can be calculated by equation 2.1 as per Horvath (1982).

$$RF = \frac{\bar{\Delta r}}{r_s} \times \frac{L_t}{L_s}$$

5) The time for the completion of the primary creep, t_p, for piers in weak rock maybe estimated from Fig. 9.15.

6) The modified creep function, $J(t)^*$, may then be calculated using equation 10.14 and the calculated values of parameters, A, B and α and factor, n, and time, t.

$$J(t)^* = nA + B \log (1 + \alpha t)$$

7) The estimated total settlement, S(t), may then be determined using equations 10.15 and 10.16 using the socket pier settlement influence factor, I_s, as per Pells and Turner (1979).

$$S(t) = \frac{Q_a}{D} I_s J(t)^* \qquad \text{for } t < t_p$$

$$S(t) = \frac{Q_a}{D} I_s J(t)^* + 0.033(\log t - \log t_p)$$

$$\text{for } t > t_p$$

CHAPTER 11

CONCLUSIONS

11.1 GENERAL

This study was undertaken to obtain a better understanding of the long-term behaviour of drilled piers socketed in weak rock. The results of this study clearly indicate that for short-term and long-term conditions, the performance of grooved socketed piers are better than that of conventional socketed piers.

11.2 LONG-TERM TEST

11.2.1 Settlement Behaviour

The settlement performance of the grooved socketed piers was found to be superior to that exhibited by the conventional socketed piers. Based on normalized settlement, S_n, the total settlement (200 days) of conventional concrete piers (RF = 0.025) was about 1.5 times the settlement for the grooved socketed piers (RF = 0.303) (Figs. 9.13 and 9.14).

The ratio of the long-term and short-term settlement was found to be about 3.3 and 2.3 for the conventional (RF = 0.025) and grooved (RF = 0.303) socketed piers respectively (Table 9.4).

The present study indicates that although satisfactory from the load point of view, the design method based on short-term load test may

not be satisfactory from the settlement point view.

11.2.2 Rate of Creep

Primary and secondary creep rate was observed for the concrete model piers. These creep rates were found to largely depend on the stress level, the compressive strength of weak rock and the roughness of the pier-rock interface. Based on normalized displacement, S_n, the initial displacement and the creep rate for piers were found to increase with decreasing roughness of socket wall (Table 9.1 and Figs. 9.13 and 9.14).

Test on the concrete model piers showed that the rate of creep decreased after a certain period of time. The time for the transition from primary to secondary creep was found to be greater for piers with lower roughness of the pier-rock interface (Table 9.1).

11.2.3 Load Transfer Behaviour

Both the steel and the concrete model piers exhibited load-redistribution effect under sustained loading. Tests on steel model pier, SP-CL(0.033), showed that the magnitude of the load transferred to the base increased with time. The average increase in base load due to load-redistribution effect was found to be around 3.0 % of applied load, Q_a, for up to the elastic loading range ($Q_a = Q_E$) (Table 8.3).

For steel model pier, SP-CL(0.033), the measured value of load transferred to the base were found to be reasonably agreement with the

values obtained using the elastic analysis. As pointed out earlier, the discrepancies observed between the measured value and the estimated values from the elastic analysis in case of concrete piers are believed to be due to the lower sensitivity of the load measuring system with flat jack load cells. However, the qualitative comparison of the values confirm that percent load transfer to the base is greater for conventional pier than for grooved pier (Fig. 9.12).

11.3 ESTIMATING LONG-TERM BEHAVIOUR OF SOCKET PIER

The settlements calculated using the Booker and Poulos (1976) method for piles in clay soils were compared with those obtained for the concrete model socketed piers in weak rock. The Young's modulus of rock, E_r, and settlement influence factor, I_s, for the socket pier (Pells and Turner 1979) were used in the calculations. The predicted values were found to be in all cases smaller than those observed values (Figs. 10.3 to 10.7). The original Booker and Poulos method was, therefore, modified. The suggested method for the estimation of the long-term settlement of socket pier is given in section 10.4.

11.4 SHORT-TERM TEST

The major conclusions obtained from short-term tests on model piers are given below:

11.4.1 Shaft Resistance

The value of the shaft resistance at failure, q_{sf}, for the gro-

oved piers was found to be about 3 times the value of the shaft resistance compared to the conventional piers (Table 6.4). The shaft resistance to failure occured at the displacement of 0.29 % of pier diameter for concrete conventional pier and 0.85 % of pier diameter for grooved pier (Table 6.4).

11.4.2 Load Transfer

The load transfer data for the model steel pier were found to agree with the elastic analysis (Table 7.2). However, the system used for the measurement of base load in case of concrete model piers did not function as anticipated. The test results for the concrete piers were found to be not in agreement with the values estimated using the elastic analysis.

CHAPTER 12

RECOMMENDATIONS

The present study indicates that additional studies should be carried out in order to obtain further understanding of socket pier behaviour under long-term loading condition. The possible research areas are briefly outlined in the following sections.

12.1 TIME-DISPLACEMENT

Time-settlement behaviour of full-scale socket piers should be studied using long-term field loading tests. The results obtained from full-scale tests could then be compared with the available published results. Creep parameters obtained from this model study and the analytical methods proposed in this study for predicting long-term behaviour could be verified.

12.2 LOAD DISTRIBUTION AND LOAD TRANSFER

The long-term behaviour of load distribution along the pier shaft and load transfer to the base of the pier should be studied further both for model and full-scale socket piers.

12.3 ROUGHNESS OF PIER-ROCK INTERFACE

Further study should investigate the effects of roughness of pier-rock interface on the long-term behaviour of socket piers. Also,

at a given Roughness Factor (RF), the effects of shape of grooves should be examined.

12.4 RADIAL STRESS

Grooved socket piers may induce a large amount of radial stress. It is, therefore, be of interest to study the distribution of the radial stress affected by the loading conditions, grooves and roughness of pier-rock interface.

12.5 MEASURING DEVICES

Experience gained in the present research show that the load measuring system used, comprising of flat jack load cells and pressure gauges, were not sensitive enough for the small-scale model tests. The load measurements were found to be affected by the room temperature.

Further studies are, therefore, suggested to improve load measuring technique or to modify the existing ones for use in the long-term testing of socket piers.

12.6 FACTOR, n, AND NORMALIZED CREEP RATE, C_{rn}.

The relationships for factor, n, (Fig. 10.10) and normalized creep rate, C_{rn}, (Fig. 10.11) presented in this report are based on a very limited amount of data. Further study is suggested to better define these parameters for successful application to the actual design problems.

REFERENCES

Al-Shaikh-Ali, M.M.H. 1977. Rock socket piles at Coventry Point, Market Way, Coventry: Discussion. Symposium on Piles in Weak Rock, ICE, London, pp. 205-208.

Al-Shaikh-Ali, M.M.H., and Davis, A.G. 1975. The in-situ creep in soft rocks using a prolonged model pile test. Proceedings of the Istanbul Conference on Soil Mechanics and Foundation Engineering. pp. 213-229.

Aurora, R.P., and Reese, L.C. 1976. Behaviour of axially loaded drilled shaft in clay-shales. Research Report 176-4, Centre for Highway Research, The University of Texas at Austin, Austin, Texas.

Bauer, G.E. 1980. The measurement and analysis of load transfer from a caisson to its rock socket. Proceedings of the International Conference on Structural Foundation on Rock, Sydney, Australia. Edited by P.J.N. Pells, Vol. 1, pp. 235-240.

Bjerrum, L. 1967. Progressive failure in slops of overconsolidated plastic clay and clay shale. Journal of the Soil Mechanics and Foundations Division, ASCE, Vol. 93, No. SM5, pp. 1-49.

Bjerrum, L. 1973. Problems of soil mechanics and construction on soft clays and structurally unstable soils. Proceedings, 8th International Conference on Soil Mechanics and Foundation Engineering. Session 4, Moscow, pp. 111-159.

Booker, J.R., and Poulos, H.G. 1976. Analysis of creep settlement of pile foundation. Journal of the Geotechnical Engineering Division, ASCE, Vol. 102, No. GT1, pp. 1-14.

Butler, H.D., and Hoy, H.E. 1977. Users manual for the Texas quick-load method for foundation load testing. Federal Highway Administration, Office of Development, Washington.

Casagrande, A. 1948. Classification and identification of soils. Transactions, ASCE, Vol. 113, pp. 901-930.

Casagrande, A., and Wilson, S.D. 1951. Effect of rate of loading on the strength of clays and shales at constant water content. Geotechnique, Vol. 2, No. 3, pp. 251-263.

Chellis, R.D. 1961. Pile foundations. McGraw-Hill Book Co., Inc., New York

Coates, D.F., and Yu, Y.S. 1970. Three dimensional stress distributions around a cylindrical hole and anchor. Proceedings, 2nd Congress International Society of Rock Mechanics, Belgrade, Vol. 3, pp. 175-182.

Cole, K.W., and Stroud, M.A. 1977. Rock socket piles at Coventry Point Market Way, Coventry. Symposium on Piles in Weak Rock, ICE, London, pp. 47-62.

Davies, P., Webb, D.L., Hooley, P., and Yeats, J.A. 1979. Geotechnical parameters for design of bored piles founded in weathered siltstone rock. Proceedings, 7th European Conference on Soil Mechanics and Foundation Engineering. pp. 43-50.

Deere, D.U. 1968. Geological considerations. in Rock Mechanics in Engineering Practis. Edited by K.G. Stagg and O.C. Zienkiewicz, John Wiley & Sons Ltd., London, pp. 1-54.

Donald, I.B., Chiu, H.K., and Sloan, S.W. 1980. Theoretical analyses of rock socketed piles. Proceedings of the International Conference on Structural Foundations on Rock, Sydney, Australia. Edited by P.J.N. Pells, Vol. 1, pp. 303-316.

Edide, O., Hutchinson, J.N., and Landva, A. 1961. Short and long-term test loading of a friction pile in clay. Proceedings, 5th International Conference on Soil Mechanics and Foundation Engineering. Paris, Vol. 2, pp. 45-53.

Ellison, R.D., D'Appolonia, E., and Thiers, G.R. 1971. Load deformation mechanism for bored piles. Journal of the Soil Mechanics and Foundations Division, ASCE, Vol. 97, No. SM4, pp. 661-678.

England, G.L. 1965. Method of estimating creep and shrinkage strains in concrete from properties of constituent materials. Journal of ACI, Vol. 62, No. 11, pp. 1411-1418.

Freeman, C.F., Klajnerman, D., and Prasad, G.D. 1972. Design of deep socketed caissons into shale bedrock. Canadian Geotechnical Journal, Vol. 9, pp. 105-114.

Freudenthal, A.M., and Roll, F. 1958. Creep and creep recovery of concrete under high compressive stress. Journal of ACI, Vol. 29, No. 12, pp. 1111-1141.

Gamble, J.C. 1971. Durability-plasticity classification of shales and other argillaceous rocks. Ph. D Thesis, University of Illinois.

Gibson, G.L. 1973. Field and laboratory investigation for a multi-story building founded in sound limestone. Master of Engineering Thesis, Carleton University, Ottawa.

Glos, G.H., and Briggs, O.H. 1983. Rock sockets in soft rock. Journal of the Geotechnical Engineering Division, ASCE, Vol. 109, No. GT4, pp. 525-535.

Green, H. 1961. Long-term loading of short-bored piles. Geotechnique, Vol. 11, No. 1, pp. 47-53.

Goodman, R.E. 1980. Introduction to rock mechanics. John Wiley & Sons, New York.

Guillet, G.R. 1977. Clay and shale deposits of Ontario. Ontario Geological Survey Mineral Deposits Circular MDC 15, Ministty of Natural Resources.

Horvath, R.G. 1982. Behaviour of rock-socketed drilled pier foundation. Ph. D. Thesis, University of Toronto, Toronto.

Horvath, R.G., Kenney, T.C., and Kozicki, P. 1983. Methods of improving the performance of drilled piers in weak rock. Canadian Geotechnical Journal, Vol. 20, No. 4, pp. 758-772.

Horvath, R.G., Kenney, T.C., and Trow, W.A. 1980. Results of tests to determine shaft resistance of rock-socketed drilled piers. Proceedings of the International Conference on Structural Foundations on Rock, Sydney, Australia. Edited by P.J.N. Pells, Vol. 1, pp. 349-361.

Jackson, W.T., Perez, J.Y., and Lacroix, Y. 1973. Foundation, construction and performance for a 34-story building in St. Louis. Geotechnique, Vol. 24, No. 1, pp. 63-90.

Kenney, T.C., Lee, L.C., and Gagg, C. 1975. Laboratory investigation of preloading as a method of improving the load-displacement performance of socketed piles. University of Toronto, Department of Civil Engineering Publication 75-09.

Kenney, T.C. 1977. Factors to be considered in design of piers socketed into rock. Proceedings of the Conference on the Design and Construction of Deep Foundations, Canadian Society for Civil Engineering, Sudbury, Ontario.

Koutsoftas, D.C. 9181. Caissons socketed in sound Mica Schist. Journal of the Soil Mechanics and Foundations Divison, ASCE, Vol. 107, No. GT6, pp. 743-757.

Ladanyi, B. 1971. Friction and end-bearing tests on bedrock for high capacity socket design: Discussion. Canadian Geotechnical Journal, Vol. 14, pp. 153-155.

Leach, B.A., and Thompson, R.P. 1979. The Design and performance of large diameter bored piles in weak mudstone rocks. Proceedings, 7th European Conference on Soil Mechanics and Foundation Engineering. pp. 101-108.

Matich, M.A.J., and Kozicki, P. 1967. Some load tests on drilled cast-in-place concrete caissons. Canadian Geotechnical Journal, Vol. 4, pp. 367-375.

Mattes, N.S. 1969. The influence of radial displacement comparatability on pile settlements. Geotechnique, Vol. 19, pp. 157-159.

Mattes, N.S., and Poulos, H.G. 1969. Settlement of single compressible pile. Journal of the Soil Mechanics and Foundations Division, Vol. 95, No. SM1, pp. 189-207.

Nelson, J.D., and Thompson, E.G. 1974. Creep failure of slopes in clay and clay shales. Proceedings, 12th Annual Symposium on Engineering Geology and Soil Engineering, Boise, Idaho, pp. 177-195.

Neville, A.M. 1972. Properties of concrete. Pitman Ltd., New York.

Ngab, A.S., Nilson, A.H., and Slate, F.O. 1981. Shrinkage and creep of high strength concrete. Journal of ACI, Vol. 78, No. 4, pp. 255-261.

O'Neill, M.W., and Reese, L.C. 1970. Behaviour of axially loaded drilled shafts in Beaumont clay. Research Report 89-8, Centre for Highway Research, The University of Texas at Austin, Austin, Texas.

Osterberg, J.O., and Gill, S.A. 1973. Load transfer mechanism for piers socketed in hard soils or rock. Proceedings, 9th Canadian Rock Mechanics Symposium, Montreal, Quebec, pp. 235-262.

Peck, R.B. 1965. Pile and pier foundations. Journal of the Soil Mechanics and Foundations Division, ASCE, Vol. 91, No. SM2, pp. 33-38.

Peck, R.B. 1976. Rock foundations for structures. Proceedings of the Specialty Conference on Rock Engineering for Foundation and Slopes, Boulder, Colorado, Vol. 2, pp. 1-21.

Pells, P.J.N. 1978. Investigation into the allowable loading for bored piles founded on Hawkesberg sandstone. Progress Report 1 & 2, Investigation Report No. S226, School of Civil Engineering, University of Sydney, Australia.

Pells, P.J.N., Rowe, R.K., and Turner, R.M. 1980. An experimental investigation into side shear for socketed piles in sandstone. Proceedings of the International Conference on Structural Foundations on Rock, Sydney, Australia. Edited by P.J.N. Pells, Vol. 1, pp. 291-302.

Pells, P.J.N., and Turner, R.M. 1979. Elastic solutions for the design and analysis of rock-socketed piles. Canadian Geotechnical Journal, Vol. 16, No. 3, pp. 481-487.

Poulos, H.G., and Davis, E.H. 1968. The settlement behaviour of single axially loaded incompressible piles and piers. Geotechnique, Vol. 18, No. 3, pp. 351-371.

Rosenberg, P., and Journeaux, N.L. 1976. Friction and end-bearing tests on bedrock for high capacity socket design. Canadian Geotechnical Journal, Vol. 13, pp. 324-333.

Schmertmann, J.M., and Osterberg, J.O. 1960. An experimental study of the development of cohesion and friction with axial strain in saturated cohesive soils. ASCE, Research Conference on Shear Strength of Cohesive Soil, Boulder, Colorado, pp. 643-694.

Scott, J.S., and Brooker, E.W. 1968. Geotechnical and engineering aspects of Upper Cretaceous Shales in Weatern Canada. Paper 66-37, Geological Survey of Canada, Department of Energy, Mines and Resources, Ottawa.

Sower, G.F. 1962. Shallow Foundations. in Foundation Engineering, Edited by G.A. Leonards, McGraw-Hill Book Co., Inc., pp. 525-632.

Terzaghi, K. 1936. Stability of slopes in natural clay. Proceedings, 1st International Conference on Soil Mechanics and Foundation Engineering. Cambridge, Mass., Vol. 1, pp. 161-165.

Troxell, G.E., Raphael, J.M., and Davis, R.E. 1958. Long-time creep and shrinkage tests of plain reinforced concrete. Proceedings of the American Society for Testing Materials, Vol. 58, pp. 1101-1120.

Vijayvergiya, V.N., Hudson, W.R., and Reese, L.C. 1969. Load distribution for a drilled shaft in clay-shale. Research Report 89-5, Center for Highway Research, The University of Texas at Austin, Austin, Texas.

Williams, A.F. 1980. The design and performance of piles socketed into weak rock. Ph. D. Thesis, Monash University, Victoria, Australia.

Williams, A.F., Donald, I.B., and Chiu, H.K. 1980. Stress distributions in rock socketed piles. Proceedings of the International Conference on Structural Foundations on Rock, Sydney, Australia. Edited by P.J.N. Pells, Vol. 1, pp. 317-325.

Wooley, J.A., and Reese, L.C. 1974. Behaviour of an axially loaded drilled shaft under sustained loading. Research Report 176-2, Center for Highway Research, The University of Texas at Austin, Texas.

York, G.P., Kennedy, T.W., and Perry, E.S. 1970. Experimental investigation of creep in concrete subjected to multiaxial compressive stresses and elevated temperatures. Research Report 2864-2, Department of Civil Engineering, The University of Texas at Austin, Austin, Texas.

APPENDIX A

COMPRESSION TESTS ON PSEUDO-ROCK

A.1 PSEUDO-ROCK

The pseudo-rock was mixed in single batches. Twelve standard control cylinders, 152.4 mm (6.0 in) in diameter and 304.8 mm (12.0 in) in hight, were cast and tested to determine the compressive strength and the rate of strength gains with time. The compressometer and four electrical resistance strain gauges were used to measured the axial and circumferential displacements of pseudo-rock concrete cylinders during the uniaxial compression tests.

All standard control cylinder were cured in a curing room at 23 ^{o}C and 100 % relative humidity. Three such cylinders were, however, taken out from the curing room and kept in laboratory near the set up when the model tests were started. These cylinders were stored as long as the model tests with steel piers were run and were then tested for compressive strength tests as usual.

The rate of strength gains for the pseudo-rock concrete is shown in Fig. A-1.

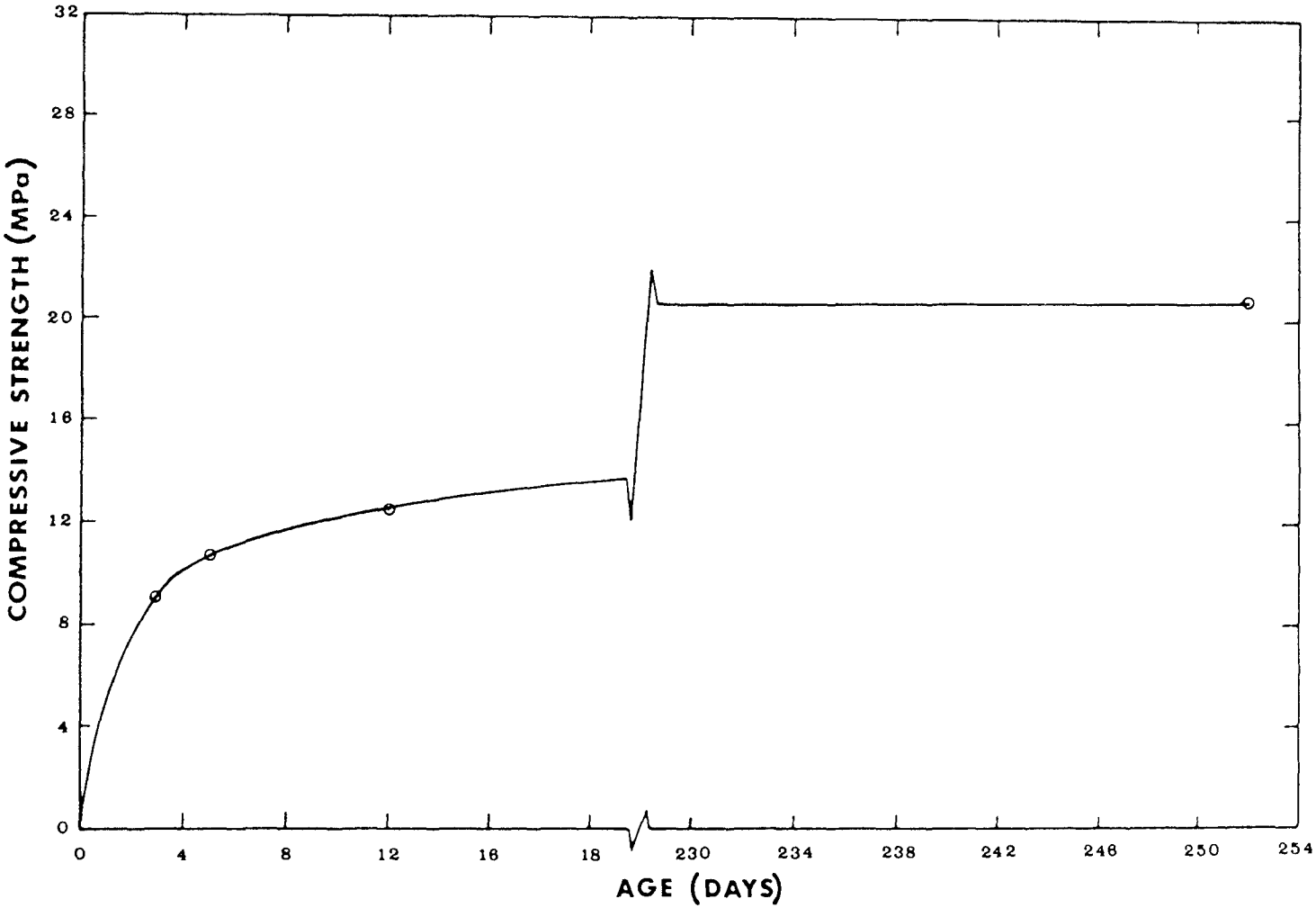

Fig. A-1 Compressive strength versus pseudo-rock age relationship.

APPENDIX B

GEOLOGY AND MINEROLOGICAL COMPOSITION OF QUEENSTON SHALE

B.1 QUEENSTON SHALE

The Queenston Shale of Southern Ontario is red in colour, argillaceous and arenaceous. These sedimentary shales were formed during the upper Ordovician age. The Queenston Shale samples for the present investigation were obtained from the National Sewer Pipe Quarry in Burlington, Ontario. The thickness of the shale formation in the surrounding area has been reported to be around 180.0 m (590.6 ft) (Guillet 1977).

The Queenston Shale samples were found to have thin beds of lime rich calcareous shale. These thin beds were found to be green in colour and were 10 mm - 150 mm (0.4 in - 5.9 in) in thickness. The green calcareous shale were found to be much hader than Queenston Shale and were thus, less affected by the weathering actions. The samples were collected in such a way that the green beds could be removed and the test for the present research were conducted on the red Queenston Shale only.

The Queenston Shale is reported to be fairly uniform in chemical and mineral compositions. The minerological composition of this shale as per Guillet (1977) is given in Table B-1.

TABLE B-1 MINERAL ANALYSES ON QUEENSTON SHALE

(AFTER GUILLET 1977)

Non-Clay Minerals		Clay Minerals	
Name	% Retain	Name	Index
Quartz	26.0	Illite	A
Calcite	11.0	Chlorite	B
Dolomite	1.8	Expanding* Minerals	D
Feldsper	1.3		

* Vermiculite

A = Abundant B = Moderate D = Trace

APPENDIX C

V-3 GROUT PROPERTIES

TABLE C-1 TYPICAL PROPERTIES OF V-3 GROUT SUGGESTED BY MANUFACTURER.

PROPERTIES (typical for pourable consistency)

PROPERTY		V-1 GROUT		V-3 GROUT	
Compressive Strength* (ASTM C109 70T)		psi	(MPa)	psi	(MPa)
Elapsed Time	24 hours	5800	40	4500	30
	3 days	8700	60	6500	45
	7 days	10500	70	7800	50
	28 days	12000	80	9000	60
	915 days	12000	80	9000	60
Controlled Expansion (unrestrained)		1.0% (approx.)		0.4% (approx.)	
Controlled Internal Pressure Development		1.0 psi (7 Kpa) (approx.)		0.5 psi (3.5 Kpa) (approx.)	
Tensile Strength (after 28 days)		625 psi (4.3 MPa)		540 psi (3.7 MPa)	
Pull Out Resistance					
1" re-bar grouted to 4.7" depth		27,200 psi (12,300 Kg)		20,800 psi (9,400 Kg)	
3/4" re-bar grouted to 4" depth		—			
Flow Index (10 drops)		125		115	
Initial Set Time (Laboratory Tests)		3h		4h	
Final Set Time (Laboratory Tests)		4h		6h	

*Plastic mixes up to 10% higher. Damp pack up to 20% higher.

Chemical Analysis No metallic elements. No evidence of corrosives

Dynamic Loading Increase of 5% in compressive strength to 10 million load plays

Freeze/Thaw Resistance Density of V-1 and V-3 grouts allows little water absorption resulting in only slight surface scaling after 180 cycles from —60°F to 40°F (—51°C to 4°C)

MEADOWS SEALTIGHT®

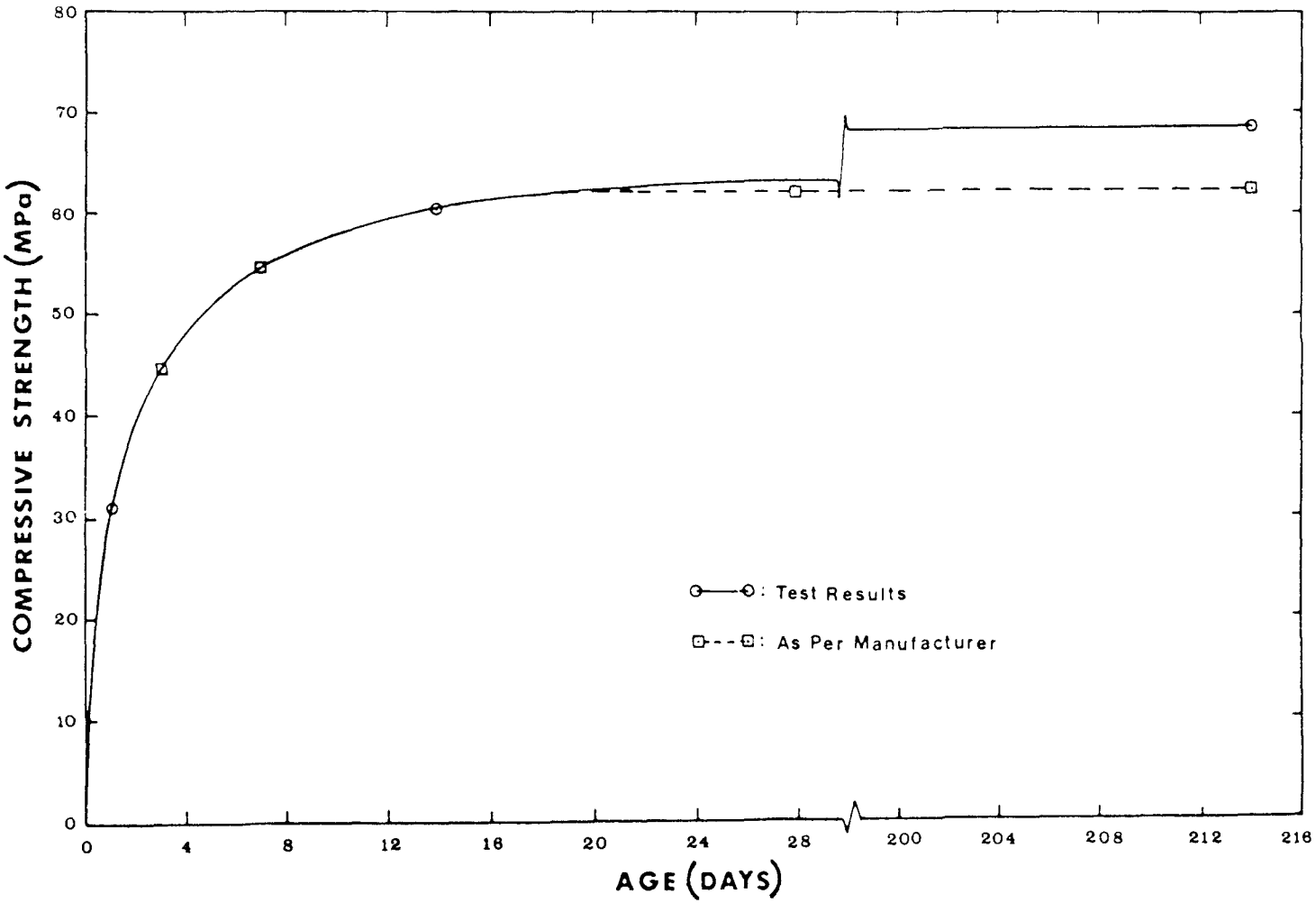

Fig. C-1 Compressive strength versus V-3 grout age relationship.